Title
The Molecular Basis for Calcium-dependent Regulation of Cardiac Structure and Function

Author
Shimizu, Hirohito

Publication Date
2014

Peer reviewed|Thesis/dissertation

UNIVERSITY OF CALIFORNIA

LOS ANGELES

The Molecular Basis for Calcium-dependent Regulation of Cardiac Structure and Function

A dissertation submitted in partial satisfaction of the requirements for the degree Doctor of Philosophy in Molecular, Cell and Developmental Biology

by

Hirohito Shimizu

2014

ABSTRACT OF THE DISSERTATION

The Molecular Basis for Calcium-dependent Regulation

of Cardiac Structure and Function

by

Hirohito Shimizu

Doctor of Philosophy in Molecular, Cell and Developmental Biology

University of California, Los Angeles, 2014

Professor Jau-Nian Chen, Chair

Calcium homeostasis is essential for regulating a wide spectrum of biological processes. In the heart, Ca^{2+} plays a key role in excitation-contraction coupling, electrophysiological processes, activation of contractile proteins, energy metabolism, cell death, and transcriptional regulation. Alteration of Ca^{2+} homeostasis is often associated with cardiac pathology such as contractile dysfunction, arrhythmias and heart failure. In order to discover novel molecular mechanisms by which Ca^{2+} regulates cardiac structure and function, I have utilized a zebrafish mutant *tremblor* (*tre*), as a model for cardiac defects induced by aberrant Ca^{2+} homeostasis. With this model system, I discovered a new mechanism by which Ca^{2+} homeostasis is regulated in cardiomyocytes and revealed its implication in normal and diseased physiology. First, I found

that mitochondria play a critical role in modulating Ca^{2+} homeostasis and maintaining cardiac rhythmicity. By a multidisciplinary approach including biochemistry, genetics and physiology, I demonstrated that Ca^{2+} transfer into mitochondria through the outer mitochondrial membrane protein, voltage-dependent anion channel (VDAC2), is an essential fine-tuning mechanism of normal intracellular Ca^{2+} homeostasis that prevents the propagation of arrhythmogenic Ca^{2+} waves. Second, I discovered that normal Ca^{2+} homeostasis is required to maintain myofibrillar integrity in cardiomyocytes. Aberrant Ca^{2+} homeostasis leads to upregulation of an E3 ubiquitin ligase, Muscle-specific RING Finger protein 1 (MuRF1), and induces degradation of contractile proteins via a proteasome-dependent protein degradation mechanism. Taken together, my dissertation research has revealed diverse roles of Ca^{2+} homeostasis in the heart and its regulatory mechanism. These findings provide new insights into cardiac diseases associated with Ca^{2+} mishandling in cardiomyocytes and may lead to the development of novel therapeutic approaches for these diseases.

The dissertation of Hirohito Shimizu is approved.

Karen Lyons

Atsushi Nakano

Michael Collins

Jau-Nian Chen, Committee Chair

University of California, Los Angeles

2014

To Father and Mother, without whose tireless support and

encouragement I would have given up long ago.

TABLE OF CONTENTS

LIST OF FIGURES AND TABLES

ACKNOWLEDGEMENTS

I would like to extend my sincere gratitude to my academic advisor, Professor Jau-Nian Chen for the valuable training and constant encouragement provided throughout my doctoral studies. Without her persistent guidance and help, this dissertation would not have been possible. I would also like to appreciate my committee members, Drs. Michael Collins, Karen Lyons, and Atsushi Nakano for the valuable comments and suggestions for my doctoral research and critical reading of my dissertation. Many thanks also go to past and present members of the Chen lab: Ann Cavanaugh, Jayoung Choi, Joseph Gheorghe, Jie Huang, Adam Langenbacher, Fei Lu, Kevin Mouillesseaux, Catherine Nguyen, Johann Schredelseker, and Kevin Wang. Their assistance and cooperation in every aspect of my research were imperative for the completion of my dissertation research, and they each have made my time in the Chen lab more valuable and enjoyable.

The following manuscripts in preparation for publication are incorporated in this dissertation. I would like to express deepest gratitude to the co-authors who have contributed to these works:

CHAPTER 2

Hirohito Shimizu*, Johann Schredelseker*, Jie Huang*, Kui Lu*, Shamim Naghdi, Fei Lu, Sarah Franklin, Huanqi Zhu, Cheng Tien, Hannah D.G. Fiji, Kevin Wang, Billy Lin, Adam Stieg, James Gimzewski, Atushi Nakano, Joshua I. Goldhaber, Thomas M. Vondriska, György Hajnóczky , Ohyun Kwon and Jau-Nian Chen. Activation of voltage-dependent anion channel suppresses aberrant Ca^{2+} handling-induced cardiac arrhythmia.

CHAPTER 3

Hirohito Shimizu, Jie Huang, Kevin Wang, Georg Otto, Robert Giesler, Jau-Nian Chen. Aberrant Ca^{2+} homeostasis leads to proteasome-mediated myofibrillar disarray via the calcineurin-FoxO signaling pathway.

(*) indicates that the authors contributed equally to the manuscript in preparation.

I would also like to acknowledge with much appreciation the Nakajima Foundation for a pre-doctoral fellowship supporting my doctoral study. This research was also supported by grants from RO1 HL096980, RO1 HL81700 to Dr. Jau-Nian Chen.

And finally, I am highly indebted to my family for their support and understanding during my graduate study.

VITA

Education

2005	M.S. in Toxicology Department of Environmental Health Sciences, Toxicology Track, School of Public Health, University of California, Los Angeles, CA
2003	B.S. in Biology Division of Biological Sciences School of Science Tokyo Metropolitan University, Tokyo, Japan

Professional Experience

2010, 2011	Teaching Assistant Department of Molecular, Cell and Developmental Biology University of California, Los Angeles, CA
2008	Publication Committee (*ad hoc* student member) Teratology Society
2006-2008	Research Technician The National Research Institute for Child Health and Development Tokyo, Japan
2003	Temporary Part-Time Biology Teacher International Christian University High School, Tokyo, Japan

Fellowships and Awards

2008-2013	Pre-Doctoral Fellowship The Nakajima Foundation
2012	Best Oral Award The 18th Japanese Medaka and Zebrafish Meeting
2011	Best Poster Award UCLA MCDB Departmental Retreat
2008	James G. Wilson Publication Award Teratology Society
2004-2005	Atlantic Richfield Company Fellowship Fund UCLA School of Public Health

Conference Presentations

2012	Activation of voltage-dependent anion channel 2 suppresses Ca^{2+}-induced cardiac arrhythmia (Talk & Poster) The 18th Japanese Medaka and Zebrafish Meeting, Kyoto, Japan
2012	Activation of voltage-dependent anion channel 2 suppresses Ca^{2+}-induced cardiac arrhythmia (Talk & Poster) Weinstein Cardiovascular Development Conference, Chicago, IL
2012	The Molecular Mechanism Underlying Aberrant Ca^{2+} Homeostasis-Induced Cardiac Myofibrillar Disarray" (Talk) Southern California Zebrafish Meeting, Los Angeles, CA
2009	EMBRYS: A digital atlas of gene expression patterns in the developing mouse embryo (Talk) 49th Annual Meeting for the Teratology Society, Rio Grande, Puerto Rico
2008	Altered localization of gene expression in both ectoderm and mesoderm is associated with a murine strain difference in retinoic acid-induced forelimb ectrodactyly (Talk) 48th Annual Meeting for the Teratology Society (as a recipient of the James G. Wilson Publication Award), Monterey, CA

Publications

Shimizu H, Kubo A, Uchibe K, Hashimoto M, Yokoyama S, Takada S, Mitsuoka K, Asahara H. The AERO system: a 3D-like approach for recording gene expression patterns in the whole mouse embryo. PLoS One. 2013;8(10):e75754.

Lee GS*, Liao X*, Shimizu H*, Collins MD. Genetic and pathologic aspects of retinoic acid-induced limb malformations in the mouse. Birth Defects Res A Clin Mol Teratol. 2010;88(10):863-82.

Shimizu H, Uchibe K, Asahara H. Large-scale whole mount in situ hybridization of mouse embryos. Methods Mol Biol. 2009;577:167-79.

Shimizu H, Yokoyama S, Asahara H. Growth and differentiation of the developing limb bud from the perspective of chondrogenesis. Dev Growth Differ. 2007;49(6):449-54.

Shimizu H, Lee GS, Beedanagari SR, Collins MD. Altered localization of gene expression in both ectoderm and mesoderm is associated with a murine strain difference in retinoic acid-induced forelimb ectrodactyly. Birth Defects Res A Clin Mol Teratol. 2007;79(6):465-82.

(*) indicates that the authors contributed equally to the manuscript.

CHAPTER 1

Calcium homeostasis in the heart

The heart functions as a pump to perfuse blood throughout the entire body, delivering oxygen, hormones and nutrients to and retrieving wastes and carbon dioxide away from tissues and organs. To carry out this task efficiently, cardiac muscle cells (cardiomyocytes) contract and relax in a coordinated manner. In the absence of this synchrony, the pump function is impaired, leading to circulatory failure.

Like skeletal muscle cells, cardiomyocytes maintain a negative membrane potential at rest. When stimulated, voltage-gated channels on the plasma membrane open, allowing the influx of cations and thereby depolarize cardiomyocytes. The repolarization of cardiomyocytes requires the opening of potassium channels to bring the membrane potential back to the resting state [1]. In the early embryonic heart, the coupling of cardiomyocytes via gap junctions is sufficient to transduce the electrical impulses through the primitive heart tube. As the heart matures, a specialized cardiac conduction system (CCS) is required for the efficient transduction of electrical impulses through the heart; action potentials generated from the sinoatrial (SA) node travel across the atria, pause at the atrioventricular (AV) node and then propagate through the ventricles via the His-Purkinje system [2-3].

At the cellular level, Ca^{2+} has a primary role in coordinating the electrical signals and muscle contractions, a mechanism known as Excitation-Contraction (E-C) Coupling. In this mechanism, the influx of Ca^{2+} through the opening of voltage-gated Ca^{2+} channels on the plasma membrane induces the release of Ca^{2+} from the sarcoplasmic reticulum (SR), which triggers

muscle contraction by inducing the sliding of thick and thin filaments in sarcomeres. Aberrant Ca^{2+} homeostasis or defects in myofibril integrity has been linked to cardiac dysfunctions such as hypertrophic cardiomyopathy, dilated cardiomyopathy and arrhythmogenic right ventricular cardiomyopathy [4]. Thus, dissecting the molecular network critical for regulating Ca^{2+} handling and myofibril integrity will not only further our understanding of basic cardiac physiology but also provide insights into disease mechanisms.

A. Cardiac E-C coupling

An essential function of Ca^{2+} in the heart is to enable E-C coupling (Figure 1-1), which is a tightly orchestrated process coordinating electrical signals and the contractile activity on a beat-to-beat basis. Upon membrane depolarization, voltage-dependent L-type Ca^{2+} channels (LTCCs) allow the influx of a relatively small amount of Ca^{2+} into the cytoplasm. This process triggers a larger Ca^{2+} release from the internal Ca^{2+} store, sarcoplasmic reticulum (SR), via clusters of ryanodine receptors (RyRs). This mechanism termed "calcium-induced calcium release" (CICR) serves as a fundamental mechanism underlying E-C coupling [1, 5-7]. As a result of CICR, Ca^{2+} released from the SR binds to troponin C of the troponin-tropomyosin complex and induces a sequence of allosteric changes in the myosin filaments to facilitate formation of cross bridges between actin and myosin, driving contraction [8]. During diastole, muscle relaxation is largely achieved by the SR Ca^{2+}-ATPase (SERCA)-mediated reuptake of cytoplasmic Ca^{2+} into the SR. In addition, a relatively small amount of Ca^{2+} is extruded from cardiomyocytes primarily through an antiporter membrane protein, Na^{+}/Ca^{2+} exchanger (NCX)

[9]. Thus, Ca^{2+} cycling between the extracellular space, cytoplasm and SR is the core mechanism underlying the rapid repetition of cardiac contraction and relaxation.

Defective intracellular Ca^{2+} homeostasis is known to be a hallmark cause of contractile dysfunction and arrhythmias in the failing myocardium. For example, failing heart is frequently characterized by elevated diastolic $[Ca^{2+}]_i$ caused by several distinct mechanisms both in cytoplasmic and transmembrane components such as reduced Ca^{2+} uptake by SERCA, increased diastolic Ca^{2+} leakage via RyR2, reduced Ca^{2+} extrusion via NCX and increased influx of extracellular Ca^{2+} via LTCC [10-11]. In fact, numerous genetic mutations in these Ca^{2+} handling proteins have been identified in human patients [7, 12]. Therefore, an amelioration of aberrant Ca^{2+} homeostasis has been considered as a promising therapeutic strategy to treat heart failure. Interestingly, recent studies suggest that, in addition to the SR, other organelles such as mitochondria play a role in regulating intracellular Ca^{2+} homeostasis.

B. Local control of Ca^{2+} homeostasis –mitochondrial Ca^{2+} uptake

Although classically viewed as a cellular power plant, identification of a variety of proteins involved in mitochondrial Ca^{2+} signaling and ER/SR-mitochondria interactions has greatly spurred our enthusiasm for research on the mechanism of mitochondrial Ca^{2+} uptake and its functional importance [13-16].

Mitochondrial Ca^{2+} uptake is primarily mediated by the mitochondrial Ca^{2+} uniporter (MCU), a recently identified pore-forming protein located in the inner mitochondrial membrane [17-18]. However, previous studies demonstrated the low Ca^{2+} affinity of MCU ($EC50 \approx 10$ mM) [19], which would limit mitochondria's ability to transport Ca^{2+} from the cytoplasm, where

normal Ca^{2+} concentrations are much lower (0.1 to 10 μM [20]). Paradoxically, a classical study using mitochondria-selective Ca^{2+} indicators reported that IP3-induced Ca^{2+} release from ER rapidly increases mitochondrial Ca^{2+} levels in quiescent cells [21]. In addition, a more recent study revealed distinct beat-to-beat Ca^{2+} transients in mitochondria during spontaneous Ca^{2+} pacing in cardiomyocytes [22]. These lines of study suggest a mechanism that can overcome the low affinity of MCU to achieve rapid transfer of Ca^{2+} into mitochondria. This mechanism is currently postulated by the concept of Ca^{2+} microdomain [21]. Experimental evidence and a computational model suggest that cytoplasmic Ca^{2+} is not uniformly distributed within a cell [23]. Ca^{2+} concentrations near the Ca^{2+} release sites of the organelles are significantly higher than the global $[Ca^{2+}]_i$. In fact, it is reported that $[Ca^{2+}]$ in the microdomains on the outer mitochondrial membrane (OMM) reaches 5- to 10-fold higher than $[Ca^{2+}]_i$ [24].

Consistently, a number of Ca^{2+} hotspots were directly observed on the outer mitochondrial membrane (OMM) surface in cardiomyocytes during cytoplasmic Ca^{2+} transients [22, 25]. From this observation, it is expected that mitochondria are present in close proximity to SR Ca^{2+} release sites. In fact, accumulating evidence has established that Ca^{2+} is locally transferred to mitochondria from SR through RyR2 in cardiomyocytes. For example, induction of Ca^{2+} release from the RyR2 results in a rapid increase in mitochondrial Ca^{2+} levels even when the cytosolic Ca^{2+} is buffered [26-27]. Also, RyR2-mediated Ca^{2+} sparks are capable of causing miniature mitochondrial Ca^{2+} transients [28]. Furthermore, cardiac mitochondria co-purified with a subfraction of the SR are capable of transferring Ca^{2+} upon stimulation of RyR with caffeine [29]. All these findings clearly indicate the importance of local control of intracellular Ca^{2+}

dynamics. However, the question still remains whether this inter-organelle Ca^{2+} transfer has functional relevance to cardiac rhythmicity and contractility [30].

C. Transcriptional control by Ca^{2+}

In excitable cells, the intracellular Ca^{2+} transients discussed above are evoked by the rapid signaling on a millisecond time scale. At the synaptic junctions, Ca^{2+} operates even faster and triggers exocytosis on a microsecond time scale. In addition, Ca^{2+} manifests long-term effects on an hour time scale through its ability to regulate gene expression by activating a variety of cytoplasmic and/or nuclear signaling pathways [31]. While Ca^{2+} passively diffuses into the nucleus and directly activates Ca^{2+}-dependent transcription factors, it also binds to cytoplasmic signaling molecules, which then transmit the signal to downstream targets to control nuclear translocation of transcription factors [32].

In cardiomyocytes, calmodulin (CaM), an intracellular Ca^{2+} sensor protein, coordinates Ca^{2+}-dependent signaling pathways including the calcineurin (CN) and Ca^{2+}-calmodulin-dependent protein kinase II (CaMKII) pathways. Misregulation of these signaling pathways due to aberrant Ca^{2+} homeostasis results in several disease states in the heart. A good example is cardiac hypertrophy, which is an adaptive response of the heart characterized by the change in cardiomyocyte size and structural remodeling of the myocardium. CN, a Ca^{2+}-calmodulin-activated serine/threonine phosphatase, dephosphorylates nuclear factor of activated T-cells (NFAT), thereby inducing NFAT translocation from the cytoplasm to the nucleus where it activates the hypertrophic gene program [33]. CaMKIIγ, a predominant isoform in the heart, regulates nuclear translocation of the downstream target MEF2, a cardiac remodeling mediator,

via phosphorylation of class II HDACs [34]. The nuclear splice variant CaMKIIδ_B phosphorylates HDAC4, allowing its export out of the nucleus as a complex with the chaperone protein 14-3-3, and thus MEF2 is relieved from the repression by HDAC4 [35]. The cytoplasmic splice variant CaMKIIδ_C, on the other hand, phosphorylates HDAC4 in the cytoplasm, preventing its translocation to the nucleus [36].

A major problem in understanding Ca^{2+}-dependent transcriptional regulation in the heart is the fact that the heart is subjected to the oscillation of cytoplasmic Ca^{2+} levels on a beat-to-beat basis. In this regard, it is interesting to note that Ca^{2+}-dependent signaling molecules are proposed to sense the temporal patterns of Ca^{2+} increase (i.e. frequency and duration) rather than the amplitude of Ca^{2+} input [37-38].

D. Zebrafish as a model organism to study cardiac Ca^{2+} homeostasis

The zebrafish has made significant contributions to our understanding of cardiac development. There is a wide spectrum of attributes underpinning the use of zebrafish as a model system: ease in embryo culture, external fertilization, high fecundity, a sequenced genome, embryological manipulability and suitability in high-throughput phenotype-based screenings. The zebrafish heart is located at a prominent ventral position of this translucent embryo allowing direct inspection of cardiac morphology and function. Furthermore, because oxygen can diffuse through the tissues during the first week of life, zebrafish embryos can survive in the total absence of blood circulation, allowing us to investigate the impact of cardiac dysfunction for a longer period of time than in mammalian models [39].

The zebrafish model has great potential to assist study in cardiac physiology for the following reasons. First, the heart rate as well as action potential shape and duration of zebrafish embryos closely resemble those in humans. Second, electrophysiological approaches are available to evaluate cardiac excitability by using optogenetic methods such as Ca^{2+}- and voltage-sensitive fluorescent dyes and transgenes [40]. Third, a number of mutations affecting cardiac contractility and/or rhythmicity have been identified from large-scale mutagenesis screens [41-42]. For example, the *island beat* (*isl*) mutant, characterized by atrial fibrillation, carries a null mutation in LTCC [43]. Embryos lacking a functional repolarizing potassium channel gene *kcnh2* display complete atrioventricular block and ventricular asystole serving as a model for human long QT syndrome, a repolarization disorder possibly leading to sudden cardiac death [44]. On the other hand, *reggae* (*reg*) mutant embryos carry a gain-of-function mutation in *kcnh2* and have a shorter duration of action potential, serving as a model for human short QT syndrome, [45].

Our laboratory has previously demonstrated that the zebrafish *tremblor* (*tre*) locus encodes the cardiac-specific *ncx1h* gene [46-47]. Loss-of-function of NCX1h results in a Ca^{2+} extrusion defect and causes abnormal Ca^{2+} transients in cardiomyocytes. The *tre* mutant embryo manifests phenotypes similar to those commonly seen in human heart failure patients including cardiac fibrillation and myofibril disarray. In my thesis research, I used *tre* as an animal model for aberrant Ca^{2+} homeostasis-induced cardiac dysfunction in order to: 1) dissect the molecular network required for the regulation of cardiac Ca^{2+} homeostasis, 2) examine the consequence of aberrant Ca^{2+} homeostasis and the molecular mechanism behind it.

E. New discoveries in this thesis

In CHAPTER 2, I describe and discuss new findings on the molecular basis for Ca^{2+}-dependent regulation of cardiac function. By using a zebrafish *tre* mutant as a model for aberrant Ca^{2+} homeostasis-induced cardiac dysfunction, I discovered a new mechanism by which Ca^{2+} homeostasis is regulated in cardiomyocytes and gained new insight into its implication in normal and disease physiology. I show that, in addition to SR, mitochondria play an essential role in modulating Ca^{2+} homeostasis and maintaining cardiac rhythmicity. From a chemical suppressor screen, we identified a novel synthetic compound named efsevin due to its potent effect on restoring rhythmic cardiac contractions in *tre*. Biochemical and molecular evidence indicate that the outer mitochondrial membrane protein, voltage-dependent anion channel (VDAC2) is directly targeted by efsevin. We further showed that efsevin treatment potentiates the Ca^{2+} transporting activity of VDAC2, accelerates Ca^{2+} transfer from SR into mitochondria, and thereby restores cardiac rhythmicity in tre embryos. These data suggest a critical role for mitochondrial Ca^{2+} uptake in maintaining normal intracellular Ca^{2+} homeostasis by preventing the propagation of arrhythmogenic Ca^{2+} waves.

In CHAPTER 3, I discuss my findings that aberrant Ca^{2+} homeostasis in *tre* cardiomyocytes results in myofibrillar disarray via the proteasome-dependent protein degradation mechanism. I showed that an E3 ubiquitin ligase, Muscle-specific RING Finger protein 1 (MuRF1), is significantly upregulated in the *tre* mutant heart and that this alteration is mediated by the calcineurin-FoxO signaling pathway induced by Ca^{2+} overload. These data reveal the function of Ca^{2+} as a molecular switch required to regulate the stoichiometry of cardiac muscle structure via transcriptional regulation.

Taken all together, the research described in my thesis provides new insights into mechanisms underlying a variety of cardiac diseases that have a root in aberrant Ca^{2+} handling. These new findings may help develop new diagnostic approaches or novel therapeutic strategies for these diseases.

Figure 1-1. Schematic representation of Excitation-Contraction coupling in cardiomyocytes. In response to an electrical pulse, L-type Ca^{2+} channels (LTCC) are activated, allowing influx of Ca^{2+} into cardiomyocytes. Ca^{2+} then stimulates ryanodine receptors (RyR) in the membrane of the sarcoplasmic reticulum (SR) and induces the release of larger amounts of Ca^{2+} to the cytoplasm, which is required for muscle contraction. Following contraction, Ca^{2+} is either taken up by the SR through the sarco/endoplasmic reticulum Ca^{2+}-ATPase (SERCA) or extruded from cardiomyocytes by the sodium-calcium exchanger (NCX) in the plasma membrane.

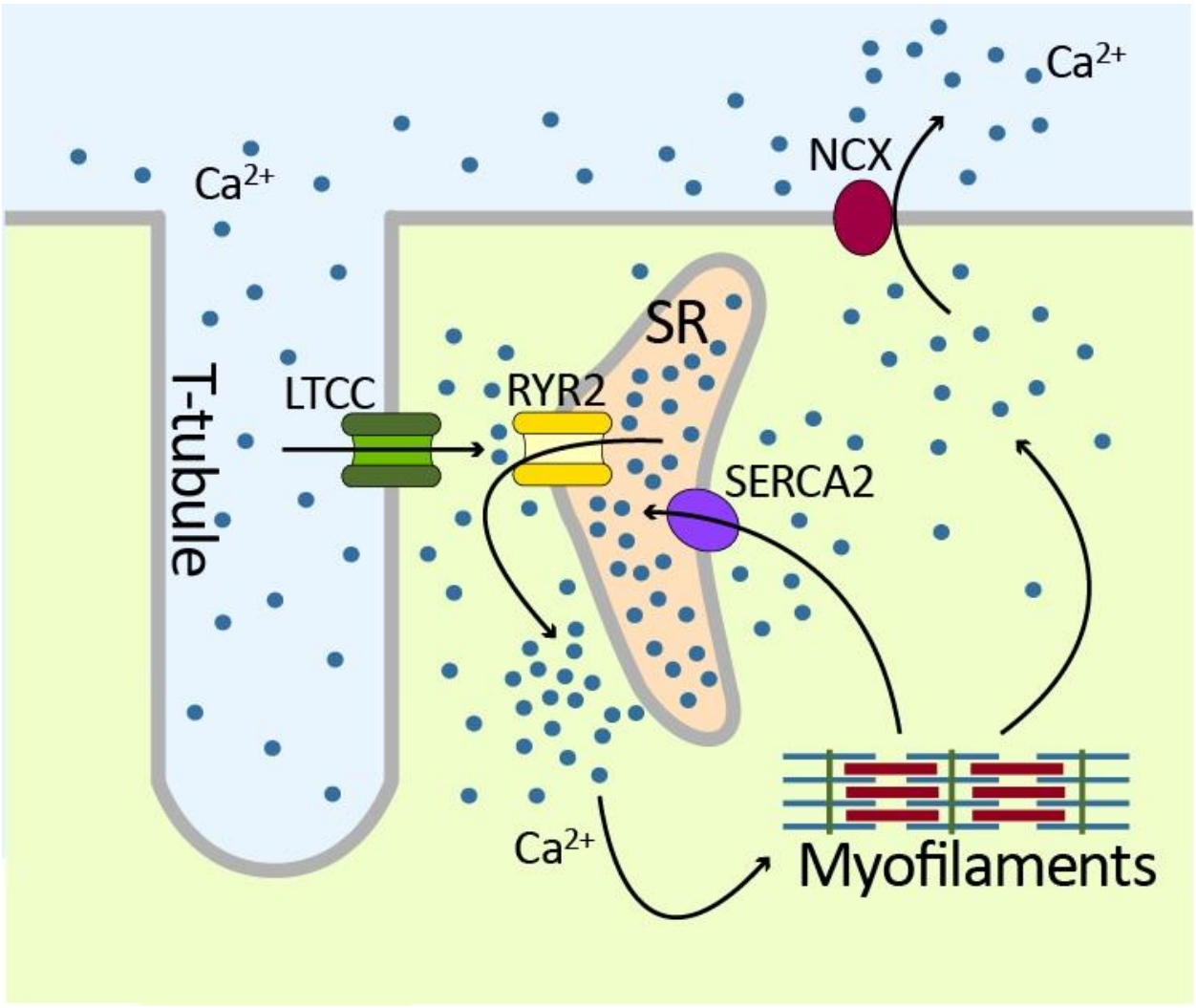
Ca2+
Ca2+
NCX
SR
T-tubule
LTCC
RYR2
SERCA2
Ca2+
Myofilaments

F. References

1. Bers DM. Cardiac excitation-contraction coupling. Nature. 2002;415(6868):198-205.

2. Pennisi DJ, Rentschler S, Gourdie RG, Fishman GI, Mikawa T. Induction and patterning of the cardiac conduction system. Int J Dev Biol. 2002;46(6):765-75.

3. Fishman GI. Understanding conduction system development: a hop, skip and jump away? Circ Res. 2005;96(8):809-11.

4. Ghosh N, Haddad H. Recent progress in the genetics of cardiomyopathy and its role in the clinical evaluation of patients with cardiomyopathy. Curr Opin Cardiol. 2011;26(2):155-64.

5. Bers DM. Calcium cycling and signaling in cardiac myocytes. Annu Rev Physiol. 2008;70:23-49.

6. Cannell MB, Kong CH. Local control in cardiac E-C coupling. J Mol Cell Cardiol. 2012;52(2):298-303.

7. Venetucci L, Denegri M, Napolitano C, Priori SG. Inherited calcium channelopathies in the pathophysiology of arrhythmias. Nat Rev Cardiol. 2012;9(10):561-75.

8. Davison FD, D'Cruz LG, McKenna WJ. Molecular motors in the heart. Essays Biochem. 2000;35:145-58.

9. Terentyev D, Viatchenko-Karpinski S, Valdivia HH, Escobar AL, Györke S.Luminal Ca^{2+} controls termination and refractory behavior of Ca2+-induced Ca^{2+} release in cardiac myocytes. Circ Res. 2002;91(5):414-20.

10. Yano M, Ikeda Y, Matsuzaki M. Altered intracellular Ca^{2+} handling in heart failure. J Clin Invest. 2005;115(3):556-64.

11. Luo M, Anderson ME. Mechanisms of altered Ca^{2+} handling in heart failure. CircRes. 2013;113(6):690-708.

12. Morita H, Seidman J, Seidman CE. Genetic causes of human heart failure. J Clin Invest. 2005;115(3):518-26.

13. Rizzuto R, Marchi S, Bonora M, Aguiari P, Bononi A, De Stefani D, Giorgi C,Leo S, Rimessi A, Siviero R, Zecchini E, Pinton P. Ca^{2+} transfer from the ER to mitochondria: when, how and why. Biochim Biophys Acta. 2009;1787(11):1342-51.

14. Contreras L, Drago I, Zampese E, Pozzan T. Mitochondria: the calcium connection. Biochim Biophys Acta. 2010;1797(6-7):607-18.

15. Dorn GW 2nd, Maack C. SR and mitochondria: calcium cross-talk between kissing cousins. J Mol Cell Cardiol. 2013;55:42-9.

16. Eisner V, Csordás G, Hajnóczky G. Interactions between sarco-endoplasmic reticulum and mitochondria in cardiac and skeletal muscle - pivotal roles in $Ca^{2+}$and reactive oxygen species signaling. J Cell Sci. 2013;126(Pt14):2965-78.

17. De Stefani D, Raffaello A, Teardo E, Szabò I, Rizzuto R. A forty-kilodalton protein of the inner membrane is the mitochondrial calcium uniporter. Nature. 2011;476(7360):336-40.

18. Baughman JM, Perocchi F, Girgis HS, Plovanich M, Belcher-Timme CA, Sancak Y,Bao XR, Strittmatter L, Goldberger O, Bogorad RL, Koteliansky V, Mootha VK.Integrative genomics identifies MCU as an essential component of the mitochondrial calcium uniporter. Nature. 2011;476(7360):341-5.

19. Kirichok Y, Krapivinsky G, Clapham DE. The mitochondrial calcium uniporter is a highly selective ion channel. Nature. 2004;427(6972):360-4.

20. Carafoli E, Santella L, Branca D, Brini M. Generation, control, and processing of cellular calcium signals. Crit Rev Biochem Mol Biol. 2001;36(2):107-260.

21. Rizzuto R, Brini M, Murgia M, Pozzan T. Microdomains with high Ca^{2+} close to IP3-sensitive channels that are sensed by neighboring mitochondria. Science. 1993;262(5134):744-7.

22. Trollinger DR, Cascio WE, Lemasters JJ. Mitochondrial calcium transients in adult rabbit cardiac myocytes: inhibition by ruthenium red and artifacts caused by lysosomal loading of Ca^{2+}-indicating fluorophores. Biophys J. 2000;79(1):39-50.

23. Wang SQ, Wei C, Zhao G, Brochet DX, Shen J, Song LS, Wang W, Yang D, Cheng H. Imaging microdomain Ca^{2+} in muscle cells. Circ Res. 2004;94(8):1011-22.

24. Giacomello M, Drago I, Bortolozzi M, Scorzeto M, Gianelle A, Pizzo P, Pozzan T. Ca^{2+} hot spots on the mitochondrial surface are generated by Ca^{2+} mobilization from stores, but not by activation of store-operated Ca^{2+} channels. Mol Cell. 2010;38(2):280-90.

25. Drago I, De Stefani D, Rizzuto R, Pozzan T. Mitochondrial Ca^{2+} uptake contributes to buffering cytoplasmic Ca^{2+} peaks in cardiomyocytes. Proc Natl AcadSci U S A. 2012;109(32):12986-91.

26. Sharma VK, Ramesh V, Franzini-Armstrong C, Sheu SS. Transport of Ca^{2+} from sarcoplasmic reticulum to mitochondria in rat ventricular myocytes. J Bioenerg Biomembr. 2000;32(1):97-104.

27. Szalai G, Csordás G, Hantash BM, Thomas AP, Hajnóczky G. Calcium signal transmission between ryanodine receptors and mitochondria. J Biol Chem. 2000;275(20):15305-13.

28. Pacher P, Csordás P, Schneider T, Hajnóczky G. Quantification of calcium signal transmission from sarco-endoplasmic reticulum to the mitochondria. JPhysiol. 2000;529 Pt 3:553-64.

29. García-Pérez C, Hajnóczky G, Csordás G. Physical coupling supports the local Ca^{2+} transfer between sarcoplasmic reticulum subdomains and the mitochondria in heart muscle. J Biol Chem. 2008;283(47):32771-80.

30. Rizzuto R, Pozzan T. Microdomains of intracellular Ca^{2+}: molecular determinants and functional consequences. Physiol Rev. 2006;86(1):369-408.

31. Berridge MJ, Bootman MD, Roderick HL. Calcium signalling: dynamics, homeostasis and remodelling. Nat Rev Mol Cell Biol. 2003;4(7):517-29.

32. Barbado M, Fablet K, Ronjat M, De Waard M. Gene regulation by voltage-dependent calcium channels. Biochim Biophys Acta. 2009;1793(6):1096-104.

33. Molkentin JD, Lu JR, Antos CL, Markham B, Richardson J, Robbins J, Grant SR, Olson EN. A calcineurin-dependent transcriptional pathway for cardiac hypertrophy. Cell. 1998;93(2):215-28.

34. Backs J, Backs T, Neef S, Kreusser MM, Lehmann LH, Patrick DM, Grueter CE, Qi X, Richardson JA, Hill JA, Katus HA, Bassel-Duby R, Maier LS, Olson EN. The delta isoform of CaM kinase II is required for pathological cardiac hypertrophy and remodeling after pressure overload. Proc Natl Acad Sci U S A. 2009;106(7):2342-7.

35. Backs J, Song K, Bezprozvannaya S, Chang S, Olson EN. CaM kinase II selectively signals to histone deacetylase 4 during cardiomyocyte hypertrophy. J Clin Invest. 2006;116(7):1853-64.

36. Zhang T, Kohlhaas M, Backs J, Mishra S, Phillips W, Dybkova N, Chang S, Ling H, Bers DM, Maier LS, Olson EN, Brown JH. CaMKIIdelta isoforms differentially affect calcium handling but similarly regulate HDAC/MEF2 transcriptional responses. J Biol Chem. 2007;282(48):35078-87.

37. Li L, Stefan MI, Le Novère N. Calcium input frequency, duration and amplitude differentially modulate the relative activation of calcineurin and CaMKII. PLoS One. 2012;7(9):e43810.

38. De Koninck P, Schulman H. Sensitivity of CaM kinase II to the frequency of Ca^{2+} oscillations. Science. 1998;279(5348):227-30.

39. Stainier DY. Zebrafish genetics and vertebrate heart formation. Nat Rev Genet. 2001;2(1):39-48.

40. Verkerk AO, Remme CA. Zebrafish: a novel research tool for cardiac (patho)electrophysiology and ion channel disorders. Front Physiol. 201;3:255.

41. Stainier DY, Fouquet B, Chen JN, Warren KS, Weinstein BM, Meiler SE, Mohideen MA, Neuhauss SC, Solnica-Krezel L, Schier AF, Zwartkruis F, Stemple DL, Malicki J, Driever W, Fishman MC. Mutations affecting the formation and function of the cardiovascular system in the zebrafish embryo. Development. 1996;123:285-92.

42. Chen JN, Haffter P, Odenthal J, Vogelsang E, Brand M, van Eeden FJ, Furutani-Seiki M, Granato M, Hammerschmidt M, Heisenberg CP, Jiang YJ, Kane DA, Kelsh RN, Mullins MC, Nüsslein-Volhard C. Mutations affecting the cardiovascular system and other internal organs in zebrafish. Development. 1996;123:293-302.

43. Rottbauer W, Baker K, Wo ZG, Mohideen MA, Cantiello HF, Fishman MC. Growth and function of the embryonic heart depend upon the cardiac-specific L-type calcium channel alpha1 subunit. Dev Cell. 2001;1(2):265-75.

44. Arnaout R, Ferrer T, Huisken J, Spitzer K, Stainier DY, Tristani-Firouzi M, Chi NC. Zebrafish model for human long QT syndrome. Proc Natl Acad Sci U S A. 2007;104(27):11316-21.

45. Hassel D, Scholz EP, Trano N, Friedrich O, Just S, Meder B, Weiss DL, Zitron E, Marquart S, Vogel B, Karle CA, Seemann G, Fishman MC, Katus HA, Rottbauer W. Deficient zebrafish ether-à-go-go-related gene channel gating causes short-QT syndrome in zebrafish reggae mutants. Circulation. 2008;117(7):866-75.

46. Langenbacher AD, Dong Y, Shu X, Choi J, Nicoll DA, Goldhaber JI, Philipson KD, Chen JN. Mutation in sodium-calcium exchanger 1 (NCX1) causes cardiac fibrillation in zebrafish. Proc Natl Acad Sci U S A. 2005;102(49):17699-704.

47. Ebert AM, Hume GL, Warren KS, Cook NP, Burns CG, Mohideen MA, Siegal G, Yelon D, Fishman MC, Garrity DM. Calcium extrusion is critical for cardiac morphogenesis and rhythm in embryonic zebrafish hearts. Proc Natl Acad Sci U S A. 2005;102(49):17705-10.

CHAPTER 2

Mitochondrial Ca^{2+} uptake via voltage-dependent anion channel modulates cardiac rhythmicity

A. Abstract

Abnormal Ca^{2+} handling in cardiac muscle cells is associated with a wide range of human cardiac diseases, including heart failure and cardiac arrhythmias [1-2]. To better understand the regulatory network for cardiac Ca^{2+} handling, we conducted a chemical suppressor screen on zebrafish *tremblor* mutants, which manifest uncoordinated irregular cardiac contractions due to a Ca^{2+} extrusion defect [3-4]. We identified a synthetic compound named efsevin with potent activity to restore persistent, coordinated and rhythmic contractions in *tremblor* hearts. From affinity purification we detected a direct interaction between efsevin and the outer mitochondrial membrane voltage-dependent anion channel VDAC2. Overexpression of VDAC restores rhythmic cardiac contractions in *tremblor* embryos whereas attenuating VDAC activity blocks efsevin's rescue effects. Potentiating the Ca^{2+} transporting activity of VDAC proteins accelerates the transfer of Ca^{2+} from intracellular stores into mitochondria. Through this mechanism, efsevin restricts the temporal and spatial boundaries of Ca^{2+} sparks, inhibits the propagation of Ca^{2+} overload-induced erratic Ca^{2+} waves and restores rhythmic contractions in cardiomyocytes. The critical role for mitochondria in regulating cardiac rhythmicity was further supported by the finding that enhancing mitochondrial Ca^{2+} uptake by overexpression of MCU, a mitochondrial inner membrane Ca^{2+} transporter likewise restores cardiac contractions in

tremblor. Together these findings demonstrate a VDAC-dependent mechanism by which mitochondria modulate cardiac Ca^{2+} homeostasis and control cardiac contractions.

B. Introduction

Aberrant Ca^{2+} handling and Ca^{2+} overload, for example during cardiac ischemia/reperfusion, are well known causes of contractile dysfunction and many types of arrhythmias including early and delayed afterdepolarizations [1-2, 5]. To ensure proper cardiac rhythmicity and contractility, Ca^{2+} homoeostasis in the myocardium is tightly regulated at the temporal and spatial levels by a network involving multiple subcellular compartments [6]. While the primary mechanisms governing Ca^{2+} release and re-uptake by the sarcoplasmic reticulum (SR) to trigger contraction and relaxation of the myocardium are well-investigated [6], regulatory pathways and contributions of other cellular organelles such as mitochondria to cardiac Ca^{2+} handling require further study [7-8].

Zebrafish *tremblor* (*tre*) embryos offer an in vivo model for aberrant Ca^{2+} handling-induced cardiac dysfunction. Homozygous *tre* embryos lack functional NCX1h (also known as slc8a1a), a cardiac-specific isoform of Na^{+}/Ca^{2+} exchanger 1 responsible for Ca^{2+} extrusion, and manifest chaotic Ca^{2+} signals in the myocardium leading to uncoordinated contractions [3-4] (Figure 2-1a).

C. Results and Discussion

To further dissect the molecular network of Ca^{2+} handling in cardiomyocytes and to identify mechanisms of arrhythmogenesis and targets for treatment thereof, we performed a

small molecule suppressor screen on *tre* embryos. A dihydropyrrole carboxylic ester compound named efsevin (Figure 2-1b) was identified from this screen based on its ability to restore persistent, rhythmic and robust cardiac contractions in *tre* mutant embryos (Figure 2-1a, and Supplementary Movies 1-4) as well as NCX1h morpholino knockdown embryos (Supplementary Figure 2-1) in a dose-dependent manner (Figure 2-1c). Fractional shortening of efsevin treated *tre* mutant hearts was comparable to that of their wild type siblings (Figure 2-1d) and heart rate was restored to approximately 40% of that observed in controls (Figure 2-1e). Rhythmic electrical pulses accompanying each heartbeat were detected in wild type and efsevin treated *tre* embryos (Figure 2-1f). Furthermore, while only sporadic Ca^{2+} signals were detected in *tre* hearts, *in vivo* Ca^{2+} imaging showed that steady Ca^{2+} waves propagate through efsevin-treated *tre* hearts (Figure 2-1g, supplementary Movies 5-7), demonstrating that cardiomyocytes are coupled and that efsevin treatment restores Ca^{2+} transients in *tre*.

We next examined whether efsevin could suppress Ca^{2+} overload induced defects in mammalian cardiomyocytes. As the extracellular Ca^{2+} level increases, an increased number of Ca^{2+} waves was observed in isolated adult murine ventricular cardiomyocytes [9-10] (Figure 2-2a). Remarkably, efsevin treatment significantly reduced the number of propagating Ca^{2+} waves in a dosage-dependent manner (Figure 2a, b). In addition, increased extracellular Ca^{2+} level induces irregular contractions of mouse embryonic stem cell derived cardiomyocytes and efsevin treatment restores rhythmic contractions (Figure 2c). These findings indicate that efsevin affects a Ca^{2+} handling mechanism conserved between fish and mammals.

To identify the protein target of efsevin, we generated an N-Boc-protected 2-aminoethoxyethoxyethylamine linker-attached efsevine ($efsevine^{L}$) (Supplementary Figure 2-2).

This modified compound retained the activity of efsevin to restore cardiac contractions in *tre* embryos (Supplementary Figure 2-2b, d) and allowed us to create efsevin-conjugated agarose beads (efsevin^{LB}). A 32kD protein species was detected from zebrafish lysate due to its binding ability to efsevin^{LB} and OK-C125^{LB}, an active efsevin derivative conjugated to beads, but not to beads capped with ethanolamine alone or beads conjugated with an inactive efsevin analog (OK-C19^{LB}) (Figure 2-3a, Supplementary Figure 2-2). Furthermore, preincubation of zebrafish lysate with excess efsevin prevented the 32kD protein from binding to efsevin^{LB} or OK-C125^{LB} (Figure 2-3a). These findings demonstrate a specific interaction between efsevin and the 32 kD protein. Mass spectrometry followed by phylogenetic and immunostaining analyses revealed that this 32kD band represents a zebrafish homologue of the mitochondrial voltage-dependent anion channel 2 (VDAC2) (Figure 2-3b, c, Supplementary Figure 2-3, 2- 4, 2-5).

VDAC2 is expressed in the developing zebrafish heart, making it a good candidate for mediating efsevin's effect on cardiac Ca^{2+} handling (Figure 2-3d). To examine this possibility, we injected in vitro synthesized VDAC2 RNA into *tre* embryos and found that the majority of these embryos had coordinated cardiac contractions similar to those subjected to efsevin treatment (Figure 2-3d, Supplementary Figure 2-6, Movies 8-11). In addition, we generated *myl7:VDAC2* transgenic fish in which VDAC2 expression can be induced in the heart by tebufenozide (TBF) (Supplementary Figure 2-7). Knocking down NCX1h in *myl7:VDAC2* embryos results in chaotic cardiac movement similar to *tre*. Remarkably, upon TBF treatment, coordinated and rhythmic contractions were restored in *myl7:VDAC2 /NCX1h* morphant hearts (Figure 2-3e, Supplementary Movies 12,13). Together, these findings demonstrate the ability for VDAC2 to restore rhythmic cardiac contractions in ncx1h deficient embryos. Interestingly,

despite the association of VDACs with mechanisms of cell survival [11-13], efsevin-treated and VDAC2 overexpressing embryos do not manifest apparent morphological defects or excessive cell death (Supplementary Figure 2-8).

VDAC1 shares a high degree of homology with VDAC2 and has been proposed to have a comparable channel activity [14-15]. In zebrafish, VDAC1 is expressed in the embryonic heart and the hearts of those *tre* embryos that received synthetic VDAC1 RNA established rhythmic contractions, indicating that VDAC1 and VDAC2 have a redundant role in embryonic zebrafish hearts (Figure 2-3f,g).

We next asked whether efsevin's effect in *tre* hearts is primarily mediated by VDAC proteins. As shown in Fig. 3, knocking down VDAC1 or VDAC2 (Supplementary Movies 14-16) significantly reduces efsevin's ability to restore cardiac contraction in *tre* embryos, and knockdown of both genes simultaneously further blocked efsevin's effect (Figure 2-3h). In addition, we generated VDAC2 null embryos by Zinc Finger Nuclease targeting (Supplementary Figure 2-9). Similar to that observed in morpholino knockdown embryos, efsevin's effect is attenuated in homozygous VDAC2$^{zfn/zfn}$; NCX1MO embryos and is further blocked in NCX1/VDAC1/VDAC2 triple deficient embryos (Figure 2-3i). These findings indicate that VDAC is the major, if not the only, mediator for efsevin's effect on *ncx1h* deficient hearts.

VDAC is an abundant channel located on the outer mitochondrial membrane serving as a primary pathway for the passage of metabolites and ions including Ca^{2+} [16-18]. We examined whether efsevin would modulate mitochondrial Ca^{2+} uptake via VDAC proteins. Since VDAC1 and VDAC2 have redundant roles in mediating efsevin's activity, we focused this line of study on VDAC2. We transfected HeLa cells with VDAC2 and noted increased mitochondrial Ca^{2+}

uptake after perfusion with high Ca^{2+}. In addition, treatment with efsevin on permeabilized VDAC2 transfected cells further enhanced mitochondrial Ca^{2+} uptake (Figure 2-4a), demonstrating that efsevin modulates Ca^{2+} handling by potentiating the mitochondrial Ca^{2+} transporting activity of VDAC2. In cardiomyocytes, mitochondria are located in close proximity to Ca^{2+} release sites of the SR [19-20] and an extensive crosstalk between the two organelles exists [7-8, 21]. In permeabilized VDAC1/VDAC3 double knockout (V1/V3DKO) MEFs [14], treatment with efsevin increased the amount of Ca^{2+} transferred into mitochondria during IP_3-induced Ca^{2+} release (Figure 2-4b). Also, in intact V1/V3 DKO MEFs, we noted that efsevin accelerated the transfer of Ca^{2+} released from intracellular store into mitochondria during stimulation by an IP_3-linked agonist (Figure 2-4c). In murine ventricular cardiomyocytes, efsevin treatment does not change the amplitude or activation kinetics of paced Ca^{2+} transients, but induced a faster inactivation kinetics (Figure 2-2d,e and Supplementary Table 2-1). Similarly, efsevin treatment did not alter the frequency, amplitude and Ca^{2+} release flux of spontaneous Ca^{2+} sparks, unitary SR Ca^{2+} release events [22], but accelerated the decay phase resulting in a shorter duration and narrower width of individual sparks (Figure 2-2f,g and Supplementary Table 2-2). Taken together, these findings indicate that efsevin does not affect SR Ca^{2+} load or RyR Ca^{2+} release, but increases Ca^{2+} removal from the cytosol and raise the possibility that efsevin modulates the spatial and temporal pattern of cytosolic Ca^{2+} by influencing mitochondrial Ca^{2+} uptake via VDAC proteins.

We reasoned that if enhancing mitochondrial Ca^{2+} uptake indeed has a suppressive effect on aberrant Ca^{2+} handling-associated arrhythmic cardiac contractions, activating other mitochondrial Ca^{2+} uptake mechanisms should also restore coordinated contractions in *tre*

mutants. To test this model, we cloned zebrafish MCU, the inner mitochondrial membrane Ca^{2+} transporter [24-25]. MCU is expressed in the developing zebrafish heart (Figure 2-3j). Overexpression of MCU restored coordinated contractions in *tre* mutants, just like VDAC2 did (Figire 2-3k), supporting the hypothesis that mitochondria regulate cardiac rhythmicity by modulating Ca^{2+} handling. *tre* embryos injected with suboptimal concentration of MCU or VDAC2 had fibrillating hearts. However, embryos receiving both VDAC2 and MCU at the suboptimal concentration manifested coordinated contractions (Figure 2-3l), demonstrating a synergistic effect of these genes. Furthermore, overexpression of MCU fails to suppress the *tre* phenotype in the absence of VDAC2 activity and VDAC2 cannot restore coordinated contractions in *tre* without functional MCU (Figure 2-3k,m), demonstrating that both outer and inner membrane transporters are required for mitochondrial Ca^{2+} uptake. These observations indicate that mitochondrial Ca^{2+} uptake mechanisms on the OMM and IMM act cooperatively and challenge the common assumption that the OMM is freely permeable for ions, such as Ca^{2+}.

Together, our study provides genetic and physiologic evidence supporting a critical role for mitochondria in regulating cardiac rhythmicity and VDAC proteins as a modulator of Ca^{2+} handling in cardiomyocytes. Potentiating the Ca^{2+} transporting activity of VDAC restores rhythmic cardiac contractions in a zebrafish model of aberrant Ca^{2+} handling and blocks Ca^{2+}-overload induced erratic Ca^{2+} waves and irregular contractions in murine cardiomyocytes. These findings, together with the observation that the OMM and IMM are in close proximity at the contacts sites of the OMM with the SR [26], suggest an attractive model in which mitochondria facilitate an efficient clearance mechanism in the Ca^{2+} microdomain around Ca^{2+} release sites. In this model, VDAC-dependent Ca^{2+} uptake plays a modulatory role for local Ca^{2+} signals, which

sets up a spatial and temporal boundary for Ca^{2+} sparks in the Ca^{2+} microdomain and limits cytosolic diffusion of Ca^{2+} without influencing global Ca^{2+} signals. We propose that through this mechanism the propensity for propagating Ca^{2+} waves is reduced in efsevin treated cardiomyocytes, despite similar spark frequency in treated and untreated cells.

The success of our chemical suppressor screen on a zebrafish cardiac disease model offers a new paradigm for the dissection of critical gene pathways and the discovery of new therapeutic approaches. Our finding that efsevin potentiates the Ca^{2+} transporting activity of VDAC proteins and thereby allows cardiomyocytes to tolerate a higher frequency of Ca^{2+} sparks under aberrant Ca^{2+} homeostasis indicates a potential for efsevin as a pharmacological tool to prevent the propagation of arrhythmogenic Ca^{2+} waves and suggests an intriguing possibility that VDAC serves as a therapeutic target for the treatment of cardiac arrhythmias that has a root in aberrant Ca^{2+} handling.

D. Materials and Mehods

Zebrafish husbandry and transgenic lines

Zebrafish of the mutant line *tremblor* (*tre*^{tc318}) were maintained and bred as described previously [3]. Transgenic lines, *myl7:VDAC2* [27] and *myl7:gCaMP4.1* [28] were created using the Tol2kit [29]. The VDAC2$^{zfn/+}$ were created using the zinc finger array OZ523 and OZ524 generated by the zebrafish Zinc Finger Consortium [30], supported by NIH R01 GM088040.

Molecular Biology

Full length VDAC1 and VDAC2 cDNA were purchased from Open Biosystems and were cloned into pCS2+ or pCS2+3XFLAG. Full length cDNA fragments of zebrafish MCU (Accession number: JX424822) were amplified from 2 dpf embryos and cloned into pCS2+. For mRNA synthesis, plasmids were linearized and mRNA synthesized using the SP6 mMESSAGE mMachine kit according to the manufacturers manual (Ambion).

Zebrafish injections

mRNA and morpholino antisense oligos (VDAC1: 5'-ATATGTGGGAGGAACAGCCATAGTC-3'), VDAC2: 5'-GGGAACGG CCATTTTATCTGTTAAA-3'; MCU: ATCTACACACTTTCGCAGCCATCTC-3') (Genetools) were injected into one-cell stage embryos collected from crosses of *tre*^{tc318} heterozygotes. Cardiac performance was analysed by visual inspection on 1 dpf. The *tre* mutant embryos were identified either by observing the fibrillation phenotype at 2-3 dpf or by genotyping as previously described [3].

Chemical Screen

A synthetic chemical library containing 168 compounds [31-32] and 300 chemicals from Biomol International LP, consisting of 72 ion channel inhibitors (Cat No. 2805), 84 kinase/phosphatase inhibitors (Cat No. 2831), 84 orphan ligands (Cat No. 2825), and 60 endocannabinoids (Cat No. 2801) were screened for their ability to partially or completely restore persistent heartbeat in tre embryos. 12 embryos collected from crosses of *tre*^{tc318}

heterozygotes were raised in the presence of individual compounds at a concentration of 10μM from 4 hpf [33]. Cardiac function was analyzed by visual inspection at 1 and 2 dpf. The hearts of *tre*^{tc318} embryos manifest a chaotic movement resembling cardiac fibrillation with intermittent contractions in rare occasion [3-4]. Compounds that elicit persistent coordinated cardiac contractions were validated on large number of *tre* mutant embryos and NCX1h morphants (>500 embryos).

Zebrafish cardiac imaging

Movies of GFP-labelled Tg(*myl7:GFP*) hearts were taken at 30 frames per second. Line-scan analysis was performed along a line through the atria of these hearts [34]. Fraction of shortening was deduced from the ratio of diastolic and systolic width and heart rate was determined by beats per minute.

Zebrafish optical mapping

36 hpf *myl7:gCaMP4.1* embryos were imaged with Zeiss Axioplan2 equipped with Axiocam camera (Zeiss) at a frame rate of 30ms/frame. Electromechanical isolation was achieved by tnnt2MO [35]. The fluorescence intensity of each pixel in a 2D map was normalized and heatmaps were generated with a custom-written C Sharp program based on the method previously described [36]. Isochronal lines at 33 ms intervals were obtained by identifying the maximal spatial gradient for a given time point.

Mouse embryonic stem cells

The mouse ESC E14Tg2a were cultured and differentiated as previously described [37-38]. At day 10 of differentiation, beating EBs were exposed to external solution containing 10mM $CaCl_2$ for 10 minutes before DMSO or efsevin (10 μM) treatment. Images of beating EBs were acquired at a rate of 30 frames/sand analyzed by motion-detection software.

Ca^{2+} imaging

Murine ventricular cardiomyocytes were isolated as previously described [39]. Cells were loaded with 5 μM fluo-4 AM in external solution containing (in mM): 138.2 NaCl, 4.6 KCl, 1.2 MgCl, 15 glucose, 20 HEPES for 1 hr [23] and imaged on a Zeiss PASCAL confocal microscope in external solution supplemented with 2, 5 or 10 mM $CaCl_2$. For the recording of Ca^{2+} sparks and transients, the external solution contained 2 mM $CaCl_2$. For Ca^{2+} transients, cells were field stimulated at 0.5Hz with a 5ms pulse at a voltage of 20% above contraction threshold. For all measurements, efsevin was added 2 hours prior to the actual experiment. Images were recorded on a Zeiss LSM 5 Pascal confocal microscope. Data analysis was carried out using the Zeiss LSM Image Browser and ImageJ with the SparkMaster plugin [40]. Cells were visually inspected prior to and after each recording. Only those recordings from healthy looking cells with distinct borders, uniform striations and no membrane blebs or granularity were included in the analysis.

Biochemistry

For pull down assays mono-N-Boc protected 2,2'-(ethylenedioxy)bis(ethylamine) was attached to the carboxylic ester of efsevin and its derivatives through the amide bond. After removal of the Boc group using TFA, the primary amine was coupled to the carboxylic acid of Affi-Gel 10 Gel (Biorad). Two-day-old zebrafish embryos were deyolked by centrifugation before being lysed with Rubinfeld's lysis buffer [41]. The lysate was precleaned by incubation with Affi-Gel 10 Gel to eliminate non-specific binding. Precleaned lysate was incubated with affinity beads overnight. Proteins were eluted from the affinity beads and separated on SDS-PAGE. Protein bands of interest were excised. Gel plugs were dehydrated in acetonitrile (ACN) and dried completely in a Speedvac. Samples were reduced and alkylated with 10 mM dithiotreitol and 10mM TCEP solution in 50 mM NH_4HCO_3 (30 min at 56°C) and 100 mM iodoacetamide (45 min in dark), respectively. Gel plugs were washed with 50 mM NH_4HCO_3, dehydrated with ACN, and dried down in a Speedvac. Gel pieces were then swollen in digestion buffer containing 50mM NH_4HCO_3, and 20.0 ng/μL of chymotrypsin (25°C, overnight). Peptides were extracted with 0.1%TFA in 50%ACN solution, dried down and resuspended in LC buffer A (0.1% formic acid, 2% ACN).

Mass spectrometry analyses and database searching

Extracted peptides were analyzed by nano-flow LC/MS/MS on a Thermo Orbitrap with dedicated Eksigent nanopump using a reversed phase column (New Objective). The flow rate was 200 nL/min for separation: mobile phase A contained 0.1% formic acid, 2% ACN in water, and mobile phase B contained 0.1% formic acid, 20% water in ACN. The gradient used for

analyses was linear from 5% B to 50% B over 60 min, then to 95% B over 15 min, and finally keeping constant 95% B for 10 min. Spectra were acquired in data-dependent mode with dynamic exclusion where the instrument selects the top six most abundant ions in the parent spectra for fragmentation. Data were searched against the Danio rerio IPI database v3.45 using the SEQUEST algorithm in the BioWorks software program version 3.3.1 SP1. All spectra used for identification had deltaCN>0.1 and met the following Xcorr criteria: >2 (+1), >3 (+2), >4 (+3), and >5 (+4). Searches required full cleavage with the enzyme, $\leq$4 missed cleavages and were performed with the differential modifications of carbamidomethylation on cysteine and methionine oxidation.

Phylogenetic Analysis

Alignments of VDAC amino acid sequences were generated using multalign (http://multalin.toulouse.inra.fr/multalin). Phylogenetic trees and bootstrap values were calculated using TreeTop (http://www.genebee.msu.su/services/phtree_reduced.html).

In situ hybridisation

In situ hybridization was performed as previously described [42]. DIG-labeled RNA probe was synthesized using T7 RNA Polymerase (Promega) and the DIG RNA labeling kit (Roche).

Immunostaining

HeLa cells were transfected with a C-terminally flag-tagged zebrafish VDAC1 or VDAC2 in plasmid pCS2+ using Lipofectamine™ 2000 (Invitrogen). After staining with MitoTracker® Orange (Invitrogen) cells were fixed in 3.7% formaldehyde and permeabilized with acetone. Immunostaining was performed using primary antibody ANTI-FLAG® M2 (Sigma Aldrich) at 1:100 and secondary antibody Anti-Mouse IgG1-FITC (Southern Biotechnology Associates) at 1:200. Cells were mounted and counterstained using Vectashield® Hard Set™ with DAPI (Vector Laboratories).

Statistics

All values are expressed as mean ± SEM. Significance values are calculated by unpaired student's t-test unless noted otherwise.

Mitochondria Ca^{2+} uptake assay in HeLa cells

HeLa cells were transfected with zebrafish VDAC2 using Lipofectamine™ 2000 (Invitrogen). 36 hrs following transfection, cells were loaded with 5 µM Rhod2-AM (Invitrogen) for 1 hour at 15°C followed by a 30 min de-esterification period at 37°C. Subsequently, cells were permeabilized with 100 µM digitonin for 1 min at room temperature. Fluorescence changes in Rhod2 (excitation 506 nm, emission 531 nm) immediately after perfusion with Ca^{2+} (final free Ca^{2+} concentration of 10 µM) were monitored in internal buffer (in mM): 5 K-EGTA, 20 HEPES, 100 K-aspartate, 40 KCl, 1 $MgCl_2$, 2 maleic acid, 2 glutamic acid, 5 pyruvic acid, 0.5 KH_2PO_4, 5

mM MgATP, pH adjusted to 7.2 with Trizma base) using a FLUOSTAR plate reader (BMG Labtech).

Mitochondria Ca^{2+} uptake assay in VDAC1/VDAC3 double knockout (V1/V3 DKO) MEFs

V1/V3 DKO MEFs were cultured as previously described [12]. Efsevin-treated (15 μM for 30 min) or mock-treated MEFs were used for measurements of $[Ca^{2+}]_c$ in suspensions of permeabilized cells or imaging of $[Ca^{2+}]_m$ simultaneously with $[Ca^{2+}]_c$ in intact single cells. Permeabilization of the plasma membrane was performed by digitonin (40 μg/ml). Changes in $[Ca^{2+}]$ in the cytoplasmic buffer upon IP_3 (7.5 μM) addition in the presence or absence of ruthenium red (3 μM) was measured by fura2 in a fluorometer [43-44]. To avoid endoplasmic reticulum Ca^{2+} uptake 2 μM thapsigargin was added before IP_3. For imaging of $[Ca^{2+}]_m$ and $[Ca^{2+}]_c$, MEFs were co-transfected with plasmids encoding polycistronic zebrafish VDAC2 with mCherry and mitochondria-targeted inverse pericam for 40 hours. Cells were sorted to enrich the transfected cells and attached to glass coverslips. In the final 10 min, of the efsevin or mock-treatment, the cells were also loaded with fura2AM (2.5 μM) and subsequently transferred to the microscope stage. Stimulation with 1 μM ATP was carried out in a norminally Ca^{2+} free buffer. Changes in $[Ca^{2+}]_c$ and $[Ca^{2+}]_m$ were imaged using fura2 (ratio of ex: 340nm to 380nm) and mitochondria-targeted inverse pericam (ex: 495nm), respectively [45].

Whole-mount Acridine orange staining and TUNEL staining

Two-day-old zebrafish embryos were incubated with 5 μg/ml Acridine orange in embryo medium for 15 min at room temperature. TUNEL staining was performed using ApopTag kit

(Millipore) as previously described [46]. Embryos were imaged using fluorescence microscopy (Zeiss Axioplan2).

Figure 2-1. Efsevin restores rhythmic cardiac contractions in zebrafish *tremblor* embryos. **a**, Line scans across the atria of GFP-labelled *Tg*(*myl7:GFP*) embryonic hearts at 48 hpf. Rhythmically alternating systoles and diastoles are recorded from vehicle- (left) or efsevin-treated wild type (center left) and efsevin-treated *tre* (right) embryos, while only sporadic unsynchronized contractions are recorded from vehicle-treated *tre* embryos (center right). **b**, Structure of efsevin. **c**, Dose-response curve for efsevin. *tremblor* embryos were treated with increasing concentrations of efsevin from 24hpf and cardiac contractions were analyzed at 48hpf. **d**, Atrial fractional shortening (AFS) deduced from the line-scan traces. Similar AFS values were observed in vehicle- and efsevin-treated wild-type embryos (37±1 %, n=11 vs. 35±2 %, n=11). While cardiac contraction was not observed in *tre*, treatment with efsevin induced robust contractions (AFS=33±2 %, n=15) in *tre*. **e**, While efsevin restored a heart rate of 46±2 beats per minute (bpm) in *tre* embryos, same treatment does not affect the heart rate in wild type embryos (126±2 bpm in vehicle-treated embryos vs. 123±3 bpm in efsevin-treated wild-type embryos). ***, $p<0.001$ by one-way ANOVA. **f**, *In vivo* optical maps of Ca^{2+} activation represented by isochronal lines every 33 ms recorded from 36 hpf wild type (left), *tre* (center) and efsevin-treated *tre* embryos.

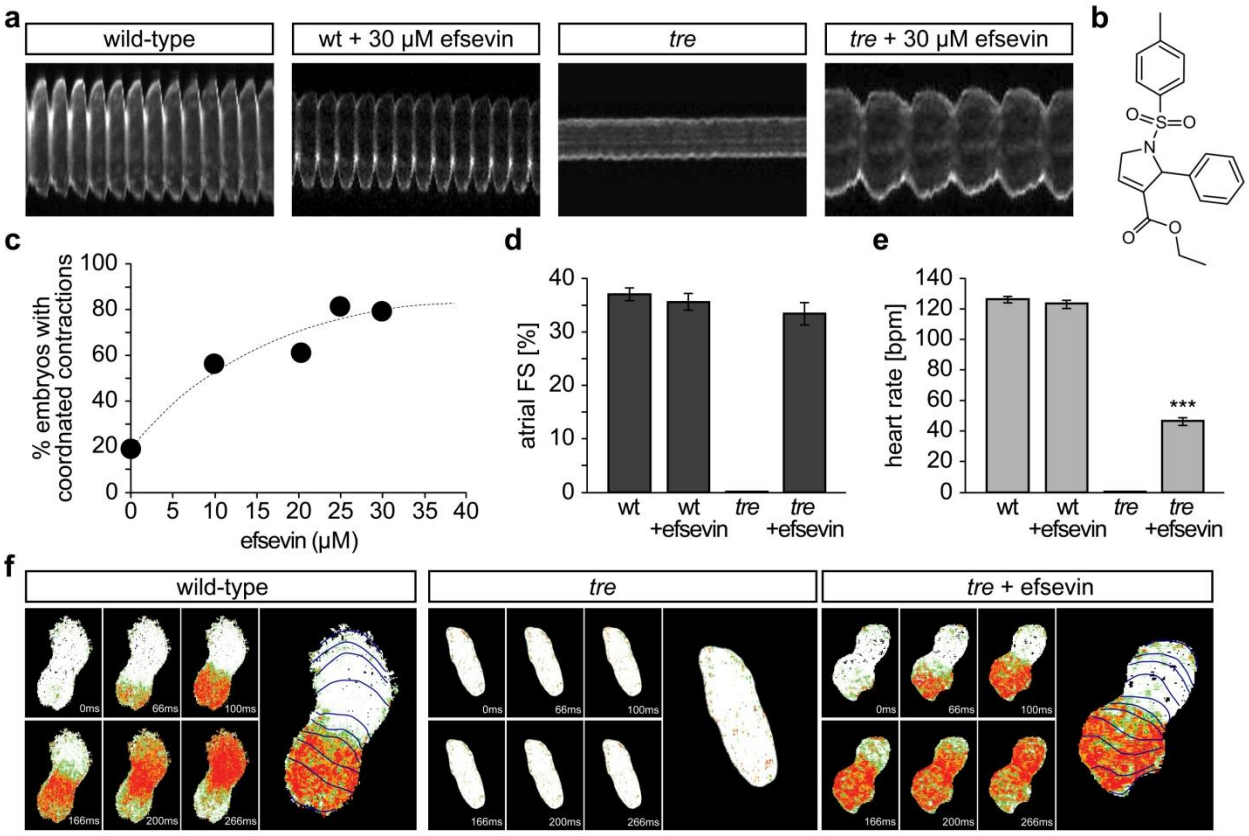
a
wild-type
wt + 30 µM efsevin
tre
tre + 30 µM efsevin
b
c
% embryos with coordnated contractions
efsevin (µM)
d
atrial FS [%]
wt
wt +efsevin
tre
tre +efsevin
e
heart rate [bpm]
***
f
wild-type
tre
tre + efsevin
0ms
66ms
100ms
166ms
200ms
266ms

Figure 2-2. Efsevin reduces arrhythmogenic events in murine cardiomyocytes.

a, Increasing concentrations of extracellular Ca^{2+} induced a higher frequency of spontaneous propagating Ca^{2+} waves in isolated adult murine ventricular cardiomyocytes. Addition of efsevin to the buffer reduced Ca^{2+} waves in a dose-dependent manner. **b,** Quantitative analysis of spontaneous Ca^{2+} waves spanning more than half of the entire cell. In vehicle-treated cardiomyocytes we observed 2.0±0.4 (n=41), 8.9±1.2 (n=42), and 11.5±1.2 (n=50) Ca^{2+} waves per minute for extracellular Ca^{2+} concentrations of 2, 5, and 10 mM, respectively (black circles). Addition of 1μM efsevin reduced Ca^{2+} waves to approximately half, specifically 0.9±0.3 (n=38), 5.1±1.1 (n=24), and 7.6±1.0 (n=61) Ca^{2+} waves per minute for 2, 5, and 10 mM Ca^{2+}_{ext} respectively (dark grey triangles). Increasing the concentration of efsevin to 10μM further reduced the number of spontaneous Ca^{2+} waves to 0.7±0.3 (n=27), 3.2±0.7 (n=36), and 4.0±0.9 (n=29) Ca^{2+} waves per minute for 2, 5, and 10 mM Ca^{2+}_{ext} respectively (light grey triangles) and 25μM efsevin almost entirely blocked the formation of Ca^{2+} waves (1.0±0.4 (n=25), 1.0±0.3 (n=23), and 1.2±0.4 (n=29) Ca^{2+} waves per minute for 2, 5, and 10 mM Ca^{2+}_{ext} respectively, white triangles). *, $p<0.05$; **, $p<0.01$; ***, $p<0.001$. **c**, (Upper left) Representative plot of mouse EB contraction after 10 days of differentiation showing regular beat-to-beat interval as 0.94±0.02s. (Upper right) Increased Ca^{2+} concentration induced an irregular contraction pattern (1.32±0.38s). (Lower lef) Efsevin treatment restores regular cardiac contractions (0.99±0.08s, right). (Lower righ) Quantitative analysis of beat-to-beat interval distributions. **d,** Confocal linescans and deducted intensity plots from vehicle- and 1 μM efsevin treated ventricular cardiomyocytes loaded with fluo-4 and paced at 0.5Hz. g, Normalized quantification of Ca^{2+} transient parameters reveals no difference for transient amplitude (efsevin-treated at 98.6±4.5%

of vehicle-treated) and time to peak (95±3.9%), but a significant decrease for the rate of inactivation (82.8±4% of vehicle- for efsevin-treated). **e**, Quantification of Ca^{2+} transient parameters reveals no difference for transient amplitude (3.1±0.1 vs 3.1±0.1 for vehicle-treated and efsevin-treated respectively) and time to peak (35.9±1.9ms vs 34.1±1.4ms), but a significant decrease for the rate of inactivation ($\tau_{inactivation}$=209.9±9.5ms vs 173.7±8.5ms). **f**, Three-dimensional representation of typical Ca^{2+} sparks recorded under 2 mM Ca^{2+}_{ext} from murine ventricular cardiomyocytes without (left) and with (right) treatment with 1µM efsevin. **g**, No differences between vehicle- and efsevin-treated cardiomyoctes were observed for spark frequency (101.1±7.7% for efsevin- compared to vehicle-treated), maximum spark amplitude (101.6±2.5%) and Ca^{2+} release flux (98.7±2.8%). In contrast, the decay phase of the single spark was significantly faster in efsevin treated cells (82.5±2.1% of vehicle-treated). Consequently, total duration of the spark was reduced to 85.7±2% and the total width was reduced to 89.5±1.4% of vehicle-treated cells.

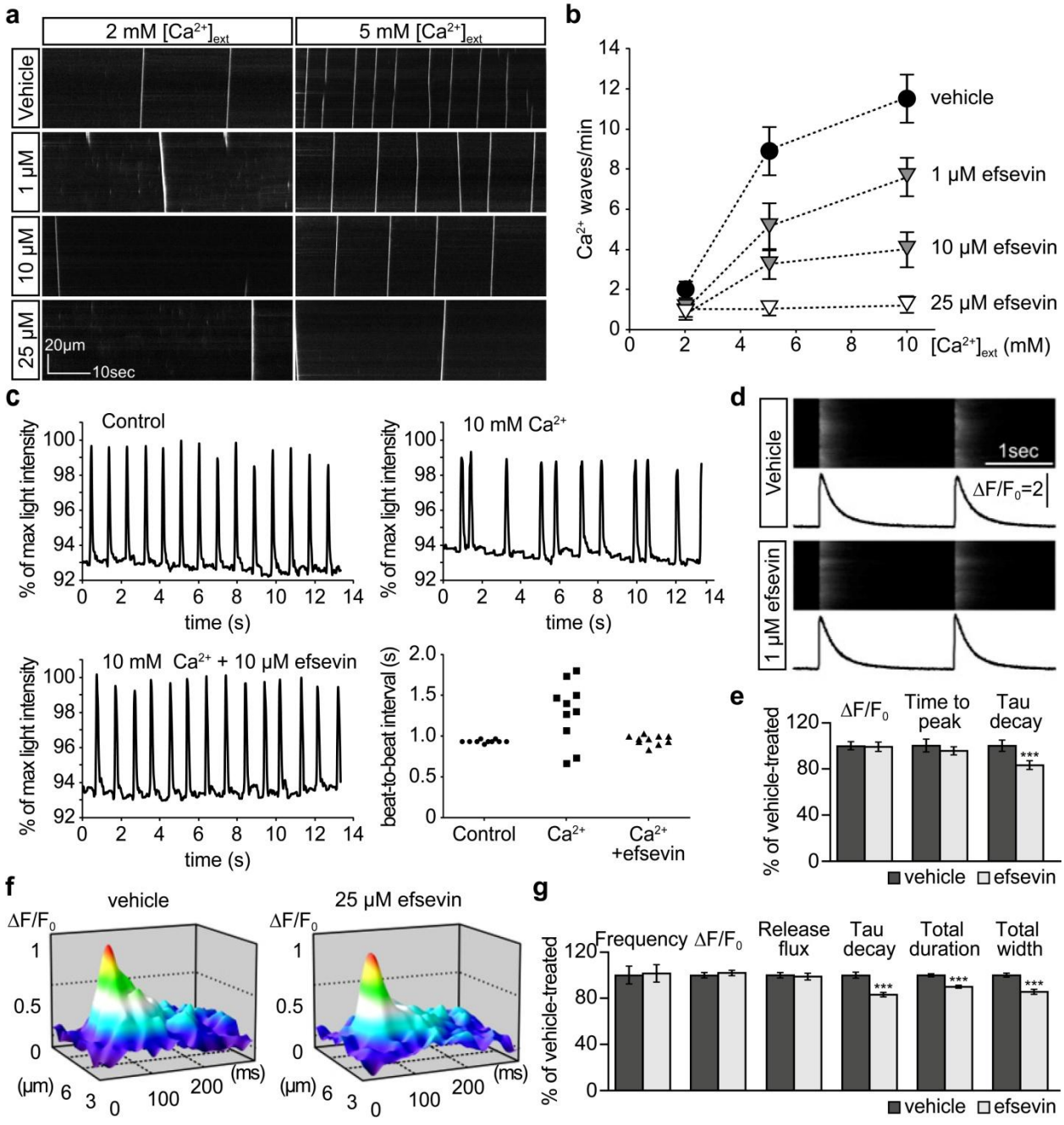
a
2 mM [Ca2+]ext
5 mM [Ca2+]ext
Vehicle
1 μM
10 μM
25 μM
20μm
10sec
b
Ca2+ waves/min
vehicle
1 μM efsevin
10 μM efsevin
25 μM efsevin
[Ca2+]ext (mM)
c
Control
10 mM Ca2+
10 mM Ca2+ + 10 μM efsevin
% of max light intensity
time (s)
beat-to-beat interval (s)
Control
Ca2+
Ca2+ +efsevin
d
Vehicle
1 μM efsevin
1sec
ΔF/F0=2
e
ΔF/F0
Time to peak
Tau decay
% of vehicle-treated
vehicle
efsevin
f
vehicle
25 μM efsevin
ΔF/F0
(μm)
(ms)
g
Frequency ΔF/F0
Release flux
Tau decay
Total duration
Total width
% of vehicle-treated
vehicle
efsevin

Figure 2-3. Mitochondria regulate cardiac rhythmicity through a VDAC dependent mechanism.

a, Affinity agarose beads covalently linked with efsevin (efsevin^{LB}) pulled down 2 protein species from zebrafish embryonic lysate, whereof one, the 32 kD upper band, was sensitive to competition with a 100 fold excess free efsevin^{L} (left gel). The 32 kD band was not detected in proteins eluted from beads capped with ethanolamine alone (beads^{C}) or beads linked to an inactive derivative of efsevin, OK-C19^{LB}, but was detected in samples eluted from beads attached with a biologically active derivative, OK-C125^{LB} (right gel). Also for OK-C125^{LB} pull-down the 32kD band was again sensitive to competition with free efsevin. Arrowheads point to the 32kD bands. **b**, In situ hybridization analysis revealed that both VDAC1 and VDAC2 are expressed in embryonic hearts at 36 hpf (upper image) and 48 hpf (lower image). Arrowheads point to the heart. **c**, Injection of 25 pg in-vitro synthesized VDAC1 mRNA restored rhythmic cardiac contractions in 53.0+-10.2% of embryos (n= 126) compared to 21.8+-5.1% in uninjected siblings (n=23/111) on day 1. Similarly, injection of 25 pg in-vitro synthesized VDAC2 mRNA restored cardiac contractions in 52.9±12.1% of one-day-old *tre* embryos (n=78), Error bars represent s.e.m.; ***p<0.001; More than 150 embryos were used in each experiment. **d**, ~20% of *myl7:VDAC2EcR;NCX1hMO* embryos have hearts displaying chaotic movements (n=116), whereas 52.3±2.4% of these embryos have rhythmic contractions after TBF induction of VDAC2 (n=154). **e**, On average, 71.2±8.8% efsevin treated embryos have coordinated cardiac contractions (n=131). Morpholino antisense oligonucleotide knock-down of VDAC2 (MO^{VDAC2}) or VDAC1 (MO^{VDAC1}) attenuates the ability of efsevin to suppress cardiac fibrillation in *tre* embryos (45.3±7.4% and 46.9±10.7% embryos with coordinated contractions, n=94 and 114,

respectively). Knocking down VDAC1/2 simultaneously further suppresses efsevin's effect (30.3±6.3%, n=75). **f**, Efsevin treatment restores coordinated cardiac contractions in 76.2±8.7% NCX1MO embryos, only 54.1±3.6% VDAC2$^{zfn/zfn}$;NCX1MO embryos and 35.7±7.1% VDAC2$^{zfn/zfn}$;VDAC1MO;NCX1MO embryos have coordinated contractions (n=250). Error bars represent s.e.m.; ***p<0.001; More than 150 embryos were used in each experiment. **g**, In situ hybridization shows that MCU is highly expressed in the developing heart (arrowheads) at 36 hpf (upper image) and 48 hpf (lower image). **h**, The ability of VDAC2 to restore rhythmic contractions in *tre* embryos (48.5±3.5% embryos, n=111) is significantly attenuated when MCU is knocked down by antisense oligonucleotide (MO^{MCU}) (25.6±2.4% embryos, n=115). **i**, Overexpression of MCU is sufficient to restore coordinated cardiac contractions in *tre* embryos (47.1±1.6% embryos as opposed to 18.3±5.3% of uninjected siblings) while this effect is significantly attenuated when co-injected with morpholino antisense oligonucleotide targeted to VDAC2 (27.1±1.9% embryos, n=135). **j**, Suboptimal overexpression of MCU (MCU^{S}) and VDAC2 (VDAC2^{S}) in combination is able to suppress cardiac fibrillation in *tre* embryos (42.9±2.6% embryos, n=129). Error bars represent s.d.; ***p<0.001; At least 110 *tre* mutant embryos were analyzed in each experiment.

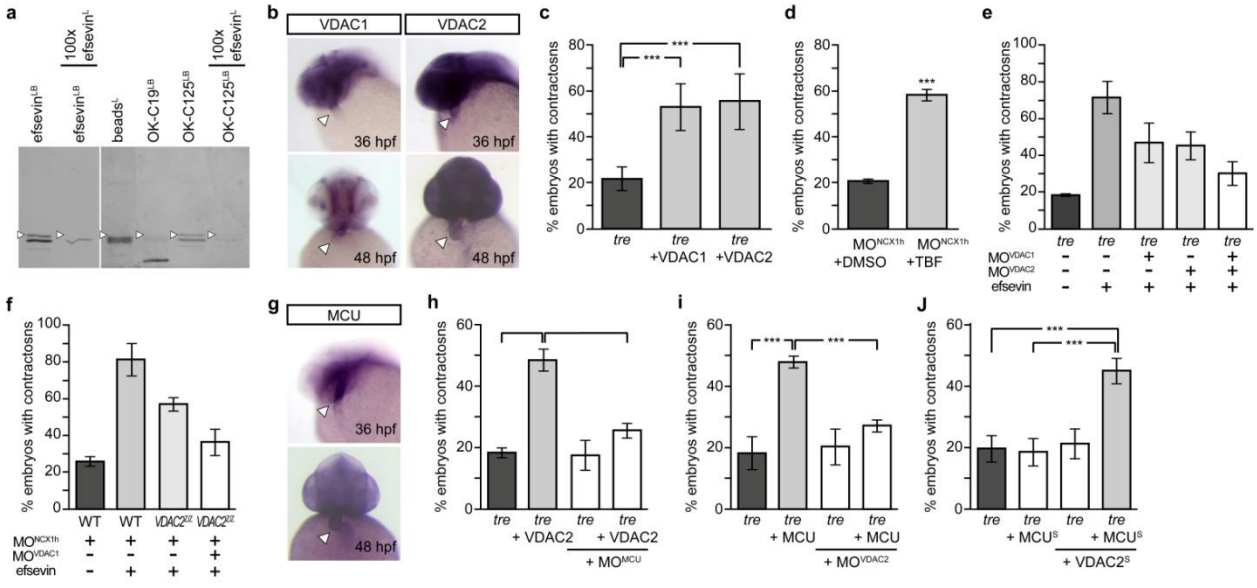
a
efsevin^LB
100x efsevin^L
efsevin^LB
beads^L
OK-C19^LB
OK-C125^LB
100x efsevin^L
OK-C125^LB
b
VDAC1
VDAC2
36 hpf
36 hpf
48 hpf
48 hpf
c
% embryos with contractosns
***
***
tre
tre +VDAC1
tre +VDAC2
d
% embryos with contractosns
***
MO^NCX1h +DMSO
MO^NCX1h +TBF
e
% embryos with contractosns
tre
MO^VDAC1
MO^VDAC2
efsevin
f
% embryos with contractosns
WT
WT
VDAC2^ZZ
VDAC2^ZZ
MO^NCX1h
MO^VDAC1
efsevin
g
MCU
36 hpf
48 hpf
h
% embryos with contractosns
tre
+ VDAC2
+ VDAC2
+ MO^MCU
i
% embryos with contractosns
***
***
+ MCU
+ MCU
+ MO^VDAC2
J
% embryos with contractosns
***
***
+ MCU^S
+ MCU^S
+ VDAC2^S

Figure 2-4. Mitochondrial Ca^{2+} uptake.

a, Representative traces of mitochondrial matrix $[Ca^{2+}]$ ($[Ca^{2+}]_m$) in digitonin-permeabilized HeLa cells detected by Rhod2, a Ca^{2+} sensitive dye compartmentalized in mitochondria. Arrows denote superfusion with 10 μM Ca^{2+}. Mitochondrial Ca^{2+} uptake was assessed when VDAC2 was overexpressed (100 or 200 ng/well; left), cells were treated with 1μM efsevin (middle) and combination of both at low doses (25 ng/well VDAC2 and 0.1 μM efsevin; right). Control-traces with ruthenium red (RuRed) show mitochondrial specificity of the signal. **b**, Representative traces of cytosolic $[Ca^{2+}]$ ($[Ca^{2+}]_c$) changes upon the application of 7.5 μM IP_3 in the presence (+) or absence (-) of RuRed in suspensions of permeabilized V1/V3 DKO MEFs. To avoid endoplasmic reticulum Ca^{2+} uptake, 2μM thapsigargin (Tg) was added before IP_3. Mitochondrial Ca^{2+} uptake was assessed by the difference of the – and + RuRed conditions normalized to the total release (n=4; mean±SE). **c**, V1/V3 DKO MEFs overexpressing zebrasfish VDAC2 (polysyctronic with mCherry), were stimulated with 1 μM ATP in a nominally Ca^{2+} free buffer. Changes in $[Ca^{2+}]_c$ and $[Ca^{2+}]_m$ were imaged using fura2 (ratio of 340 nm to 380 nm) and mitochondria-targeted inverse pericam, respectively. Black and gray traces show the $[Ca^{2+}]_c$ (in nM) and $[Ca^{2+}]_m$ (F_0/F mtpericam) time courses, respectively in two representative single cells in the presence or absence of efsevin. Bar charts: Cell population averages for the peak $[Ca^{2+}]_c$ (left), the corresponding $[Ca^{2+}]_m$ (middle), and the coupling time (time interval between the maximal $[Ca^{2+}]_c$ and $[Ca^{2+}]_m$ responses) in the presence (black, n=24) or absence (gray, n=28) of efsevin.

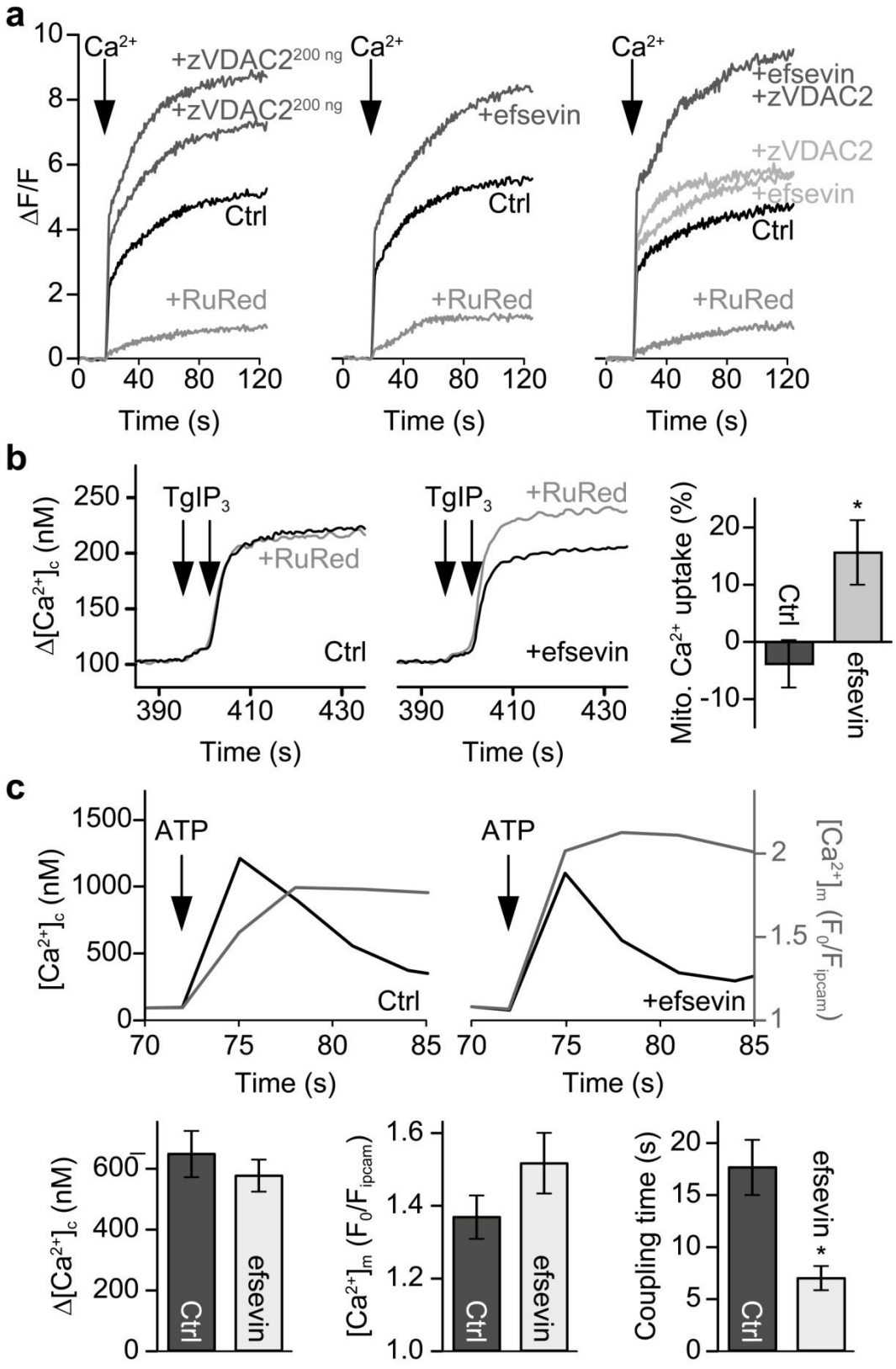
a
Ca2+
+zVDAC2200 ng
+zVDAC2200 ng
Ctrl
+RuRed
ΔF/F
Time (s)
Ca2+
+efsevin
Ctrl
+RuRed
Time (s)
Ca2+
+efsevin
+zVDAC2
+zVDAC2
+efsevin
Ctrl
+RuRed
Time (s)
b
TgIP3
+RuRed
Ctrl
Δ[Ca2+]c (nM)
TgIP3
+RuRed
+efsevin
Time (s)
Time (s)
Mito. Ca2+ uptake (%)
Ctrl
efsevin
*
c
ATP
Ctrl
[Ca2+]c (nM)
Time (s)
ATP
+efsevin
[Ca2+]m (F0/Fipcam)
Time (s)
Δ[Ca2+]c (nM)
Ctrl
efsevin
[Ca2+]m (F0/Fipcam)
Ctrl
efsevin
Coupling time (s)
Ctrl
efsevin
*

Supplementary Figure 2-1. Efsevin restores rhythmic cardiac contractions in NCX1h morphant embryos.

Injection of a morpholino antisense oligonucleotide against NCX1h (MONCX1h) recapitulated the *tremblor* phenotype (light gray bar). Treatment with 30 μM efsevin (MONCX1h + efsevin) restored rhythmic cardiaccontractions in the majority of morphant embryos (striped bar). ***, $p<0.001$.

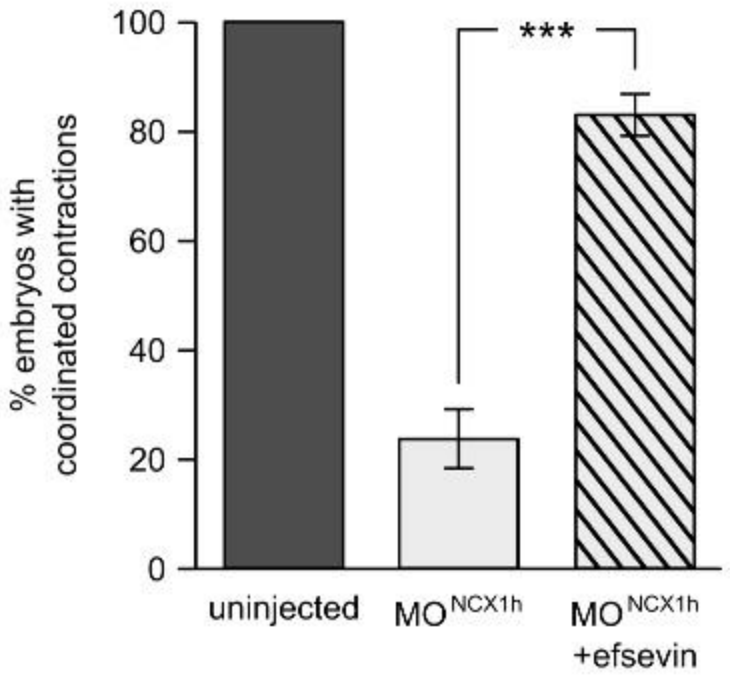
100
80
60
40
20
0
% embryos with coordinated contractions
***
uninjected
MO NCX1h
MO NCX1h +efsevin

Supplementary Figure 2-2. Derivatives of efsevin.

a, Two derivatives of efsevin, OK-C125 and OK-C19, werecreated. **b,** The ability of OK-C125 and OK-C19 to restore cardiac contractions were analyzed. OK-C125restored rhythmic contractions in the majority of *tremblor* embryos (82%, 37/45 embryos), comparable toefsevin (61%, 25/41 embryos), whereas OK-C19 failed to rescue the *tremblor* phenotype (0%, 0/20 embryos, *tre*-controls: 14%, 17/118 embryos). **c,** We attached linkers to all three compounds (indicated by superscript L).**d,** Compounds with linker were injected into one cell embryos together with a morpholino targeting NCX1h(MONCX). Compounds efsevinL and OK-C125L retained their ability to restore rhythmic contractions in MONCXinjected embryos (efsevinL: 81%, 26/32 embryos and OK-C125L: 50%, 21/42 embryos, respectively), while theinactive derivative OK-C19L was still unable to induce rhythmic contraction above background levels (OKC19L:9%, 3/32 embryos, and background: 26%, 36/138 embryos).

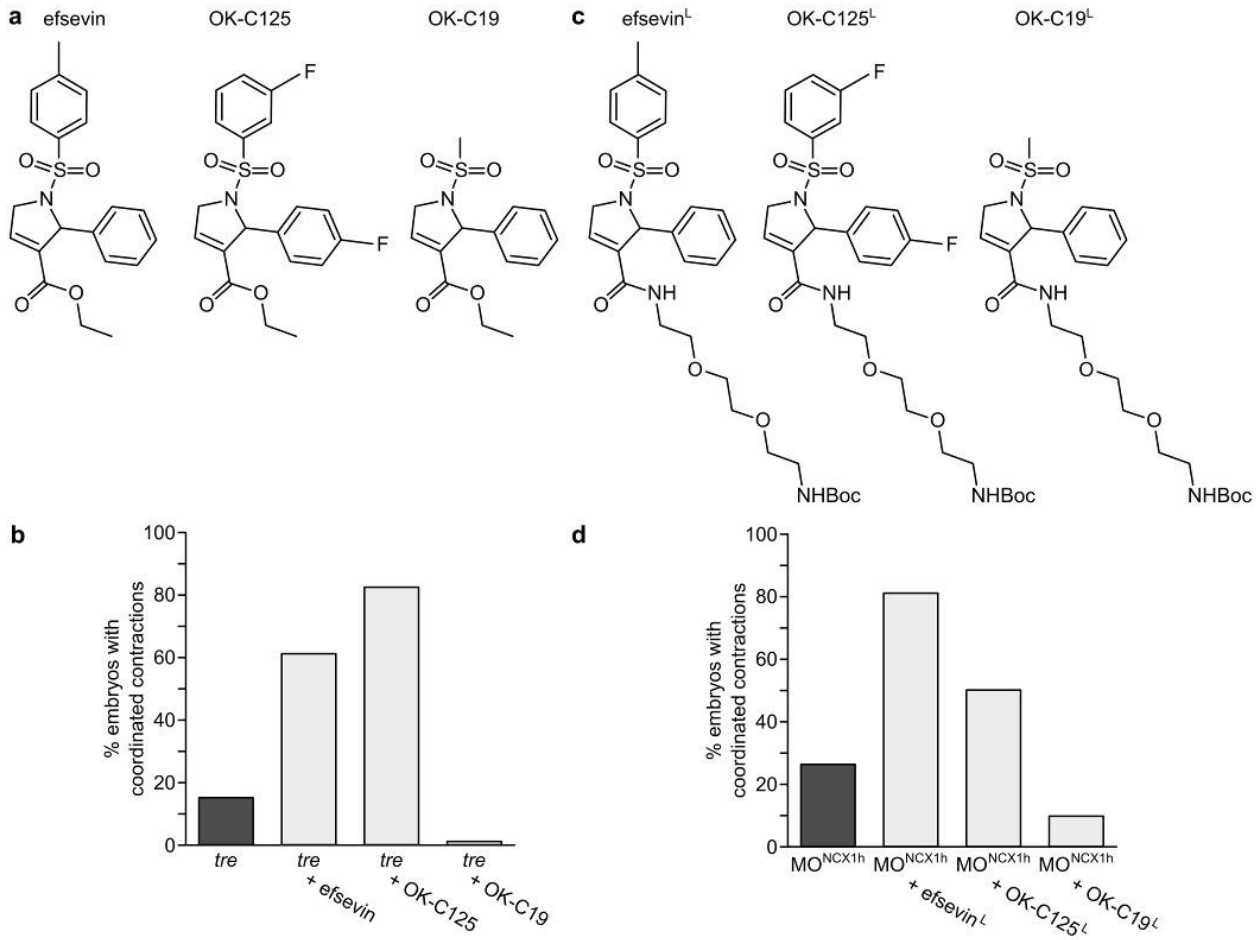
a
efsevin
OK-C125
OK-C19
c
efsevin^L
OK-C125^L
OK-C19^L
NHBoc
b
% embryos with coordinated contractions
100
80
60
40
20
0
tre
tre + efsevin
tre + OK-C125
tre + OK-C19
d
% embryos with coordinated contractions
MO^NCX1h
MO^NCX1h + efsevin^L
MO^NCX1h + OK-C125^L
MO^NCX1h + OK-C19^L

Supplementary Figure 2-3. Identification of VDAC2 as the target of efsevin by Mass Spectrometry.

The 32kD band eluted from efsevinL beads shown in Figure. 2-4 was excised and in-gel digested prior to analysis by massspectrometry. **a,** The spectrum shown allowed the identification of the VDAC 2 peptide LTFDTTFSPNTGK.Diagnostic b- and y-series ions are shown in red and blue, respectively. **b,** VDAC 2 peptides identified by massspectrometry (underlined) account for 30% of the total sequence. The peptide exemplified in (**a**) is indicated in bold.

a

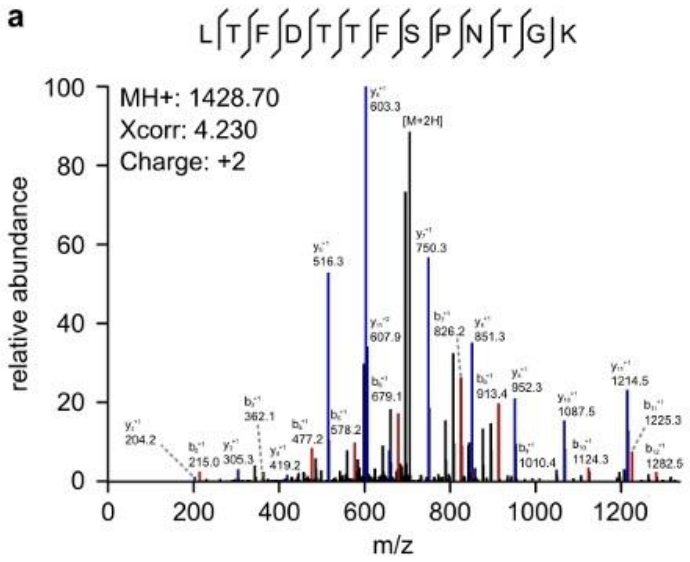

b

VDAC2 - 30% Sequence Coverage

MAVPPAYADLGKSAKDIFNKGYGFG
MVKLDVKTKSASGVEFKTSGSSNT
DTSKVVGSLETKYKRSEYGLTFTEK
WNTDNTLGTEINIEDQIAKGLK**LTFD**
TTFSPNTGKKSGKVKTAYKREFVNL
GCDVDFDFAGPTIHGAAVVGYEGW
LAGYQMSFDTAKSKMTQNNFAVGY
KTGDFQLHTNVNDGSEFGGSIYQK
VSDKLETAVNLAWTAGSNSTRFGIA
AKYQLDKDASISAKVNNTSLVGVGY
TQSLRPGIKLTLSALVDGKSINSGG
HKLGLGLELEA

Supplementary Figure 2-4. Phylogenetic analysis of vertebrate VDAC isoforms.

A phylogenetic analysisusing the amino acid sequences of (**a**) full-length and (**b**) the core domain sequence from *Homo sapiens* (h), *Musmusculus* (m), *Gallus gallus* (g), *Xenopus laevis* (x), and *Danio rerio* (d) confirmed that the 32kDa proteinspecies identified from the pulldown assay is isoform 2 of the voltage-dependent anion channel (VDAC2).Accession numbers for sequences used are: dVDAC1: AAI60655.1, dVDAC2: AAI64640.1, dVDAC3:NP_998411.1, hVDAC1: NP_003365.1, hVDAC2: CAI40911.1, hVDAC3: NP_001129166.1, xVDAC1:NP_001016492.1, xVDAC2: NP_001016193.1, xVDAC3: AAH87828.1, mVDAC1: NP_035824.1, mVDAC2:NP_035825.1, mVDAC3: NP_001185927.1, gVDAC1: NP_001029041.1, gVDAC2: NP_990072.1, gVDAC3:XP_424406.2.

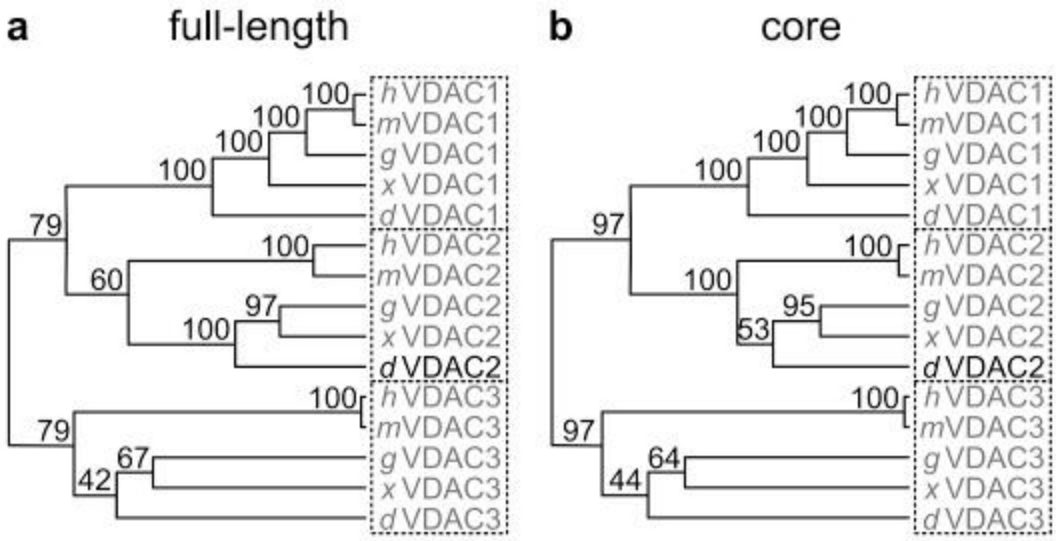
a
full-length
b
core
hVDAC1
mVDAC1
gVDAC1
xVDAC1
dVDAC1
hVDAC2
mVDAC2
gVDAC2
xVDAC2
dVDAC2
hVDAC3
mVDAC3
gVDAC3
xVDAC3
dVDAC3

Supplementary Figure 2-5. Co-localization of zebrafish VDAC proteins with mitochondria in cultured HeLa cells.

HeLa cells were transfected with a flag-tagged zebrafish VDAC1 (VDAC1flag, top panel) and VDAC2 (VDAC2flag, lower panel), immunostained against the flag epitope and counterstained for mitochondriawith MitoTracker Orange and for nuclei with DAPI. Co-localization of red and green foci in transfected cellsindicates mitochondrial localization of zebrafish VDAC1 and VDAC2.

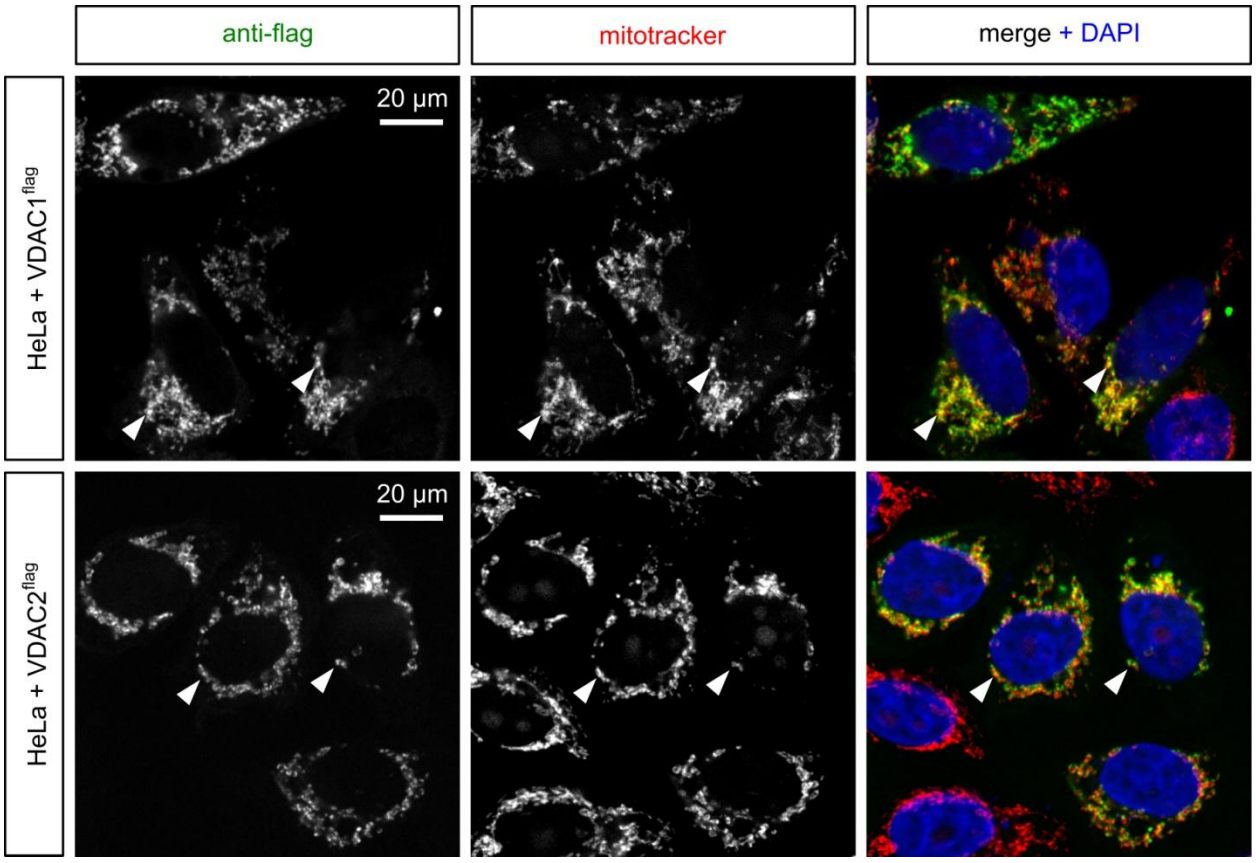
anti-flag
mitotracker
merge + DAPI
HeLa + VDAC1flag
HeLa + VDAC2flag
20 µm
20 µm

Supplementary Figure 2-6. Overexpression of VDAC2 restores rhythmic cardiac contractions in NCX1h morphant embryos.

Injection of a morpholino antisense oligonucleotide against NCX1h (MONCX1h) recapitulated the *tremblor* phenotype (light gray bar). Co-injection of VDAC2 mRNA (MONCX1h + VDAC2) significantly restored rhythmic cardiac contractions in NCX1h morphant embryos (striped bar). ***, $p<0.001$

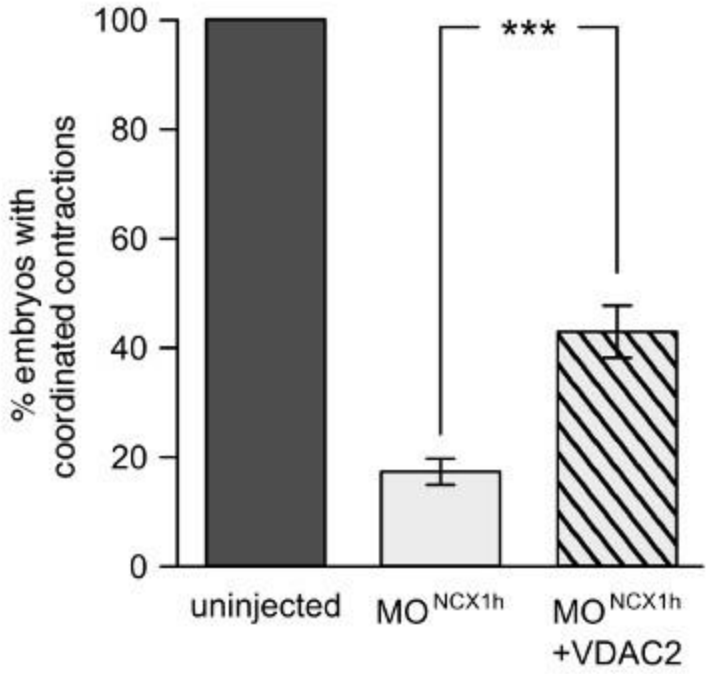
100
80
60
40
20
0
% embryos with coordinated contractions
***
uninjected
MO NCX1h
MO NCX1h +VDAC2

Supplementary Figure 2-7. Generation of drug-inducible VDAC2 transgenic fish.

a, Schematic diagram of *myl7:VDAC2EcR* construct. **b**, TBF treatment induces GFP expression in the heart of *myl7:VDAC2EcR* embryos while DMSO treatment does not induce GFP expression at all. In situ hybridization verified that VDAC2 expression is significantly upregulated in the heart by TBF treatment but not by DMSO treatment.

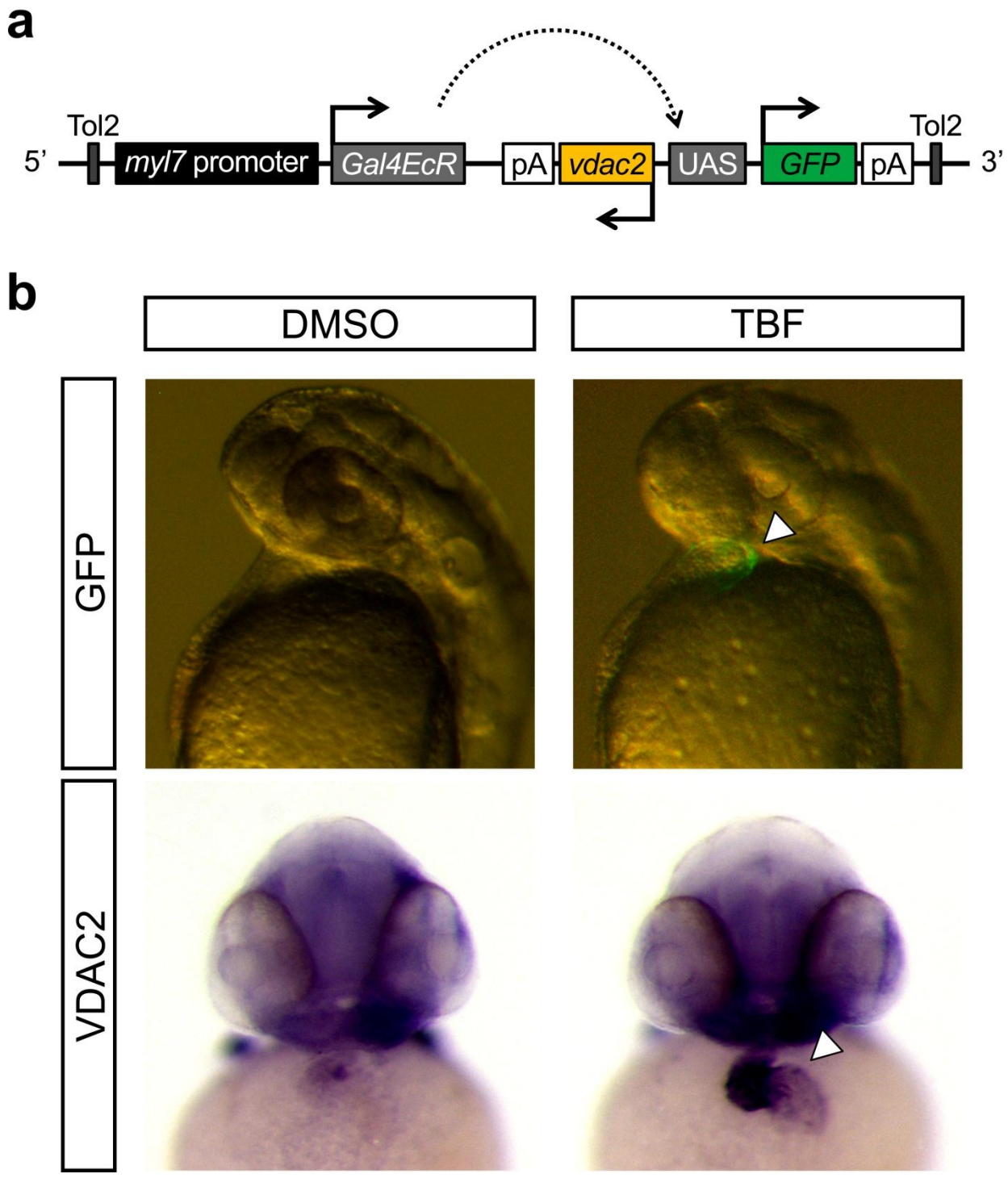
a
Tol2
5'
myl7 promoter
Gal4EcR
pA
vdac2
UAS
GFP
pA
Tol2
3'
b
DMSO
TBF
GFP
VDAC2

Supplementary Figure 8. Activating VDAC2 does not induce apoptosis in developing zebrafish embryos.

a-**c**, Live images of control (**a**), efsevin-treated (**b**) and VDAC2-overexpressing (**c**) embryos at 48 hpf. **d**-**i**, Apoptotic cells were visualized by TUNEL assays (**d**-**f**) or Acridine orange staining (**g**-**i**) at 48 hpf and imaged using fluorescence microscopy. Neither efsevin treatment nor VDAC2 overexpression significantly induce apoptosis in zebrafish embryos.

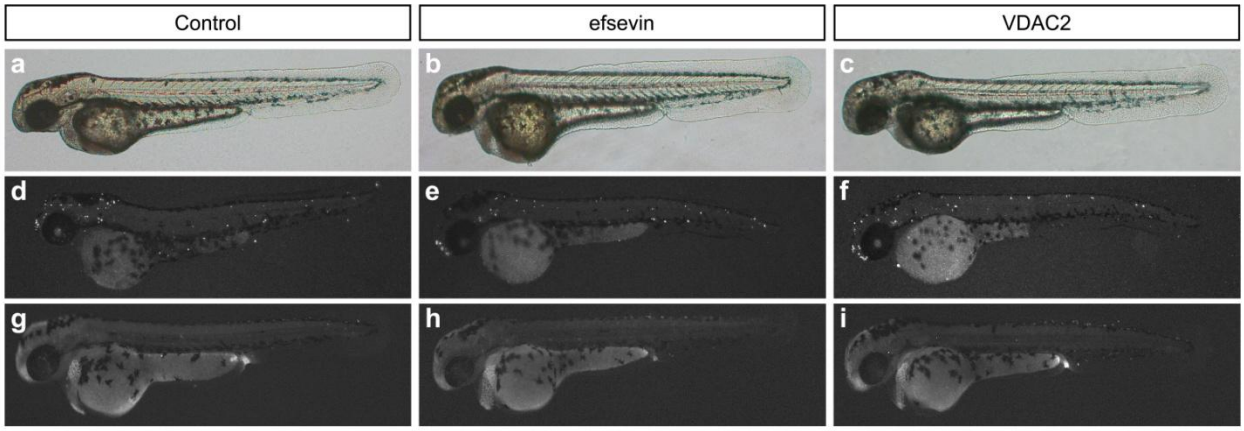
Control
efsevin
VDAC2
a
b
c
d
e
f
g
h
i

Supplementary Figure 9. Generation of VDAC2 knockout fish.

a, Diagram of Zinc finger target sites. **b**, RFLP analysis of wild type (left) and VDAC2 mutant (right) embryos. **c**, VDAC2$^{zfn/zfn}$ carries a 34bp deletion in exon 3 which results in a premature stop codon (red asterisk). **d,** In situ hybridization analysis showing loss of VDAC2 transcripts in VDAC2$^{zfn/zfn}$ embryos.

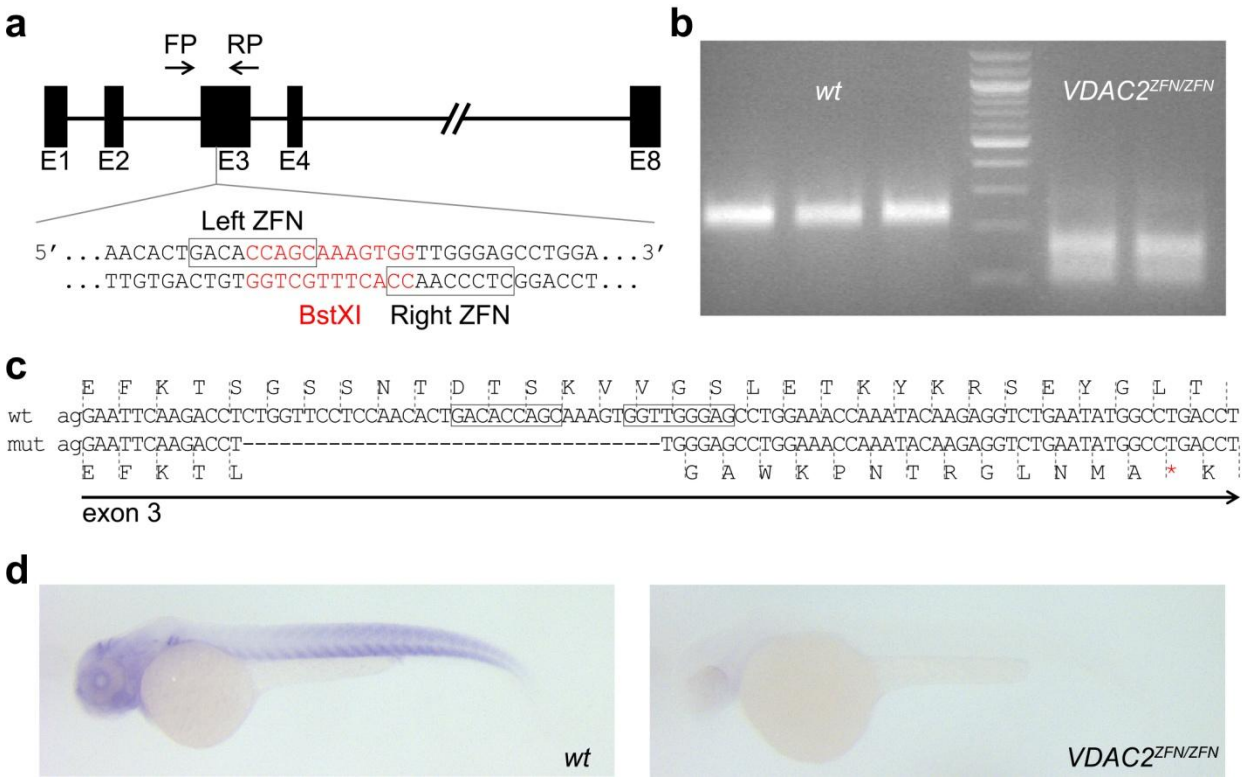
a
FP
RP
E1
E2
E3
E4
E8
Left ZFN
5′...AACACTGACACCAGCAAAGTGGTTGGGAGCCTGGA...3′
...TTGTGACTGTGGTCGTTTCACCAACCCTCGGACCT...
BstXI
Right ZFN
b
wt
VDAC2ZFN/ZFN
c
E F K T S G S S N T D T S K V V G S L E T K Y K R S E Y G L T
wt agGAATTCAAGACCTCTGGTTCCTCCAACACTGACACCAGCAAAGTGGTTGGGAGCCTGGAAACCAAATACAAGAGGTCTGAATATGGCCTGACCT
mut agGAATTCAAGACCT----------TGGGAGCCTGGAAACCAAATACAAGAGGTCTGAATATGGCCTGACCT
E F K T L
G A W K P N T R G L N M A * K
exon 3
d
wt
VDAC2ZFN/ZFN

Supplementary Table 2-1. Effect of 1μM efsevin on global Ca^{2+} transients in ventricular cardiomyocytes.

	Amplitude *($\Delta F/F_0$)*	**Time to peak** *(ms)*	**Tau activation** *(ms)*	**Tau Inactivation** *(ms)*	**n**
vehicle	3.13±0.11	35.8±1.9	6.7±0.37	209.8±9.5	78
efsevin	3.08±0.14	34.1±1.4	6.76±0.4	173.7±8.5***	57

***, $p<0.01$

Supplementary Table 2-2. Effect of 1μM efsevin on spontaneous Ca^{2+} sparks in ventricular cardiomyocytes.

	Frequency *(sparks/100μm/100s)*	n	Amplitude *($\Delta F/F_0$)*	Release flux *($\Delta F/F_0/\Delta t_{max}$)*	Tau Inactivation *(ms)*	Total width *(μm)*	Total duration *(ms)*	n
vehicle	2.46±0.18	89	0.9±0.02	96.3±2.3	52.7±1.1	5.06±0.06	106.9±1.8	847
efsevin	2.49±0.19	75	0.92±0.02	95±2.7	43.6±1.1***	4.53±0.07***	91.6±2.1***	619

***, p<0.01

E. References

1. Yano M, Yamamoto T, Kobayashi S, Ikeda Y, Matsuzaki M. Defective Ca^{2+} cycling as a key pathogenic mechanism of heart failure. Circ J. 2008;72 Suppl A:A22-30.

2. Greiser M, Lederer WJ, Schotten U. Alterations of atrial Ca^{2+} handling as cause and consequence of atrial fibrillation. Cardiovasc Res. 2011;89(4):722-33.

3. Langenbacher AD, Dong Y, Shu X, Choi J, Nicoll DA, Goldhaber JI, Philipson KD, Chen JN. Mutation in sodium-calcium exchanger 1 (NCX1) causes cardiac fibrillation in zebrafish. Proc Natl Acad Sci U S A. 2005;102(49):17699-704.

4. Ebert AM, Hume GL, Warren KS, Cook NP, Burns CG, Mohideen MA, Siegal G, Yelon D, Fishman MC, Garrity DM. Calcium extrusion is critical for cardiac morphogenesis and rhythm in embryonic zebrafish hearts. Proc Natl Acad Sci U S A. 2005;102(49):17705-10.

5. Bers DM, Pogwizd SM, Schlotthauer K. Upregulated Na/Ca exchange is involved in both contractile dysfunction and arrhythmogenesis in heart failure. Basic Res Cardiol. 2002;97 Suppl 1:I36-42.

6. Bers DM. Calcium cycling and signaling in cardiac myocytes. Annu Rev Physiol. 2008;70:23-49.

7. Brown DA, O'Rourke B. Cardiac mitochondria and arrhythmias. Cardiovasc Res. 2010;88(2):241-9.

8. Ruiz-Meana M, Fernandez-Sanz C, Garcia-Dorado D. The SR-mitochondria interaction: a new player in cardiac pathophysiology. Cardiovasc Res. 2010;88(1):30-9.

9. Sedej S, Heinzel FR, Walther S, Dybkova N, Wakula P, Groborz J, Gronau P, Maier LS, Vos MA, Lai FA, Napolitano C, Priori SG, Kockskämper J, Pieske B. Na+-dependent SR Ca^{2+} overload induces arrhythmogenic events in mouse cardiomyocytes with a human CPVT mutation. Cardiovasc Res. 2010;87(1):50-9.

10. Yang D, Zhu WZ, Xiao B, Brochet DX, Chen SR, Lakatta EG, Xiao RP, Cheng H. Ca^{2+}/calmodulin kinase II-dependent phosphorylation of ryanodine receptors suppresses Ca^{2+} sparks and Ca^{2+} waves in cardiac myocytes. Circ Res. 2007;100(3):399-407.

11. Gizak A, Pirog M, Rakus D. Muscle FBPase binds to cardiomyocyte mitochondria under glycogen synthase kinase-3 inhibition or elevation of cellular Ca^{2+} level. FEBS Lett. 2012;586(1):13-9.

12. Yagoda N, von Rechenberg M, Zaganjor E, Bauer AJ, Yang WS, Fridman DJ, Wolpaw AJ, Smukste I, Peltier JM, Boniface JJ, Smith R, Lessnick SL, Sahasrabudhe S, Stockwell BR. RAS-RAF-MEK-dependent oxidative cell death involving voltage-dependent anion channels. Nature. 2007;447(7146):864-8.

13. Cheng EH, Sheiko TV, Fisher JK, Craigen WJ, Korsmeyer SJ. VDAC2 inhibits BAK activation and mitochondrial apoptosis. Science. 2003;301(5632):513-7.

14. Roy SS, Ehrlich AM, Craigen WJ, Hajnóczky G. VDAC2 is required for truncated BID-induced mitochondrial apoptosis by recruiting BAK to the mitochondria. EMBO Rep. 2009;10(12):1341-7.

15. Arzoine L, Zilberberg N, Ben-Romano R, Shoshan-Barmatz V. Voltage-dependent anion channel 1-based peptides interact with hexokinase to prevent its anti-apoptotic activity. J Biol Chem. 2009 Feb 6;284(6):3946-55.

16. Shoshan-Barmatz V, De Pinto V, Zweckstetter M, Raviv Z, Keinan N, Arbel N. VDAC, a multi-functional mitochondrial protein regulating cell life and death. Mol Aspects Med. 2010;31(3):227-85.

17. Rapizzi E, Pinton P, Szabadkai G, Wieckowski MR, Vandecasteele G, Baird G, Tuft RA, Fogarty KE, Rizzuto R. Recombinant expression of the voltage-dependent anion channel enhances the transfer of Ca^{2+} microdomains to mitochondria. J Cell Biol. 2002;159(4):613-24.

18. Báthori G, Csordás G, Garcia-Perez C, Davies E, Hajnóczky G. Ca^{2+}-dependent control of the permeability properties of the mitochondrial outer membrane and voltage-dependent anion-selective channel (VDAC). J Biol Chem. 2006;281(25):17347-58.

19. Hayashi T, Martone ME, Yu Z, Thor A, Doi M, Holst MJ, Ellisman MH, Hoshijima M. Three-dimensional electron microscopy reveals new details of membrane systems for Ca^{2+} signaling in the heart. J Cell Sci. 2009;122(Pt 7):1005-13.

20. García-Pérez C, Hajnóczky G, Csordás G. Physical coupling supports the local Ca^{2+} transfer between sarcoplasmic reticulum subdomains and the mitochondria in heart muscle. J Biol Chem. 2008;283(47):32771-80.

21. Dorn GW 2nd, Scorrano L. Two close, too close: sarcoplasmic reticulum-mitochondrial crosstalk and cardiomyocyte fate. Circ Res. 2010;107(6):689-99.

22. Cheng H, Lederer WJ, Cannell MB. Calcium sparks: elementary events underlying excitation-contraction coupling in heart muscle. Science. 1993;262(5134):740-4.

23. Hove-Madsen L, Llach A, Bayes-Genís A, Roura S, Rodriguez Font E, Arís A, Cinca J. Atrial fibrillation is associated with increased spontaneous calcium release from the sarcoplasmic reticulum in human atrial myocytes. Circulation. 2004;110(11):1358-63.

24. Baughman JM, Perocchi F, Girgis HS, Plovanich M, Belcher-Timme CA, Sancak Y, Bao XR, Strittmatter L, Goldberger O, Bogorad RL, Koteliansky V, Mootha VK. Integrative genomics identifies MCU as an essential component of the mitochondrial calcium uniporter. Nature. 2011;476(7360):341-5.

25. De Stefani D, Raffaello A, Teardo E, Szabò I, Rizzuto R. A forty-kilodalton protein of the inner membrane is the mitochondrial calcium uniporter. Nature. 2011;476(7360):336-40.

26. García-Pérez C, Schneider TG, Hajnóczky G, Csordás G. Alignment of sarcoplasmic reticulum-mitochondrial junctions with mitochondrial contact points. Am J Physiol Heart Circ Physiol. 2011;301(5):H1907-15.

27. Esengil H, Chang V, Mich JK, Chen JK. Small-molecule regulation of zebrafish gene expression. Nat Chem Biol. 2007;3(3):154-5.

28. Shindo A, Hara Y, Yamamoto TS, Ohkura M, Nakai J, Ueno N. Tissue-tissue interaction-triggered calcium elevation is required for cell polarization during Xenopus gastrulation. PLoS One. 2010;5(2):e8897.

29. Kwan KM, Fujimoto E, Grabher C, Mangum BD, Hardy ME, Campbell DS, Parant JM, Yost HJ, Kanki JP, Chien CB. The Tol2kit: a multisite gateway-based construction kit for Tol2 transposon transgenesis constructs. Dev Dyn. 2007;236(11):3088-99.

30. Foley JE, Yeh JR, Maeder ML, Reyon D, Sander JD, Peterson RT, Joung JK. Rapid mutation of endogenous zebrafish genes using zinc finger nucleases made by Oligomerized Pool ENgineering (OPEN). PLoS One. 2009;4(2):e4348.

31. Castellano S, Fiji HD, Kinderman SS, Watanabe M, Leon Pd, Tamanoi F, Kwon O. Small-molecule inhibitors of protein geranylgeranyltransferase type I. J Am Chem Soc. 2007;129(18):5843-5.

32. Cruz D, Wang Z, Kibbie J, Modlin R, Kwon O. Diversity through phosphine catalysis identifies octahydro-1,6-naphthyridin-4-ones as activators of endothelium-driven immunity. Proc Natl Acad Sci U S A. 2011;108(17):6769-74.

33. Choi J, Mouillesseaux K, Wang Z, Fiji HD, Kinderman SS, Otto GW, Geisler R, Kwon O, Chen JN. Aplexone targets the HMG-CoA reductase pathway and differentially regulates arteriovenous angiogenesis. Development. 2011;138(6):1173-81.

34. Nguyen CT, Lu Q, Wang Y, Chen JN. Zebrafish as a model for cardiovascular development and disease. Drug Discov Today Dis Models. 2008;5(3):135-140.

35. Milan DJ, Giokas AC, Serluca FC, Peterson RT, MacRae CA. Notch1b and neuregulin are required for specification of central cardiac conduction tissue. Development. 2006;133(6):1125-32.

36. Chi NC, Shaw RM, Jungblut B, Huisken J, Ferrer T, Arnaout R, Scott I, Beis D, Xiao T, Baier H, Jan LY, Tristani-Firouzi M, Stainier DY. Genetic and physiologic dissection of the vertebrate cardiac conduction system. PLoS Biol. 2008;6(5):e109.

37. Blin G, Nury D, Stefanovic S, Neri T, Guillevic O, Brinon B, Bellamy V, Rücker-Martin C, Barbry P, Bel A, Bruneval P, Cowan C, Pouly J, Mitalipov S, Gouadon E, Binder P, Hagège A, Desnos M, Renaud JF, Menasché P, Pucéat M. A purified population of multipotent cardiovascular progenitors derived from primate pluripotent stem cells engrafts in postmyocardial infarcted nonhuman primates. J Clin Invest. 2010;120(4):1125-39.

38. Arshi A, Nakashima Y, Nakano H, Eaimkhong S, Evseenko D, Reed J, Stieg AZ, Gimzewski JK, Nakano A. Rigid microenvironments promote cardiac differentiation of mouse and human embryonic stem cells. Sci Technol Adv Mater. 2013;14(2).

39. Reuter H, Han T, Motter C, Philipson KD, Goldhaber JI. Mice overexpressing the cardiac sodium-calcium exchanger: defects in excitation-contraction coupling. J Physiol. 2004;554(Pt 3):779-89.

40. Picht E, Zima AV, Blatter LA, Bers DM. SparkMaster: automated calcium spark analysis with ImageJ. Am J Physiol Cell Physiol. 2007;293(3):C1073-81.

41. Rubinfeld B, Souza B, Albert I, Müller O, Chamberlain SH, Masiarz FR, Munemitsu S, Polakis P. Association of the APC gene product with beta-catenin. Science. 1993;262(5140):1731-4.

42. Chen JN, Fishman MC. Zebrafish tinman homolog demarcates the heart field and initiates myocardial differentiation. Development. 1996;122(12):3809-16.

43. Csordás G, Renken C, Várnai P, Walter L, Weaver D, Buttle KF, Balla T, Mannella CA, Hajnóczky G. Structural and functional features and significance of the physical linkage between ER and mitochondria. J Cell Biol. 2006;174(7):915-21.

44. Roy SS, Madesh M, Davies E, Antonsson B, Danial N, Hajnóczky G. Bad targets the permeability transition pore independent of Bax or Bak to switch between Ca^{2+}-dependent cell survival and death. Mol Cell. 2009;33(3):377-88.

45. Csordás G, Várnai P, Golenár T, Roy S, Purkins G, Schneider TG, Balla T, Hajnóczky G. Imaging interorganelle contacts and local calcium dynamics at the ER-mitochondrial interface. Mol Cell. 2010;39(1):121-32.

46. Mouillesseaux K, Chen JN. Mutation in utp15 disrupts vascular patterning in a p53-dependent manner in zebrafish embryos. PLoS One. 2011;6(9):e25013.

CHAPTER 3

Aberrant Ca^{2+} homeostasis leads to proteasome-mediated myofibrillar disarray via the calcineurin-FoxO-Trim63 signaling pathway

A. Abstract

Abnormal Ca^{2+} homeostasis is associated with multiple cardiac conditions including arrhythmias, hypertrophy and myopathy. Here we use the zebrafish as a genetic model to explore the regulatory relationship between Ca^{2+} signaling and the sarcomere integrity. In zebrafish, deficiency in *ncx1h*, a cardiac-specific sodium-calcium exchanger gene, disrupts normal Ca^{2+} transients in cardiomyocytes and causes arrhythmic cardiac contractions and severe myofibril disarray. Gene profiling analysis revealed a significant elevation of *trim63* expression in *ncx1h* deficient hearts. Overexpression of *trim63* disrupts the sarcomere structure in zebrafish cardiomyocytes and knock-down of *trim63* or inhibiting proteasome activity protects myofibrils from degradation in *ncx1h* deficient embryos, demonstrating a causal relationship between *trim63* gene expression and the myofibril defects. Molecular analysis showed that elevated Ca^{2+} level is sufficient to enhance *trim63* expression in zebrafish hearts and that inhibiting calcineurin activity blocks aberrant Ca^{2+} homeostasis-induced *trim63* expression. We next showed that calcineurin regulates *trim63* expression by determining the subcellular localization of FoxO. In *tre* hearts, FoxO is accumulated in the nucleus. Overexpression of a dominant negative form of calcineurin sequesters FoxO in the cytoplasm, suppresses *trim63* expression and protects sarcomere integrity in *tre* cardiomyocytes. Furthermore, overexpression of FoxO in the heart induces *trim63a* expression and leads to myofibril disarray, whereas overexpression of a

dominant negative form of FoxO protects sarcomere integrity in *ncx1h* deficient embryos. Together, these studies uncovered a novel mechanism by which Ca^{2+} regulates *trim63a* expression in cardiomyocytes.

B. Introduction

Ca^{2+} regulates critical biological processes. In the heart, Ca^{2+} plays a central role in coordinating electrical signals and cardiac contractions on a beat-to-beat basis [1]. Aberrant Ca^{2+} homeostasis often leads to contractile dysfunction, arrhythmias and heart failure [2-4]. In addition, Ca^{2+} is a critical signaling molecule controlling multiple cellular processes in the heart. Key transducers of pathological Ca^{2+} signals include Calmodulin-dependent protein kinase II (CaMKII) and calmodulin-dependent protein phosphatase calcineurin (Cn). While mechanisms by which CaMKII and Cn mediate pathological Ca^{2+} signaling in hypertrophy have been documented [5-8], the involvement of Ca^{2+}-dependent transcriptional alteration in other pathophysiological conditions requires further investigation.

The tripartite motif containing protein TRIM63 (also known as MuRF1) is an E3 ubiquitin ligase expressed in cardiac and skeletal muscles [9-10]. It adds poly-ubitiquin chains to sarcomere proteins including myBP-C, tropomyosin and troponin [10-12] and thereby facilitates sarcomere disassembly and myofibril disarray through a proteasome-dependent mechanism [13-14]. TRIM63 is implicated in the control of cardiac cell mass and contractility [10, 15-16] and loss-of-function mutations of TRIM63 are associated with hypertrophic cardiomyopathy in humans [17]. While TRIM63 deficiency does not cause obvious phenotypes in the mouse model, it markedly attenuates transverse aortic constriction (TAC) induced cardiac hypertrophy [18].

However, the causative relationship between TRIM63, sarcomere integrity and cardiac hypertrophy requires further investigation at the mechanistic level.

The Forkhead box O (FoxO) class of transcription factors, whose activity is primarily regulated by its subcellular localization, regulates a wide range of gene expression programs and cellular processes. Phosphorylated FoxO is sequestered in the cytoplasm whereas dephosphorylation leads to nuclear translocation and transcriptional activation of FoxO [19-20]. In striated muscles, FoxO mediates various signaling pathways to control muscle cell mass. This mechanism is best documented in skeletal muscles. Upon stimulation with growth factors such as IGF-1, FoxO is phosphorylated by AKT and sequestered in the cytoplasm, resulting in the repression of *trim63* transcription and the increase of cell mass [21-22]. In catabolic conditions such as glucocorticoid treatment, denervation, long-term immobilization and microgravity, the suppression of PI3-Akt pathway facilitates the accumulation of FoxO in the nucleus, leading to the induction of *trim63* expression and muscle atrophy [23-25]. Whether FoxO-TRIM63 regulation is also influenced by Ca^{2+} homeostasis has not been directly evaluated.

The zebrafish *tremblor* (*tre*) mutant lacks functional *ncx1h* gene, a cardiac-specific *ncx1* gene, resulting in abnormal Ca^{2+} transients in cardiomyocytes and cardiac fibrillation [26-27]. Interestingly, the sarcomere structures of the *tre* mutant heart are severely disrupted [27]. Similarly, severe defects in sarcomere integrity have been noted in embryonic NCX1-deficient mouse heart [28-29] and NCX1 inhibitor treated adult mouse cardiomyocytes [31]. The molecular mechanism underlying the myofibril defects observed in NCX1 deficient hearts is not known. NCX1 is a critical Ca^{2+} extrusion molecule in the heart. This raises an attractive possibility that aberrant Ca^{2+} signaling induces myofibril disarray in NCX1 compromised

cardiomyocytes. Here, we assess the molecular mechanisms by which Ca^{2+} homeostasis influences the integrity of the contractile machinery in the *tre* heart. By microarray analysis, we noted a dramatic increase of *trim63* expression in *ncx1h* deficient hearts. Our genetic and pharmacologic analyses further demonstrate a causative relationship between *trim63* upregulation and myofibril disarray. We showed that elevated intracellular Ca^{2+} levels activates calcineurin which dephosphorylates FoxO and promotes the translocation of FoxO from the cytoplasm to the nucleus and thereby upregulates expression of *trim63*. Our results provide the evidence that Ca^{2+} functions as a molecular switch required to regulate the stoichiometry of cardiac muscle structure via transcriptional regulation.

C. Results

Loss of function of *NCX1h* leads to myofibril disarray

NCX1h is a cardiac-specific NCX1 gene in zebrafish. NCX1h deficient zebrafish embryos (both *tre* mutant embryos and *ncx1h* morphants) never initiate persistent cardiac contractions [26-27] and the myofibril structures are severely dissembled after three days of development [27]. We therefore investigated whether NCX1 activity is required for sarcomere assembly. At 30 hours post fertilization (hpf), the overall morphology of the primitive heart tube and the cell shape of cardiomyocytes are indistinguishable between wild type and *tre* mutant embryos (Figure 3-1B). In addition, a nascent periodic banding pattern of α-actinin marking the Z-line is apparent in *tre* mutant hearts suggesting that the initiation of sarcomere assembly does not require NCX1 activity (Figure 3-1A). By 48 hpf, *tre* mutant hearts become dysmorphic; the ventricle is small and the atrium is collapsed at the inflow end (Figure 3-1A, B). Cardiomyocytes

assume a rounded shape and Z-lines are no longer intact as indicated by the sporadic α-actinin pattern (Figure 3-1A). The *tre* heart further deteriorated as development proceeds. By 72 hpf, both ventricle and atrium are collapsed, cardiomyocytes are misshaped and α-actinin pattern is severely disorganized in *tre* hearts (Figure 3-1A). Similar myofibril phenotype was observed in the *ncx1h* morphants (Supplementary Figure 3-1). Together, these findings suggest that myofibrils are assembled initially but the integrity of sarcomeres is not properly maintained in *tre* mutant hearts.

Elevated *trim63* expression in *tre* mutant hearts

To identify molecular pathways underlying the pathogenesis of the myofibril defect, we isolated 2-day-old embryonic hearts from wild type and *ncx1h* deficient embryos. Microarray analysis showed a significant increase of *trim63* transcripts in *ncx1h* morphant hearts compared to wild type hearts. There are two highly homologous *trim63* genes in zebrafish (*zgc_86757* and *zgc_56376*, hereafter referred to as *trim63a* and *trim63b*, respectively), both of which are clustered with mammalian *trim63* genes (Figure 3-2A). These genes share a high degree of homology and are likely to be a result of genome duplication [31]. Quantitative RT-PCR analysis using RNA extracted from 2-day-old *ncx1h* deficient hearts confirmed an elevated expression of both *trim63a* and *trim63b* (Figure 3-2B). In situ hybridization analysis showed that both *trim63a* and *trim63b* are expressed in the skeletal and cardiac muscles in developing zebrafish embryos as early as 30 hpf (Figure 3-2C). Interestingly, elevated expression levels of *trim63a* and *trim63b* are observed in the heart, but not the skeletal muscles, in *ncx1h* deficient embryos (Figure 3-2C), consistent with the fact that *ncx1h* is a cardiac-specific gene.

Upregulation of *trim63* causes myofibril disarray in embryonic zebrafish heart

Trim63 regulates cardiomyocyte mass by tagging target proteins with polyubiquitin, which leads to a proteasome-dependent degradation process [9-10]. We hypothesized that upregulation of *trim63* causes myofibrillar disarray in *ncx1h* deficient hearts. To evaluate this possibility, we generated *myl7*:*trim63a-IRES-EGFP* transgenic fish in which *myl7* promoter drives the expression of zebrafish *trim63a* and the bicistronic *EGFP* reporter specifically in the heart (Figure 3-3A). In these transgenic embryos, *trim63a* expression is significantly upregulated in the heart (Figure 3-3B). Both atrium and ventricle are dilated and cardiac looping is defective (Figure 3-3B). The heart rate and fractional shortening are reduced (Figure 3-3C, D). As a result, significant blood regurgitation, reduced periphery blood circulation as well as pericardial edema were observed in *trim63a* overexpressing hearts (Figure 3-3B, Supplementary Movie 1, 2). Furthermore, the heart in the *myl7*:*trim63a-IRES-EGFP* transgenic fish failed to maintain sarcomere structure as indicated by disorganized α-actinin pattern and actin filaments (Figure 3-3E), demonstrating that overexpression of *trim63a* is sufficient to disrupt myofibril structure in the developing heart.

We reasoned that if indeed *trim63* overexpression causes myofibril disarray in *tre* hearts, downregulation of *trim63* should alleviate this defect. We utilized antisense morpholino oligonuclotides targeting the translation initiation sites of *trim63a* and *trim63b* to knockdown these genes. While knockdown of either gene alone did not result in marked differences in *tre*, simultaneous knockdown of both *trim63a* and *trim63b* ameliorated the myofibril defect and maintained sarcomere structures in *tre* mutant hearts (Figure 3-3F, G). Furthermore, treatment with MG132, a proteasome inhibitor, restored periodic banding of α-actinin in *tre*

cardiomyocytes, as seen in *trim63* knockdown cardiomyocytes (Figure 3-3F, G), indicating that myofibril defects observed in *ncx1h* deficient hearts results from a trim63-mediated proteasome-dependent protein degradation mechanism. Taken together, our gain- and loss-of-function results suggest a causative relationship between *trim63* overexpression and the myofibril defect observed in *ncx1h* deficient embryos.

Identification of minimum regulatory element of *trim63a*

Loss of function of *ncx1* results in Ca^{2+} homeostasis defects [32]. We therefore investigated whether *trim63a* expression is responsive to Ca^{2+} signaling. A 6.9 kb genomic fragment upstream of the *trim63a* transcription initiation site was used to drive GFP expression in zebrafish embryos (Figure 3-4A) and transient GFP expression was observed in cardiac and skeletal muscles, a pattern similar to endogenous *trim63* expression revealed by in situ hybridization (Figure 3-4B). This expression pattern is further confirmed in stable germ-line transmitted transgenic embryos (Figure 3-4C). We next generated a series of deletion constructs of this 6.9 kb fragment (Figure 3-4A). By transient expression analysis, we found that the 638 bp fragment upstream of the *trim63a* transcription initiation site is sufficient to recapitulate the endogenous *trim63a* expression pattern (Figure 3-4B), suggesting that this fragment contains minimum regulatory elements required for *trim63a* expression.

Ca^{2+} regulates *trim63a* expression via the Calcineurin signaling pathway

To examine whether *trim63a* expression is responsive to changes in intracellular Ca^{2+} levels, we transfected HEK293T cells with either *trim63a* (-6906)-*Luc* or *trim63a* (-638)-*Luc*

plasmid and exposed these cells to A23187, a calcium ionophore. After A23187 treatment, *trim63a* (-6906)-*Luc* and *trim63a* (-638)-*Luc* transfected cells have similar levels of induction of luciferase activity (Figure 3-4E), indicating that *trim63a* expression is responsive to elevated levels of intracellular Ca^{2+} and that the 638bp *trim63a* proximal fragment is sufficient to direct Ca^{2+}-mediated *trim63a* transcription.

We next examined whether Ca^{2+} induces *trim63a* expression via the calcium/calmodulin-dependent protein kinase II (CaMKII) axis or the calcineurin (Cn) axis by treating *trim63a*(-638)-*Luc* transfected HEK293T cells with KN62, a chemical inhibitor of CaMKII, or FK506, an inhibitor of Cn. We then measured the luciferase activities in response to A23187 treatment. While KN62 treatment did not have significant impact on the Ca^{2+}-induced *trim63a* expression, FK506 treatment attenuated the Ca^{2+} responsiveness of the *trim63a*(-638)-*Luc* reporter (Figure 3-5A), indicating that the Cn pathway mediates the Ca^{2+} responsiveness of *trim63a* expression.

FoxO mediates *trim63a* expression in a Ca^{2+}-dependent manner

FoxO regulates *trim63* expression in cardiac and skeletal muscles [21-25, 33-34]. Interestingly, putative FoxO binding sites are detected in the zebrafish *trim63a* (-638) regulatory region (Figure 3-5C). There are seven *foxo* genes; *foxo1a*, *foxo1b*, *foxo3a*, *foxo3b*, *foxo4*, *foxo6a* and *foxo6b* in zebrafish [35]. In situ hybridization demonstrated that *foxo6a* is expressed in the primitive heart tube at 24 hpf, but this expression is diminished by 48 hpf (Supplementary Figure 3-2A). All the other zebrafish *foxo* genes are expressed in the developing heart throughout embryogenesis (Figure 3-5D, Supplementary Figure 3-2A).

We co-transfected *trim63a*(-638)-*Luc* with zebrafish FoxOs into HEK293T cells and found that FoxO induces a dose-dependent activation of *trim63a* transcription (Figure 3-5E, Supplementary Figure 3-2B). Interestingly, overexpression of FoxO further enhanced the Ca^{2+} responsiveness of the 638bp *trim63a* promoter. Furthermore, overexpression of a dominant-negative form of FoxO (DN-foxO), which lacks the transactivation domain but harbors an intact DNA binding domain of FoxO [36-37], abrogated the Ca^{2+}-induced *trim63a* expression (Figure 3-5F). Together, these findings indicate that Ca^{2+} signaling regulates *trim63a* expression via FoxO transcription factors.

Calcineurin regulates *trim63a* expression by dephosphorylating FoxO

The subcellular localization of FoxO is determined by post-translational modifications [20]. We explored the possibility that Cn regulates *trim63a* expression by modulating the phosphorylation status of FoxO. Since *foxo3* has been shown to regulate *trim63* expression in the cardiac muscle [33-34] and zebrafish *foxo3a* enhances the Ca^{2+} responsiveness of the *trim63a* promoter (Supplementary Figure 3-2B), we focus our study on *foxo3a* hereafter.

Upregulation of Ca^{2+} signaling by overexpression of Cn significantly reduced the level of phosphorylated FoxO3 whereas blocking Cn pathway by overexpression of a dominant negative form of Cn (DN-Cn) does not have significant effect on the phosphorylation status of FoxO3a (Figure 3-6A). Furthermore, overexpression of wildtype Cn enhanced FoxO3a-mediated *trim63a* expression whereas overexpression of DN-Cn significantly blunted FoxO's ability to enhance *trim63a* expression (Figure 3-6B). Together, these data demonstrate that activation of Cn induces *trim63a* expression by dephosphorylating FoxO.

trim63a expression is upregulated by FoxO in the zebrafish heart

Our findings suggest that the Cn-FoxO pathway regulates *trim63a* expression. This model predicts that *ncx1h* deficient embryos, which suffer from Ca^{2+} extrusion defects, would have a higher level of FoxO accumulated in the nucleus. To test this hypothesis, we transiently expressed FLAG-tagged FoxO3a and compared the subcellular localization of FoxO3a between wildtype and *tre* mutant cardiomyocytes. Confocal microscopy revealed that while the majority of FoxO3a is sequestered in the cytoplasm in wild type cardiomyocytes, FoxO3a is preferentially localized to the nucleus of cardiomyocytes in *tre* (Figure 3-7A).

We next manipulated Cn and FoxO activities in zebrafish embryos to evaluate their impact on *trim63a* expression. As shown in Figure 3-7B, embryos that received synthetic *foxo3a* mRNA had elevated levels of *trim63a* expression in the heart. This effect was further enhanced by overexpression of a constitutively active form of *foxo3a* (CA-*foxo3a*) in which all three phosphorylation sites were mutated (T29A, S236A, S299A) [38]. Additionally, overexpression of CA-foxo3a resulted in disruption of Z-discs (Figure 3-7C), similar to that observed in *ncx1h* deficient and *trim63a* overexpression embryos. Furthermore, overexpression of DN-*foxo* blunted *trim63a* expression (Figure 3-7B) and restored periodic banding pattern of α-actinin in *tre* mutant hearts (Figure 3-7C). Finally, FK506 treatment mimics the effect of DN-foxO on *trim63a* expression both in wildtype and *tre* embryos (Figure 3-7B). Together, these findings demonstrated a regulatory role for FoxO on *trim63a* expression in developing zebrafish hearts.

D. Discussion

While Ca^{2+} has long been implicated to induce myofibril disarray in cardiac dysfunction [39], underlying molecular mechanisms remain to be explored. Here we use *tremblor*, a zebrafish aberrant Ca^{2+} homeostasis model, to dissect molecular pathways by which Ca^{2+} signaling influences the integrity of myofibrils in cardiomyocytes. We showed that the activation of calcineurin by Ca^{2+} overload leads to a nuclear accumulation of FoxO, which induces expression of *trim63* and a proteasome-dependent degradation of sarcomere structure in cardiomyocytes, demonstrating a novel Ca^{2+} homeostasis-regulated signaling pathway that controls cardiac muscle wasting.

trim63a expression is elevated at the onset of sarcomere disassembly in *tre* mutant hearts and overexpression of *trim63* is sufficient to induce myofibril disarray and atrophy in cardiomyocytes. These findings, together with the observation that knocking down *trim63* and inhibiting ubiquitin-proteosome degradation protect the integrity of sarcomeres in *tre* hearts, demonstrate a causal relationship between the upregulation of *trim63* and myofibril disarray. This finding is consistent with previously established association between *trim63* upregulation and muscle atrophy [9, 11-12, 24, 40]. Furthermore, a ~2-fold increase of *trim63* expression detected in *tre* and *trim63* transgenic hearts is comparable to those detected in heart failure patients and in patients that develop muscle atrophy after receiving the placement of a left ventricular assist device [40-41]. These findings indicate that a modest elevation of *trim63* expression is sufficient to tilt the balance between protein synthesis and degradation to pathological conditions and thus a fine control mechanism for the stoichiometry of cardiac muscle structure is required for maintaining the cell mass of cardiomyocytes. Interestingly, while

trim63 overexpression accelerates heart failure in the TAC mouse model, *trim63* transgenic mice do not exhibit obvious ubiquitin-dependent degradation of sarcomeric proteins [42]. Further investigation is required to determine whether the differences in trim63's effects on sarcomere integrity between fish and mouse *trim63* transgenic models are due to species- or developmental stage-specific responses.

Cn is a critical downstream effector of Ca^{2+} signaling in normal heart development and in pathological conditions [43]. In this study, we present the evidence to support a Cn-mediated regulation of *trim63* gene expression, which has a critical role in controlling cell mass and sarcomere integrity in the heart. Our study showed that aberrant Ca^{2+} homeostasis induces *trim63* expression in cultured cells and in developing zebrafish hearts. This effect is primarily mediated by Cn-FoxO signaling pathway as overexpression of FoxO is sufficient to enhance *trim63* expression and blocking Cn activity by pharmacological inhibitor or by overexpression of a dominant-negative form of Cn blunted FoxO's effect on *trim63*. We propose that Cn induces *trim63* expression by dephosphorylating and promoting nuclear translocation of FoxO. This model is supported by a Cn-dependent increase of dephosphorylated FoxO upon stimulation with ionophore. In the *tre* hearts, FoxO is predominantly localized in the nucleus and *trim63* expression is high. Intriguingly, inhibiting Cn activity by dominant-negative Cn blocks nuclear translocation of FoxO, blunts *trim63* gene expression and protects sarcomere integrity in *tre* mutant hearts. Together these findings indicate a novel Cn-FoxO-TRIM63 pathway mediating Ca^{2+}-dependent regulation of cardiac cell mass and sarcomere integrity (Figure 3-7D).

FoxO transcription factor is a key regulator of *trim63* expression. In skeletal muscles, FoxO mediates PI3K-AKT signaling-controlled hypertrophy and atrophy responses. Upon

stimulation with hormones, such as insulin-like growth factor-1 (IGF-1) and insulin, the activation of AKT phosphorylates and sequesters FoxO transcription factors in the cytoplasm to prevent the induction of atrophy genes including TRIM63 leading to the increase of cell mass [21-22]. Under starvation or denervation, AKT activity is downregulated, promoting the nuclear translocation of FoxO and the induction of TRIM63 expression [23-25]. Our finding that FoxO regulates *trim63* expression in cardiomyocytes as a respond to changes in Ca^{2+} homeostasis adds to the growing evidence supporting a critical nodal point for FoxO-Trim63 in controlling the growth and atrophy of striated muscles.

E. Materials and Methods

Zebrafish husbandry and morpholino oligos

Zebrafish *tremblor* (*tre*^{tc318}) heterozygotes were bred in *Tg(cmlc2:egfp)* background. The wildtype lined used in this study is AB. These fish were maintained and bred following standard protocols [44]. Embryos were raised at 28.5 °C and were staged as previously described [45]. Embryos for in situ hybridization were raised in the presence of 0.2 mM 1-phenyl-2-thiourea from ~22 hpf to prevent pigmentation. Embryos were fixed with 4% paraformaldehyde at the stage indicated for subsequent analyses.

The morpholino-modified antisense oligonucleotides targeting the translation initiation sites of *trim63a* (5'-TTTGACCCGTTTGGATGTCCATTGC-3') and *trim63b* (5'-AAGAGGCAGTTCGCTGAATGTCCAT-3') were purchased from Gene-Tools. Morpholino oligonucleotides (8 ng each) were introduced to 1- to 2-cell stage embryos by microinjection.

Pharmacological treatment

Chemicals used in this study are A23187, FK506, KN62 (Sigma-Aldrich) and MG132 (CALBIOCHE). All chemicals were prepared in DMSO. For zebrafish embryos, chemicals were applied to the embryo media.

Microarray and quantitative PCR

For microarray analysis, zebrafish embryonic hearts were isolated at 48 hpf as previously described [46]. Total RNA was purified using RNAeasy micro kit (Qiagen). Microarray hybridization was performed in triplicate using the Affymetrix Zebrafish GeneChip containing 15,617 genes. RNA probes were prepared according to the guideline provided by the array manufacturer. For quantitative analysis, total RNAs isolated from embryonic hearts were reverse transcribed to generate first-strand cDNA using iScript kit (BIORAD) by priming with random hexamers. The relative expression levels of *trim63a* and *trim63b* in the wild type and *tre* hearts were determined by quantitative PCR using the LightCycler® 480 System (Roche Applied Science). GAPDH was served as the internal control for normalization. Primer sequences used in this study are listed in Supplementary Table.

Transmission electron microscopy

Wild type and homozygous *tre* mutant embryos at 72 hpf were fixed in 2% paraformaldehyde, 2% glutaraldehyde (electron-microscopy grade) at room temperature for 2 h. Samples were processed, embedded and sectioned according to the standard procedure and examined on a JEOL 100CX or JEM-1230 transmission electron microscope.

Construction of expression vectors

Full length cDNA fragments were cloned into either pCS2+ or pCS2+3XFLAG vectors following amplification from cDNA synthesized from wild-type embryonic mRNA at 1-2 dpf. All the point mutations were introduced by PCR-based mutagenesis. Capped mRNAs were synthesized by in vitro transcription with the mMESSAGE kit (Ambion).

Determination of transcription start site and identification of putative transcription binding motifs

5' RACE was performed using SMART RACE cDNA Amplification Kit (Clontech) to determine the transcription start site of *trim63a*. cDNA was synthesized from mRNA extracted from wild-type embryos at 36 hpf. The RACE cDNA fragment was cloned into pCDII-TOPO (Invitrogen) for sequencing.

The ECR browser (http://ecrbrowser.dcode.org/) [47] was utilized for cross-species comparison of the upstream genomic sequences of *trim63a*. TRANSFAC 6.0 (www.generegulation.com) [48] and JASPAR (http://jaspar.genereg.net/) [49] were used to identify putative transcription factor binding sites.

In vivo GFP reporter assay

An approximately 7.0-kb genomic fragment upstream of the zebrafish *trim63a* gene (ranging from –6906 to +80 bp) was amplified from genomic DNA by PCR and cloned into the pGL3-Basic vector (Promega). The luciferase gene of this construct was then substituted by the

EGFP gene at the XbaI-NcoI junctions. A deletion series of *trim63a*-EGFP construct was generated using the ERASE-A-BASE system (Promega).

For transient expression, each deletion construct was digested with NheI and SalI to release the trim63a-EGFP reporter. 80 pg of this DNA fragment was microinjected into 1-cell stage embryos. At least 20 EGFP-positive embryos were examined at 1 and 2 days post fertilization (dpf) using a Zeiss SV-11 epifluorescence microscope and photographed by Axiocam digital camera.

Cell-based luciferase assay

A *trim63a*-luciferase deletion series was generated by replacing the regulatory sequence in the *trim63a* (-6906)-luciferase plasmid with PCR-amplified *trim63a* upstream elements down to 638 bp. Primer sequences are provided in Supplementary Table. HEK293T cells were plated into 96-well plates at a density of 32000 cells per well and cultured in Dulbecco's modified Eagle's medium (DMEM; Cellgro) supplemented with 10% fetal bovine serum (FBS; Mediatech) until an approximate confluency of 90% was reached. Transient transfection was performed in Opti-Mem (Invitrogen) using Lipofectamine^{TM} 2000 (Invitrogen) with 200 ng of the *firefly* luciferase reporter construct and 50 ng of the SV40-*Renilla* luciferase reporter construct. When cells were co-transfected with expression vector(s), the total amount of DNA transfected was set constant in the same series of experiment using pCS2+ vector as filler DNA. Luciferase activities were determined by the Dual-Glo Luciferase Assay System (Promega). The assays were conducted in triplicate at least three times, and the activity of firefly luciferase was normalized to that of Renilla luciferase for transfection efficiency and cell viability. When

indicated, transfected cells were cultured in the presence of chemical(s) or DMSO (vehicle control) for 24 hrs prior to the luciferase assay. Cells were used for assays 40-48 hrs after the start of transfection.

Zebrafish transgenesis

Zebrafish transgenesis was performed using Tol2kit system developed by the lab of Chi-Bin Chien [50]. For the *cmlc2*:*trim63a-IRES-EGFP* construct, the cardiac-specific *cmlc2* promoter (-870-+34) [51] was amplified from zebrafish genomic DNA and cloned into the 5' Gateway entry vector (p5E). The PCR fragment of the *trim63a* coding region was cloned into the middle entry vector (pENTR-SH). These entry clones and the 3' entry vector (p3E) containing *IRES-EGFP*pA were subjected to the multisite recombination reaction to the pDestTol2pA2 destination vector by LR clonase II Plus (Invitrogen) to generate the transgene construct flanked by Tol2 sites. Similarly, the *cmlc2*:*FLAG-foxo3a-IRES-EGFP* construct was generated using the same 5' and 3' entry vector, and the middle entry vector containing the *FLAG*-tagged *foxo3a* gene was amplified from the pCS2+-*FLAG-foxo3a* construct. Wildtype AB embryos were injected at 1-cell stage with 10-20 pg of the transgene plasmid and 20 pg of mRNA encoding Tol2 transposase. Transiently transgenic embryos exhibiting cardiac-specific EGFP expression were screened and raised to adulthood as founders. Embryos resulting from crosses between each of the founder fish and a wild-type fish were screened for cardiac-specific EGFP expression to identify germline-transmitting founders.

Western blotting

HEK293T cells were serum-starved with 0.05% FBS in DMEM for 16 hrs, washed with phosphate-buffered saline (PBS) before lysed in RIPA buffer (50 mM Tris-HCl (pH.8.0), 150 mM NaCl, 1% NP-40, and 0.5% sodium deoxycholate) supplemented with protease and phosphatase inhibitors (Complete Mini Protease Inhibitor Cocktail and PhosStop; Roche). The whole cell lysates were subjected to SDS-PAGE. Separated proteins were transferred onto a nitrocellulose membrane, which was analyzed by immunoblotting with anti-phospho-FoxO1 (Thr24)/FoxO3a (Thr32) (1:1000, clone 9496, Cell Signaling) or anti-FLAG (1:10000, clone M2, Sigma-Aldrich) antibody.

Whole-mount in situ hybridization and immunostaining

Whole-mount in situ hybridization was performed as preciously described [52]. The antisense RNA probes used in this study (*trim63a*, trim*63b*, *foxo1a*, *foxo1b*, *foxo3a*, *foxo3b*, *foxo4*, *foxo5a*, and *foxo5b*) were synthesized from a partial genomic coding fragment (*foxo5a*) or full-length cDNA fragments (all others) and were cloned into the pCS2+ vector. Embryos were photographed using Axiocam digital camera.

For whole-mount immunefluorescence staining, embryos were permeabilized with acetone, blocked with 2% BSA in PBTx (PBS containing 1% TritonX) prior to staining. Both primary and secondary staining procedures were performed overnight in the blocking solution containing antibodies at 4°C. Staining with Phalloidin (1:50, Sigma-Aldrich) was carried out concurrently with secondary staining. The antibodies used in this study are anti-sarcomeric α-

actinin (1:10000, clone EA53, Sigma) and Zn8 (1:100, Developmental Studies Hybridoma Bank). Following staining, the pericardium was carefully removed with fine forceps to expose the heart region and fluorescence images were acquired using LSM 510 confocal microscope (Zeiss) with a 40x water objective.

Figure 3-1. Myofibrillar structures are not maintained in *tre* cardiomyocytes.

(A) Embryos were stained for F-actin (upper panel) and α-actinin (lower panel) at different time points during embryogenesis. At 30 hpf, overall cardiac morphology and filamentous network are distinguishable between wildtype and *tre* hearts. Also, nascent sarcomere structures are observed both in wildtype and *tre* hearts as indicated by periodic dots of α-actinin (arrowheads). The wildtype heart undergoes looping and ballooning processes as development progresses and myofibrils become mature and more organized. In contrast, the *tre* heart fails to undergo proper morphological change and exhibits severe myofibrillar disarray. Insets are same images at higher magnification. (B) Embryos were stained with the antibody against Zn8, a cell surface marker. Cardiomyosytes in *tre* mutant display rounded shape as development proceeds. Insets are same images at higher magnification. (C) Electron micrographs showing severe myofibrillar disarray in *tre* cardiomyocytes characterized by discontinuous myofilaments. Scale bars in main panel, 50 μm; in inset, 20 μm.

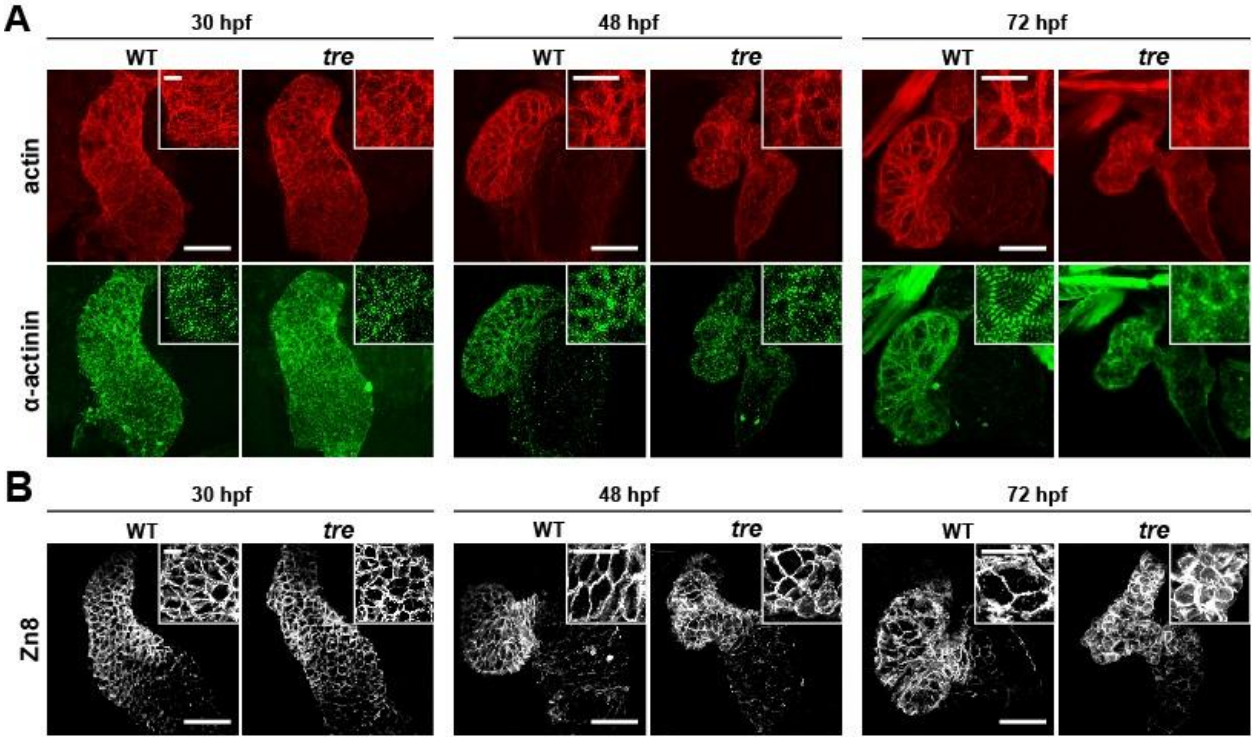
A
30 hpf
48 hpf
72 hpf
WT
tre
actin
α-actinin
B
Zn8

Figure 3-2. *trim63* genes are significantly upregulated in the *tre* mutant heart.

(A) Phylogenetic tree of vertebrate *trim63, 55* and *54* (also known as *MuRF1, 2* and *3*, respectively). The tree was constructed using ClustalX with the neighbor-joining method. Zebrafish (z), Human (h), mouse (m), rat (r), chick (g), frog (x). (B) Real-time PCR analysis of *trim63a* and *b* with SYBR Green. Total RNA was isolated from d2 embryonic hearts. The expression levels of *trim63a* and *trim63b* are both upregulated in *tre* hearts. (C) In situ hybridization analysis showed significant induction of *trim63a* and *trim63b* specifically in the heart at 48 and 72 hpf.

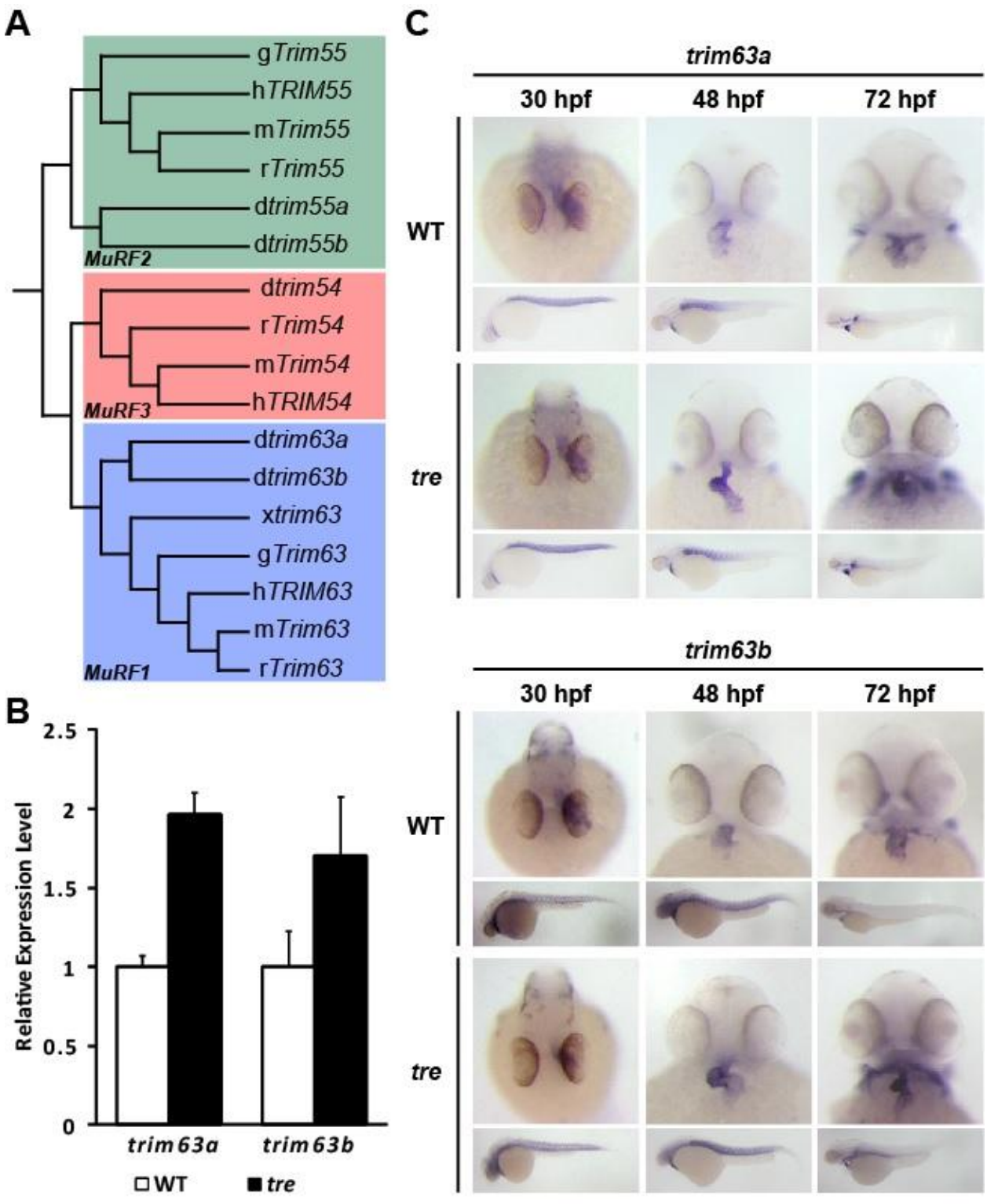
A
gTrim55
hTRIM55
mTrim55
rTrim55
dtrim55a
dtrim55b
MuRF2
dtrim54
rTrim54
mTrim54
hTRIM54
MuRF3
dtrim63a
dtrim63b
xtrim63
gTrim63
hTRIM63
mTrim63
rTrim63
MuRF1
B
Relative Expression Level
2.5
2
1.5
1
0.5
0
trim63a
trim63b
WT
tre
C
trim63a
30 hpf
48 hpf
72 hpf
WT
tre
trim63b
30 hpf
48 hpf
72 hpf
WT
tre

Figure 3-3. Upregulation of *trim63a* leads to myofibrillar disarray.

(A) Transgenic construct for the expression of *trim63a* specifically in the heart. The *trim63a* followed by an *IRES-EGFP* fragment is driven by the cardiac specific *myl7* promoter. (B) Gross cardiac morphology of wildtype and Tg(*myl7*:*trim63a-IRES-EGFP*) fish at 72 hpf. Transgenic fish exhibit dilated cardiac chambers and lack of cardiac looping with severe pericardial edema (upper panel). Inset in the upper panel shows expression of the GFP reporter in the heart that is driven bicistronically. In these transgenic fish, *trim63a* expression is strongly upregulated in the heart as revealed by in situ hybridization (lower panel). (C) Representative line-scan images of wildtype, *tre* and Tg(*myl7*:*trim63a-IRES-EGFP*) atria at 72 hpf. (D) Heart rate (upper panel) and atrial fraction shortening (lower panel) deduced from line-scan images.

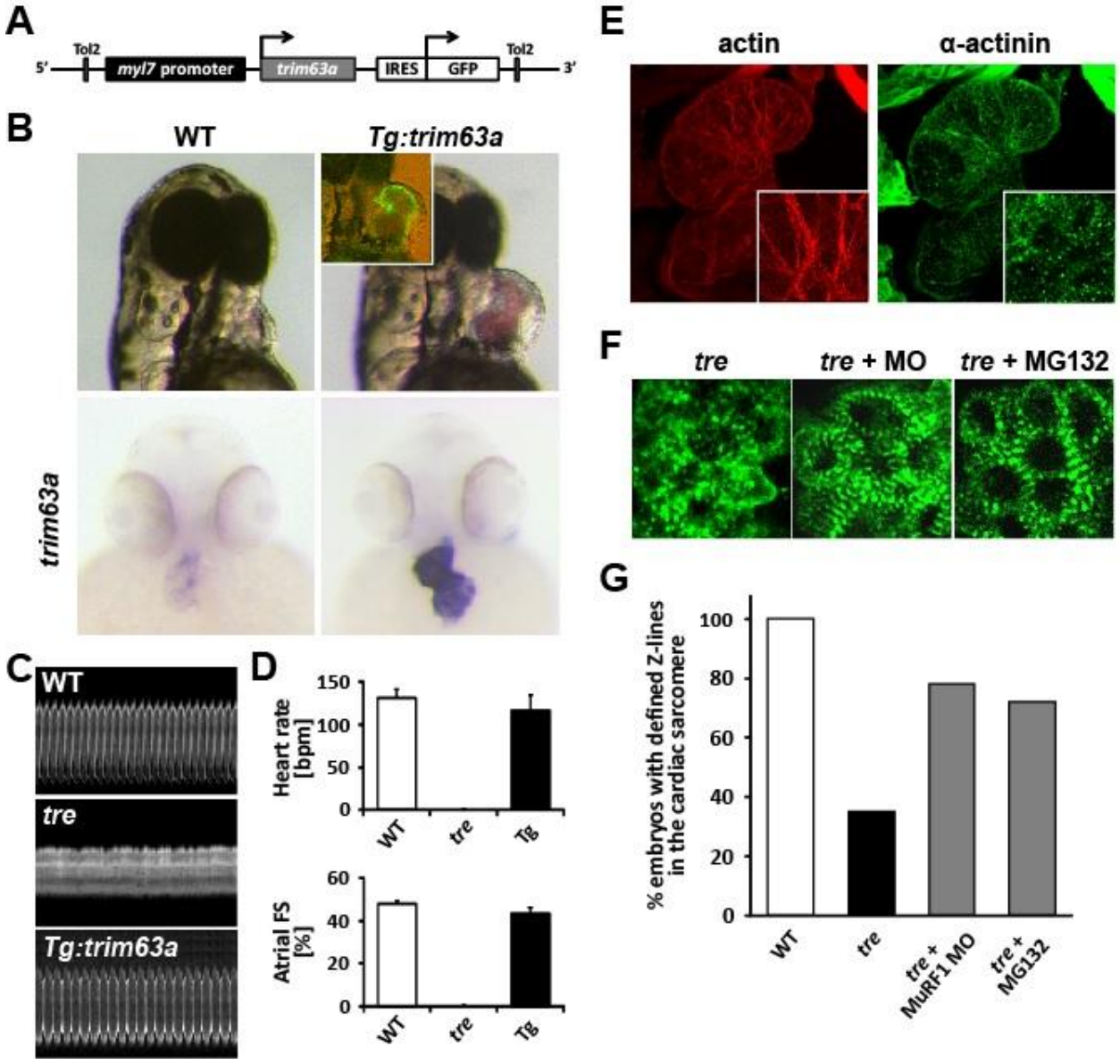
A
Tol2
5'
myl7 promoter
trim63a
IRES
GFP
Tol2
3'
B
WT
Tg:trim63a
trim63a
C
WT
tre
Tg:trim63a
D
Heart rate [bpm]
150
100
50
0
WT
tre
Tg
Atrial FS [%]
60
40
20
0
WT
tre
Tg
E
actin
α-actinin
F
tre
tre + MO
tre + MG132
G
% embryos with defined Z-lines in the cardiac sarcomere
100
80
60
40
20
0
WT
tre
tre + MuRF1 MO
tre + MG132

Figure 3-4. A 638 bp upstream regulatory element recapitulates the endogenous expression of *trim63a* and is activated in response to elevated levels of Ca^{2+}.

(A) Schematic representation of the GFP reporter with deletion series of the *trim63a* upstream sequence. Followed each construct is the presence (+) or absence (-) of the GFP expression both in the heart and somites. (B) Representative image of transient GFP expression in the somites (left panel) and the heart (right panel) of the 48 hpf embryo. Arrows indicate cardiomyocytes expressing GFP. (C) Transgenic zebrafish embryo stably expressing GFP under the control of the *trim63a* (-6906)-GFP promoter. The GFP expression recapitulates the endogenous *trom63a* expression in the somites (left panel) and the heart (right panel). The inset in the left panel shows the GFP expression in the somites at a higher magnification. The asterisk denotes auto-fluorescence from the yolk that is independent of expression of the reporter construct. (D) Luciferase assay of the *trim63a* (-638) reporter. Promoter activities were analyzed in HEK293T cells treated with either DMSO or 0.5 uM A23187 for 12 or 24 hours. Values are shown as the fold increase in luciferase activity of cells treated with DMSO for 12 hours. Activities of the *trim63a* (-638) promoter were significantly induced by A23187 in a time-dependent manner. (E) Comparison of Ca^{2+} responsiveness between *trim63a* (-638) and *trim63a* (-6906) promoters assessed by luciferase assay. Fold inductions of luciferase activities by treatment with 0.5 mM A23187 for 12 or 24 hours were shown.

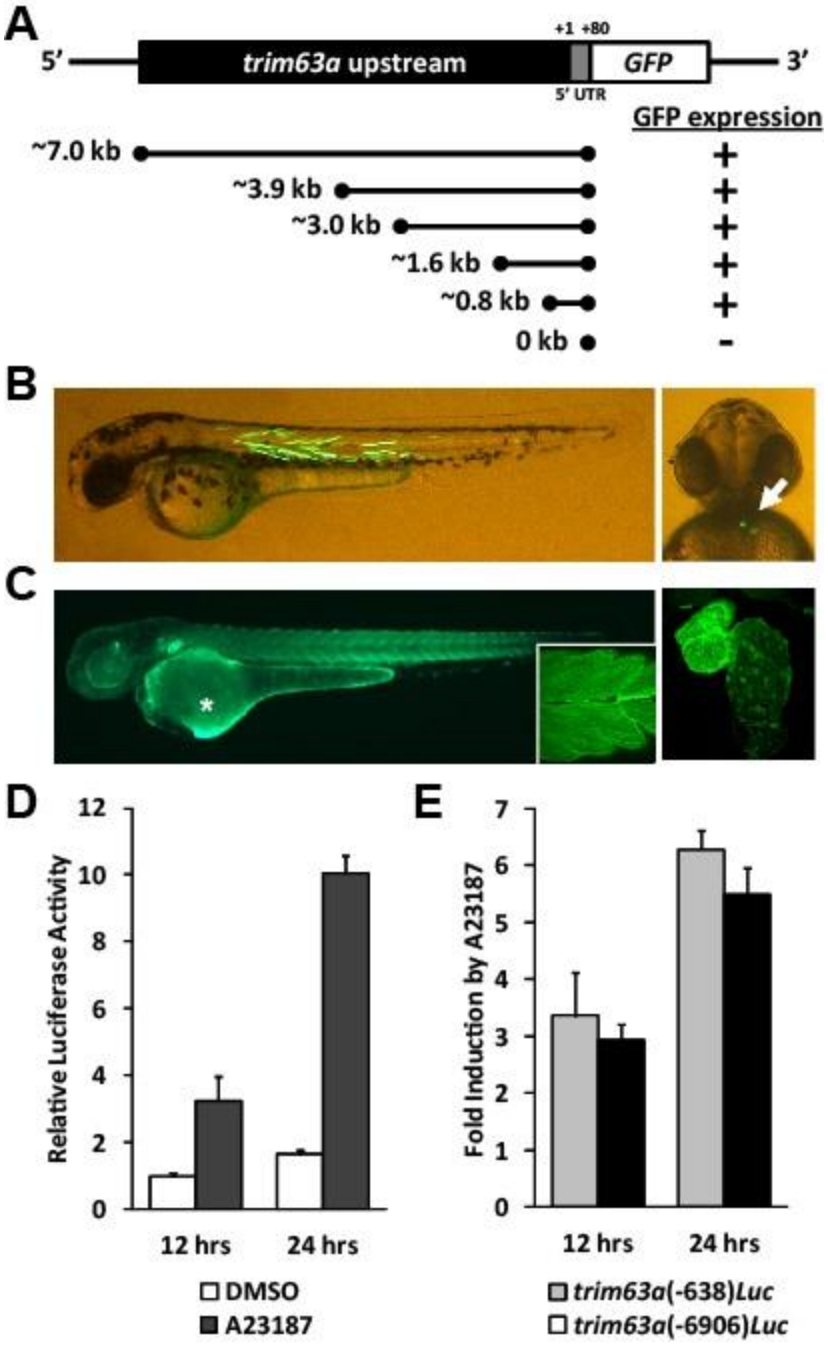
A
5'
trim63a upstream
+1 +80
GFP
3'
5' UTR
GFP expression
~7.0 kb
~3.9 kb
~3.0 kb
~1.6 kb
~0.8 kb
0 kb
+
+
+
+
+
-
B
C
*
D
Relative Luciferase Activity
0
2
4
6
8
10
12
12 hrs
24 hrs
DMSO
A23187
E
Fold Induction by A23187
0
1
2
3
4
5
6
7
12 hrs
24 hrs
trim63a(-638)Luc
trim63a(-6906)Luc

Figure 3-5. Ca^{2+}-dependent expression of *trim63a* mediated by foxO transcription factors. (A) HEK293T cells were transiently transfected with the *trim63a* (-638) luciferase reporter construct. After incubation in the presence of DMSO, FK506 or KN62, cells were treated with DMSO or A23187. Values are expressed relative to the luciferase activity of cells treated with DMSO. (B) Serial deletion fragments of the *trim63a* (-638) reporter were generated and transcriptional activities of these fragments were examined in HEK293T cells. The relative position of each deletion construct is shown on the left. Activity of each promoter reporter construct is shown relative to that of the empty expression plasmid. (C) Alignment of the Trim63/trim63a promoter sequence containing the putative NFAT- and FoxO binding elements from zebrafish, medaka, fugu, mouse and human. Putative NFAT- and FoxO-binding sites are boxed. Asterisks indicate conserved nucleotides. (D) Whole-mount in situ hybridization demonstrating the expression of foxo3a in the heart at 24 and 48 hpf. Cardiac expression of foxo3a is comparable between wildtype and *tre* embryos. (E) HEK293T cells were transiently cotransfected with different doses of nfat or foxo3a expression plasmid with the *trim63a* (-638) luciferase reporter plasmid. Values are shown relative to the luciferase activity of cells transfected with the *trim63a* (-638) reporter plasmid alone. (F) Luciferase assay of the *trim63a* (-638) reporter plasmid in HEK293T cells cotransfected with wildtype or dominant negative foxo3a expression plasmid. Following transfection, cells were stimulated with A23187. The luciferase activities in cells transfected with these expression constructs are shown relative to that in DMSO-treated cells transfected with an empty expression plasmid.

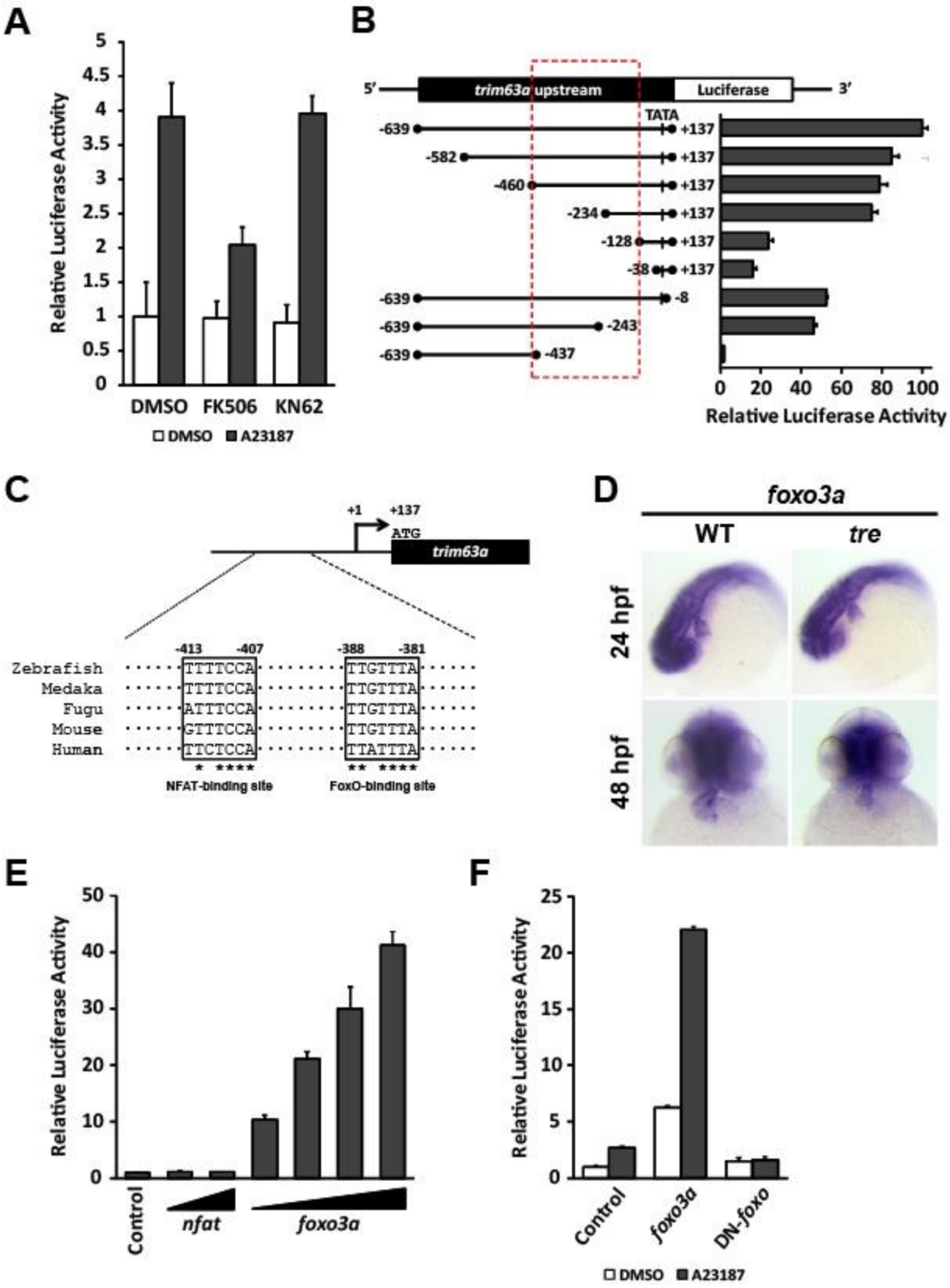
A
Relative Luciferase Activity
5
4.5
4
3.5
3
2.5
2
1.5
1
0.5
0
DMSO FK506 KN62
DMSO A23187
B
5'
trim63a upstream
Luciferase
3'
TATA
-639 +137
-582 +137
-460 +137
-234 +137
-128 +137
-38 +137
-639 -8
-639 -243
-639 -437
0 20 40 60 80 100
Relative Luciferase Activity
C
+1 +137
ATG
trim63a
-413 -407 -388 -381
Zebrafish TTTTCCA TTGTTTA
Medaka TTTTCCA TTGTTTA
Fugu ATTTCCA TTGTTTA
Mouse GTTTCCA TTGTTTA
Human TTCTCCA TTATTTA
* **** ** ****
NFAT-binding site
FoxO-binding site
D
foxo3a
WT
tre
24 hpf
48 hpf
E
Relative Luciferase Activity
50
40
30
20
10
0
Control
nfat
foxo3a
F
Relative Luciferase Activity
25
20
15
10
5
0
Control
foxo3a
DN-foxo
DMSO A23187

Figure 3-6. FoxO upregulates trim63a expression downstream of the Cn pathway.

(A) HEK293T cells transiently coexpressing FLAG-tagged zebrafish foxo3a with wildtype zebrafish calcineurin (WT-Cn) or dominant-negative form of zebrafish calcineurin (DN-Cn) were stimulated with 5 uM A23187 for 15 minutes. Changes in levels of phosphorylated FoxO3a (P-FoxO3a) were analyzed by western blotting with antibodies against p-FoxO3^{The32} (top) and β-actin (bottom). (B) Luciferase assay of the *trim63a* (-638) reporter plasmid in HEK293T cells cotransfected with wildtype calcineurin (WT-Cn) or dominant-negative form of calcineurin (DN-Cn). Cells were stimulated with A23187 and then luciferase activities were analyzed. Values are expressed relative to the luciferase activity of cells transfected with empty expression vector without A23187 stimulation.

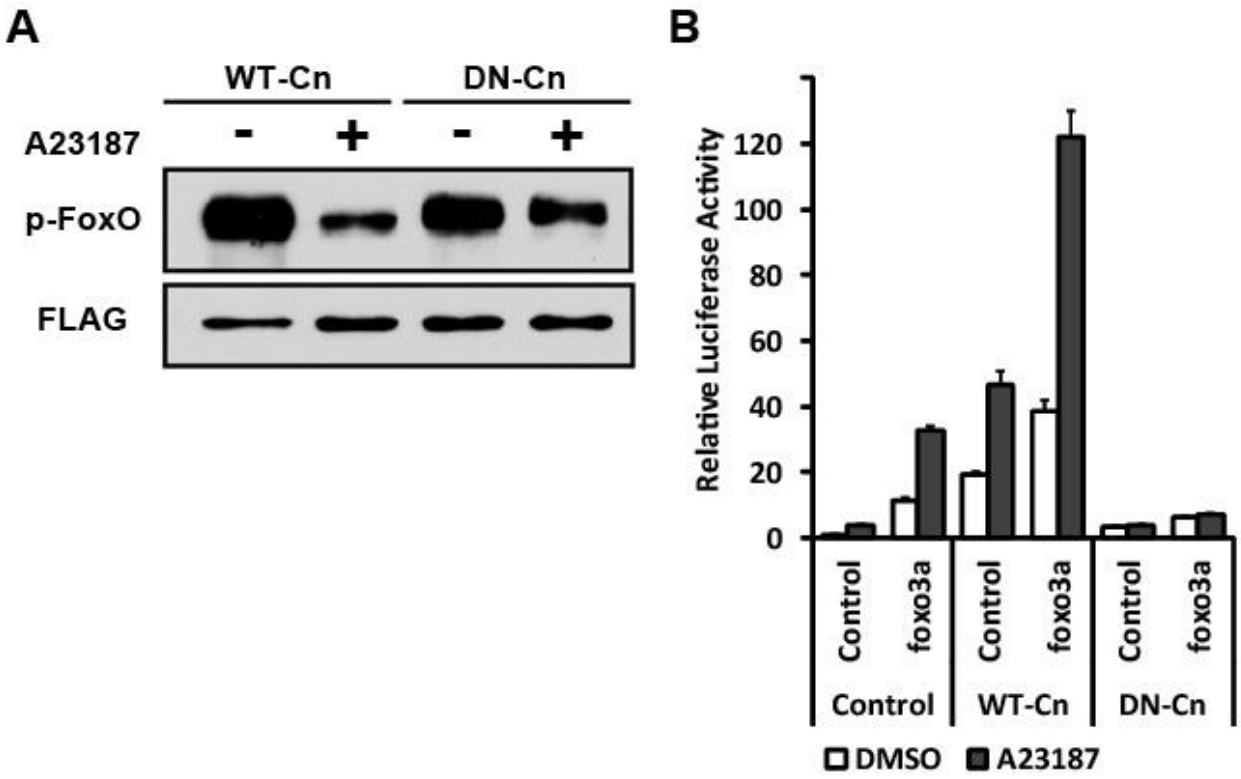
A
WT-Cn
DN-Cn
A23187
-
+
-
+
p-FoxO
FLAG
B
Relative Luciferase Activity
120
100
80
60
40
20
0
Control
foxo3a
Control
foxo3a
Control
foxo3a
Control
WT-Cn
DN-Cn
DMSO
A23187

Figure 3-7. FoxO3a induces the expression of trim63a in the zebrafish heart.

(A) Immunostaining for the FLAG epitope (red) in 30 hpf wildtype and *tre* embryos transiently expressing FLAG-tagged FoxO3a. DAPI marks nuclei (blue). FoxO3 protein is preferentially localized to nuclei in *tre* cardiomyocytes. Scale bars: 20 um. (B) In situ hybridization of 48 hpf embryos with trim63a riboprobe. The expression of trim63a in control (uninjected) embryos is compared with that in foxo3a mRNA-injected or FK506-treated embryos. (C) Immunostaining for the α-actinin protein in 48 hpf zebrafish embryos. Integrity of cardiac saromeres in control (uninjected) embryos is compared with that in mRNA-injected (constitutively active or dominant negative form of foxo3a.) embryos. (D) Schematic representation of the model for aberrant Ca^{2+}-induced myofibril disarray in the *tre* heart. Aberrant Ca^{2+} homeostasis activates the calcineurin signaling pathway, leading to phosphorylation FoxO transcription factors. Phosphorylated FoxOs are translocated into the nucleus and upregulate *MuRF1* expression, resulting in degradation of myofibril structures via proteasome-dependent protein degradation system.

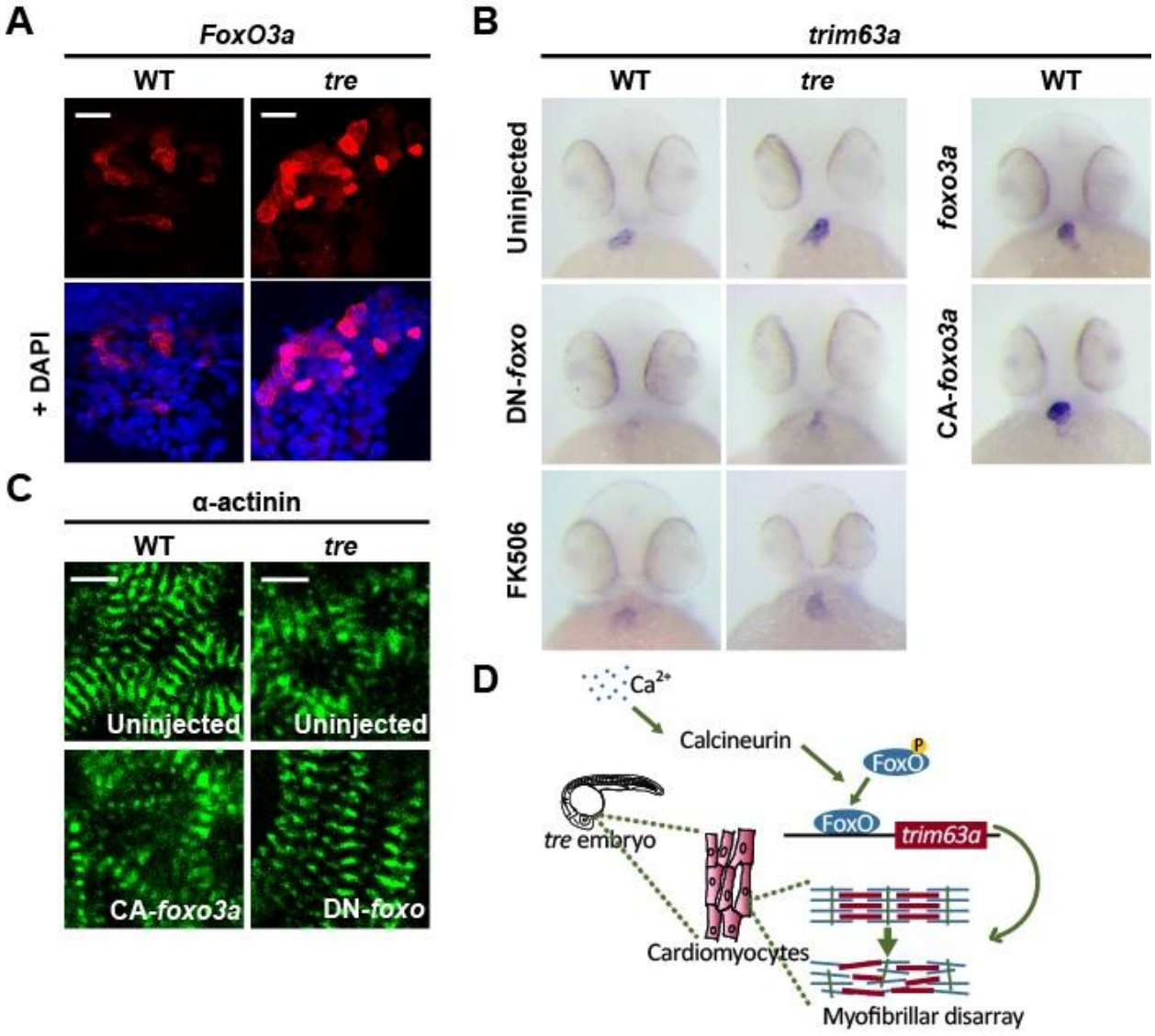
A
FoxO3a
WT
tre
+ DAPI
B
trim63a
WT
tre
WT
Uninjected
foxo3a
DN-foxo
CA-foxo3a
FK506
C
α-actinin
WT
tre
Uninjected
Uninjected
CA-foxo3a
DN-foxo
D
Ca2+
Calcineurin
FoxO
P
FoxO
trim63a
tre embryo
Cardiomyocytes
Myofibrillar disarray

Supplementary Figure 3-1. Myofibrillar structures are not maintained in the heart of *ncx1h* morphants.

(A) As seen in the *tre* heart, *ncx1h* morphant heart exhibits dysmorphologenesis and develop severe myofibrillar disarray. Insets are same images at higher magnification. Scale bars in main panel, 50 μm; in inset, 20 μm.

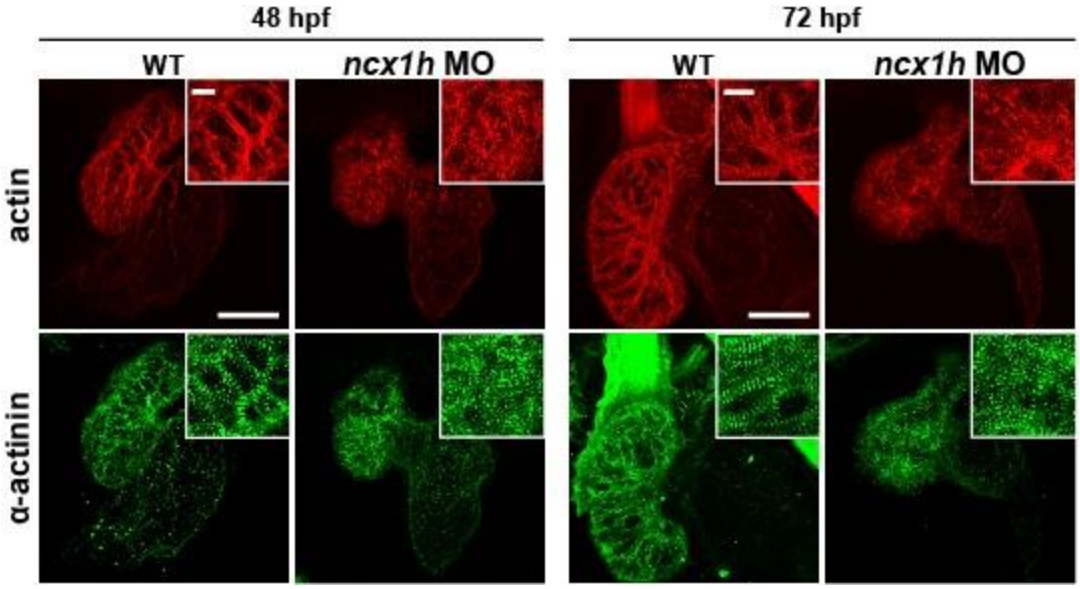
48 hpf
72 hpf
WT
ncx1h MO
WT
ncx1h MO
actin
α-actinin

Supplementary Figure 3-2. Expression patterns and Ca^{2+} responsiveness of zebrafish *foxo* genes.

(A) Whole-mount in situ hybridization analysis showing foxo expression in zebrafish embryos. While *foxo6a* expression is diminished by 48 hf, all the other foxo genes examined (*foxo1a*, *1b*, *3b*, *4*, *6a* and *6b*) are expressed in the heart throughout development. (B) Luciferase assay of the *trim63a* (-638) reporter plasmid in HEK293T cells cotransfected with different *foxo* genes. Following transfection, cells were stimulated with A23187. The luciferase activities in cells transfected with these expression constructs are shown relative to that in DMSO-treated cells transfected with an empty expression plasmid.

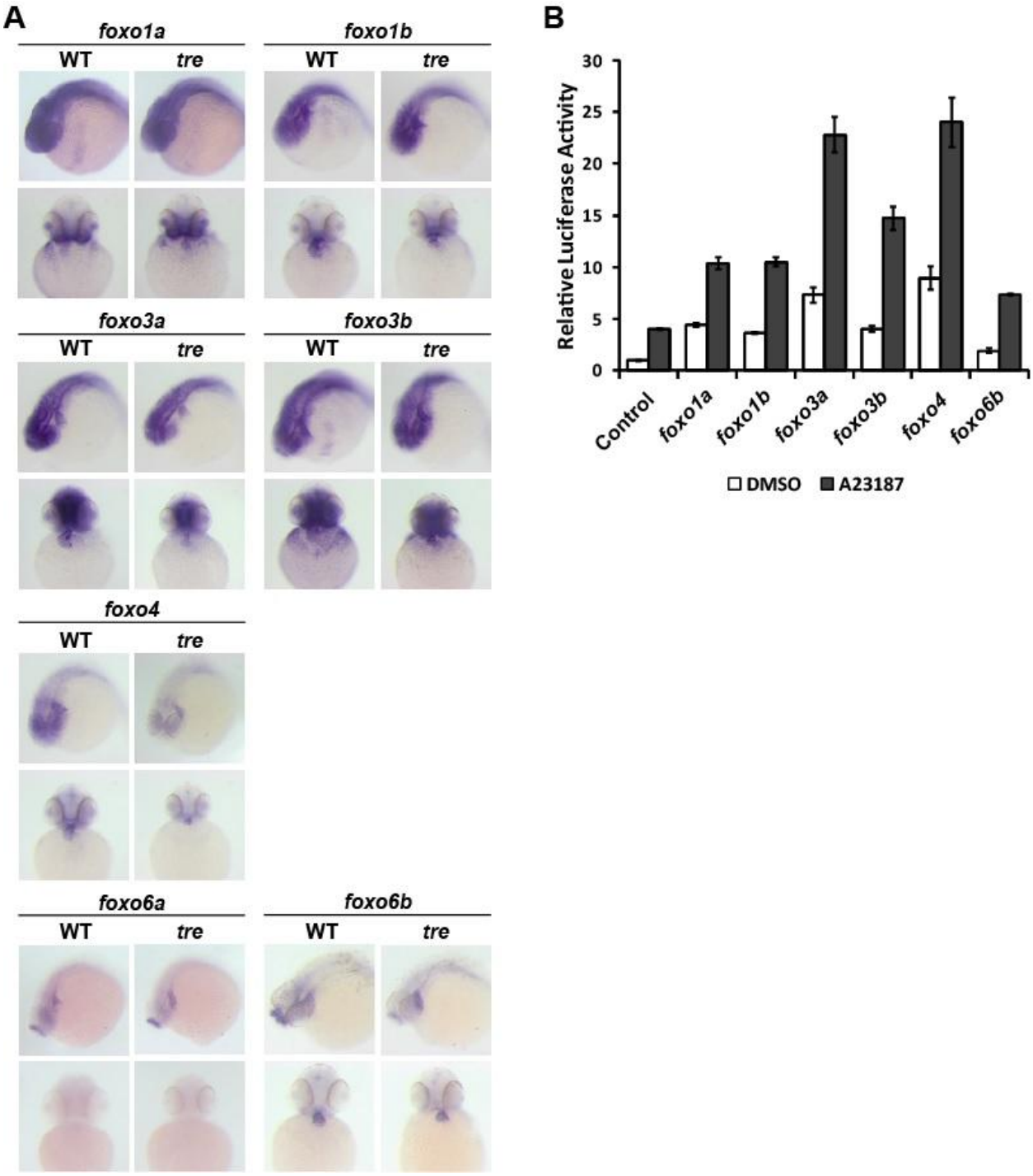
A
foxo1a
WT
tre
foxo1b
WT
tre
foxo3a
WT
tre
foxo3b
WT
tre
foxo4
WT
tre
foxo6a
WT
tre
foxo6b
WT
tre
B
Relative Luciferase Activity
30
25
20
15
10
5
0
Control
foxo1a
foxo1b
foxo3a
foxo3b
foxo4
foxo6b
DMSO
A23187

F. References

1. Bers DM. Cardiac excitation-contraction coupling. Nature. 2002;415(6868):198-205.

2. Yano M, Ikeda Y, Matsuzaki M. Altered intracellular Ca^{2+} handling in heart failure. J Clin Invest. 2005;115(3):556-64.

3. Luo M, Anderson ME. Mechanisms of altered Ca^{2+} handling in heart failure. CircRes. 2013;113(6):690-708.

4. Morita H, Seidman J, Seidman CE. Genetic causes of human heart failure. J Clin Invest. 2005;115(3):518-26.

5. Molkentin JD, Lu JR, Antos CL, Markham B, Richardson J, Robbins J, Grant SR, Olson EN. A calcineurin-dependent transcriptional pathway for cardiac hypertrophy. Cell. 1998;93(2):215-28.

6. Backs J, Backs T, Neef S, Kreusser MM, Lehmann LH, Patrick DM, Grueter CE, Qi X, Richardson JA, Hill JA, Katus HA, Bassel-Duby R, Maier LS, Olson EN. The delta isoform of CaM kinase II is required for pathological cardiac hypertrophy and remodeling after pressure overload. Proc Natl Acad Sci U S A. 2009;106(7):2342-7.

7. Backs J, Song K, Bezprozvannaya S, Chang S, Olson EN. CaM kinase II selectively signals to histone deacetylase 4 during cardiomyocyte hypertrophy. J Clin Invest. 2006;116(7):1853-64.

8. Zhang T, Kohlhaas M, Backs J, Mishra S, Phillips W, Dybkova N, Chang S, Ling H, Bers DM, Maier LS, Olson EN, Brown JH. CaMKIIdelta isoforms differentially affect calcium handling but similarly regulate HDAC/MEF2 transcriptional responses. J Biol Chem. 2007;282(48):35078-87.

9. Bodine SC, Latres E, Baumhueter S, Lai VK, Nunez L, Clarke BA, Poueymirou WT, Panaro FJ, Na E, Dharmarajan K, Pan ZQ, Valenzuela DM, DeChiara TM, Stitt TN, Yancopoulos GD, Glass DJ. Identification of ubiquitin ligases required for skeletal muscle atrophy. Science. 2001;294(5547):1704-8.

10. Kedar V, McDonough H, Arya R, Li HH, Rockman HA, Patterson C. Muscle-specific RING finger 1 is a bona fide ubiquitin ligase that degrades cardiac troponin I. Proc Natl Acad Sci U S A. 2004;101(52):18135-40.

11. Clarke BA, Drujan D, Willis MS, Murphy LO, Corpina RA, Burova E, Rakhilin SV, Stitt TN, Patterson C, Latres E, Glass DJ. The E3 Ligase MuRF1 degrades myosin heavy chain protein in dexamethasone-treated skeletal muscle. Cell Metab. 2007;6(5):376-85.

12. Cohen S, Brault JJ, Gygi SP, Glass DJ, Valenzuela DM, Gartner C, Latres E, Goldberg AL. During muscle atrophy, thick, but not thin, filament components are degraded by MuRF1-dependent ubiquitylation. J Cell Biol. 2009;185(6):1083-95.

13. Pagan J, Seto T, Pagano M, Cittadini A. Role of the ubiquitin proteasome system in the heart. Circ Res. 2013;112(7):1046-58.

14. Lyon RC, Lange S, Sheikh F. Breaking down protein degradation mechanisms in cardiac muscle. Trends Mol Med. 2013;19(4):239-49.

15. Gregorio CC, Perry CN, McElhinny AS. Functional properties of the titin/connectin-associated proteins, the muscle-specific RING finger proteins (MURFs), in striated muscle. J Muscle Res Cell Motil. 2005;26(6-8):389-400.

16. McElhinny AS, Kakinuma K, Sorimachi H, Labeit S, Gregorio CC. Muscle-specific RING finger-1 interacts with titin to regulate sarcomeric M-line and thick filament structure and may have nuclear functions via its interaction with glucocorticoid modulatory element binding protein-1. J Cell Biol. 2002;157(1):125-36.

17. Chen SN, Czernuszewicz G, Tan Y, Lombardi R, Jin J, Willerson JT, Marian AJ. Human molecular genetic and functional studies identify TRIM63, encoding Muscle RING Finger Protein 1, as a novel gene for human hypertrophic cardiomyopathy. Circ Res. 2012 Sep 14;111(7):907-19.

18. Willis MS, Ike C, Li L, Wang DZ, Glass DJ, Patterson C. Muscle ring finger 1, but not muscle ring finger 2, regulates cardiac hypertrophy in vivo. Circ Res.2007;100(4):456-9.

19. Eijkelenboom A, Burgering BM. FOXOs: signalling integrators for homeostasis maintenance. Nat Rev Mol Cell Biol. 2013;14(2):83-97.

20. van der Horst A, Burgering BM. Stressing the role of FoxO proteins in lifespan and disease. Nat Rev Mol Cell Biol. 2007;8(6):440-50.

21. Sacheck JM, Ohtsuka A, McLary SC, Goldberg AL. IGF-I stimulates muscle growth by suppressing protein breakdown and expression of atrophy-related ubiquitin ligases, atrogin-1 and MuRF1. Am J Physiol Endocrinol Metab. 2004;287(4):E591-601.

22. Stitt TN, Drujan D, Clarke BA, Panaro F, Timofeyva Y, Kline WO, Gonzalez M,Yancopoulos GD, Glass DJ. The IGF-1/PI3K/Akt pathway prevents expression of muscle atrophy-induced ubiquitin ligases by inhibiting FOXO transcription factors. Mol Cell. 2004;14(3):395-403.

23. Lecker SH, Jagoe RT, Gilbert A, Gomes M, Baracos V, Bailey J, Price SR, Mitch WE, Goldberg AL. Multiple types of skeletal muscle atrophy involve a common program of changes in gene expression. FASEB J. 2004;18(1):39-51.

24. Zhao J, Brault JJ, Schild A, Cao P, Sandri M, Schiaffino S, Lecker SH, Goldberg AL. FoxO3 coordinately activates protein degradation by the autophagic/lysosomal and proteasomal pathways in atrophying muscle cells. Cell Metab. 2007;6(6):472-83.

25. Waddell DS, Baehr LM, van den Brandt J, Johnsen SA, Reichardt HM, Furlow JD, Bodine SC. The glucocorticoid receptor and FOXO1 synergistically activate the skeletal muscle atrophy-associated MuRF1 gene. Am J Physiol Endocrinol Metab. 2008;295(4):E785-97.

26. Langenbacher AD, Dong Y, Shu X, Choi J, Nicoll DA, Goldhaber JI, Philipson KD, Chen JN. Mutation in sodium-calcium exchanger 1 (NCX1) causes cardiac fibrillation in zebrafish. Proc Natl Acad Sci U S A. 2005;102(49):17699-704.

27. Ebert AM, Hume GL, Warren KS, Cook NP, Burns CG, Mohideen MA, Siegal G, Yelon D, Fishman MC, Garrity DM. Calcium extrusion is critical for cardiac morphogenesis and rhythm in embryonic zebrafish hearts. Proc Natl Acad Sci U S A. 2005;102(49):17705-10.

28. Koushik SV, Wang J, Rogers R, Moskophidis D, Lambert NA, Creazzo TL, Conway SJ. Targeted inactivation of the sodium-calcium exchanger (Ncx1) results in the lack of a heartbeat and abnormal myofibrillar organization. FASEB J. 2001;15(7):1209-11.

29. Wakimoto K, Fujimura H, Iwamoto T, Oka T, Kobayashi K, Kita S, Kudoh S, Kuro-o M, Nabeshima Yi, Shigekawa M, Imai Y, Komuro I. Na^{+}/Ca^{2+} exchanger-deficient mice have disorganized myofibrils and swollen mitochondria in cardiomyocytes. Comp Biochem Physiol B Biochem Mol Biol. 2003;135(1):9-15.

30. Horackova M, Morash B, Byczko Z. Altered transarcolemmal Ca transport modifies the myofibrillar ultrastructure and protein metabolism in cultured adult ventricular cardiomyocytes. Mol Cell Biochem. 2000;204(1-2):21-33.

31. Meyer A, Schartl M. Gene and genome duplications in vertebrates: the one-to-four (-to-eight in fish) rule and the evolution of novel gene functions. Curr Opin Cell Biol. 1999;11(6):699-704.

32. Herrmann S, Lipp P, Wiesen K, Stieber J, Nguyen H, Kaiser E, Ludwig A. The cardiac sodium-calcium exchanger NCX1 is a key player in the initiation and maintenance of a stable heart rhythm. Cardiovasc Res. 2013;99(4):780-8.

33. Skurk C, Izumiya Y, Maatz H, Razeghi P, Shiojima I, Sandri M, Sato K, Zeng L, Schiekofer S, Pimentel D, Lecker S, Taegtmeyer H, Goldberg AL, Walsh K. The FOXO3a transcription

factor regulates cardiac myocyte size downstream of AKT signaling. J Biol Chem. 2005;280(21):20814-23.

34. Paula-Gomes S, Gonçalves DA, Baviera AM, Zanon NM, Navegantes LC, Kettelhut IC. Insulin Suppresses Atrophy- and Autophagy-related Genes in Heart Tissue and Cardiomyocytes Through AKT/FOXO Signaling. Horm Metab Res. 2013;45(12):849-55.

35. Wang M, Zhang X, Zhao H, Wang Q, Pan Y. FoxO gene family evolution in vertebrates. BMC Evol Biol. 2009;9:222.

36. van den Heuvel AP, Schulze A, Burgering BM. Direct control of caveolin-1 expression by FOXO transcription factors. Biochem J. 2005;385(Pt3):795-802.

37. Medema RH, Kops GJ, Bos JL, Burgering BM. AFX-like Forkhead transcription factors mediate cell-cycle regulation by Ras and PKB through p27kip1. Nature.2000;404(6779):782-7.

38. Brunet A, Bonni A, Zigmond MJ, Lin MZ, Juo P, Hu LS, Anderson MJ, Arden KC, Blenis J, Greenberg ME. Akt promotes cell survival by phosphorylating and inhibiting a Forkhead transcription factor. Cell. 1999 Mar 19;96(6):857-68.

39. Pearcé PC, Hawkey C, Symons C, Olsen EG. Role of calcium in the induction of cardiac hypertrophy and myofibrillar disarray. Experimental studies of a possible cause of hypertrophic cardiomyopathy. Br Heart J. 1985;54(4):420-7.

40. Willis MS, Rojas M, Li L, Selzman CH, Tang RH, Stansfield WE, Rodriguez JE, Glass DJ, Patterson C. Muscle ring finger 1 mediates cardiac atrophy in vivo. Am J Physiol Heart Circ Physiol. 2009;296(4):H997-H1006.

41. Adams V, Linke A, Gielen S, Erbs S, Hambrecht R, Schuler G. Modulation of Murf-1 and MAFbx expression in the myocardium by physical exercise training. Eur J Cardiovasc Prev Rehabil. 2008;15(3):293-9.

42. Willis MS, Schisler JC, Li L, Rodríguez JE, Hilliard EG, Charles PC, Patterson C. Cardiac muscle ring finger-1 increases susceptibility to heart failure in vivo. Circ Res. 2009;105(1):80-8.

43. Vega RB, Bassel-Duby R, Olson EN. Control of cardiac growth and function by calcineurin signaling. J Biol Chem. 2003;278(39):36981-4.

44. Westerfield, M. (1995). The Zebrafish Book. A Guide for the Laboratory Use of Zebrafish (*Danio rerio*). Eugene: University of Oregon.

45. Kimmel CB, Ballard WW, Kimmel SR, Ullmann B, Schilling TF. Stages of embryonic development of the zebrafish. Dev Dyn. 1995;203(3):253-310.

46. Burns CG, MacRae CA. Purification of hearts from zebrafish embryos. Biotechniques. 2006 Mar;40(3):274, 276, 278 passim. Erratum in: Biotechniques. 2006;40(5):596.

47. Ovcharenko I, Nobrega MA, Loots GG, Stubbs L. ECR Browser: a tool for visualizing and accessing data from comparisons of multiple vertebrate genomes. Nucleic Acids Res. 2004;32:W280-6.

48. Matys V, Kel-Margoulis OV, Fricke E, Liebich I, Land S, Barre-Dirrie A, Reuter I, Chekmenev D, Krull M, Hornischer K, Voss N, Stegmaier P, Lewicki-Potapov B, Saxel H, Kel AE, Wingender E. TRANSFAC and its module TRANSCompel: transcriptional gene regulation in eukaryotes. Nucleic Acids Res. 2006;34:D108-10.

49. Bryne JC, Valen E, Tang MH, Marstrand T, Winther O, da Piedade I, Krogh A, Lenhard B, Sandelin A. JASPAR, the open access database of transcription factor-binding profiles: new content and tools in the 2008 update. Nucleic Acids Res. 2008;36:D102-6.

50. Kwan KM, Fujimoto E, Grabher C, Mangum BD, Hardy ME, Campbell DS, Parant JM, Yost HJ, Kanki JP, Chien CB. The Tol2kit: a multisite gateway-based construction kit for Tol2 transposon transgenesis constructs. Dev Dyn. 2007;236(11):3088-99.

51. Huang CJ, Tu CT, Hsiao CD, Hsieh FJ, Tsai HJ. Germ-line transmission of a myocardium-specific GFP transgene reveals critical regulatory elements in the cardiac myosin light chain 2 promoter of zebrafish. Dev Dyn. 2003;228(1):30-40.

52. Chen JN, Fishman MC. Zebrafish tinman homolog demarcates the heart field and initiates myocardial differentiation. Development. 1996;122(12):3809-16.

CHAPTER 4

FUTURE DIRECTIONS

Aberrant Ca^{2+} homeostasis in cardiomyocytes is frequently associated with contractile dysfunction and arrhythmias, which ultimately lead to heart failure [1-3], a major cause of death worldwide. To reveal the molecular mechanism by which Ca^{2+} homeostasis is regulated in cardiomyocytes and its implication in normal physiology and diseased states, I used the zebrafish *tremblor* (*tre*) mutant [4-5] as a model and conducted research using multidisciplinary approaches including molecular and cellular analyses, genetics, biochemistry, embryology, physiology and optogenetics. My research provides novel insights into the roles for Ca^{2+} homeostasis and its downstream event in the heart and sheds light on mechanisms underlying a variety of cardiac diseases caused by abnormal Ca^{2+} homeostasis.

A. Identification of the molecular mechanism regulating Ca^{2+} homeostasis in cardiomyocytes

To dissect the molecular network of Ca^{2+} handling in cardiomyocytes, our laboratory conducted a chemical suppressor screen on *tre* embryos and identified a synthetic compound named efsevin, which exhibits potent activity to restore rhythmic cardiac contractions by potentiating Ca^{2+} uptake activity of mitochondrial Ca^{2+} channel VDAC2. By a series of experiments using this compound, my work showed that, in addition to SR, mitochondria play an

essential role in modulating Ca^{2+} homeostasis in a VDAC-dependent manner, thereby maintaining cardiac rhythmicity.

Although beat-to-beat mitochondrial Ca^{2+} transients in cardiomyocytes have been reported [6-8], it is currently a matter of debate whether mitochondrial Ca^{2+} uptake affects E-C coupling by modulating cytosolic Ca^{2+} transients [9]. My study of the zebrafish *tre* mutant embryo provides genetic and physiologic evidence suggesting a regulatory role of mitochondria for cardiac rhythmicity. To further assess the role for mitochondria in the regulation of cardiac contractility and/or rhythmicity, it would be interesting to investigate how MCU [10-11] and MICU1 [12-13], a mitochondrial inner membrane Ca^{2+} transporter and its regulator, impact on embryonic and adult hearts.

Accumulating evidence demonstrates that Ca2+ released from the SR is transferred into mitochondria and that this process is facilitated by physical interactions between these two organelles [14-16]. Recently, several protein complexes have been implicated to tether ER/SR and mitochondria in mammalian cells. For instance, mitofusin 2 (MFN2) on the ER forms heterotypic and homotypic dimer with mitofusin (MFN) 1 and 2 on the OMM [17], and the voltage-dependent anion channel 1 (VDAC1) located on the OMM forms a complex with triphosphate receptor (IP3R) on the ER through the chaperone 75 kDa glucose-regulated protein (GRP75) [18]. In cardiac cells, RyR2 on the SR was shown to interact with VDAC2 on the OMM [19]. Thus, it would be interesting to test whether SR-mitochondria crosstalk serves as a critical component of Ca^{2+} handling to regulate cardiac rhythmicity.

My work also suggests that efsevin attenuates arrhythmogenic propensity under aberrant Ca^{2+} homeostasis by potentiating the Ca^{2+} transporting activity of VDAC2. This mechanism

enhances mitochondrial Ca^{2+} uptake and restricts spatiotemporal spread of cytosolic Ca^{2+} near the Ca^{2+} microdomains. From a therapeutic perspective, my research suggests that VDAC could be an effective therapeutic target for human arrhythmias and efsevin could lead to the development of novel anti-arrhythmognic agents. Future studies focusing on the kinetics of VDAC-dependent mitochondrial Ca^{2+} uptake as well as pharmacological characterization of efsevin will be highly valuable.

B. The role for Ca^{2+} homeostasis in maintaining sarcomeric integrity in cardiomyocytes

Although substantial evidence suggests that Ca^{2+}-dependent transcription plays a major role in several cardiac diseases [20-22], transcriptional alterations caused by pathophysiological Ca^{2+} homeostasis has not been completely understood. I utilized the zebrafish *tre* mutant as a model to investigate a downstream consequence of Ca^{2+} mishandling in cardiomyocytes. My study demonstrated that an E3 ubiquitin ligase, Muscle-specific RING Finger protein 1 (MuRF1), is significantly upregulated in the *tre* mutant heart. I further demonstrated mechanistically that Ca^{2+} overload induces the calcineurin-FoxO signaling pathway to promote MuRF1 expression, which leads to proteasome-dependent myofibril degradation in *tre* hearts. My study revealed a causative relationship between pathological Ca^{2+} homeostasis and myofibril disarray, suggesting that normal Ca^{2+} homeostasis is required for maintaining stoichiometry of cardiac muscle structure via transcriptional regulation.

It would be interesting to establish an inducible MuRF1 transgenic line to assess the possibility of using it as a model for cardiomyopathy. It is conceivable that this transgenic line would facilitate chemical suppressor screens to identify molecular pathways or chemical

compounds important for protecting myofibril integrity in the heart, which will provide valuable information to develop new diagnostic approaches and novel strategies for human cardiomyopathies.

C. References

1. Braunwald E. Research advances in heart failure: a compendium. Circ Res 2013;113(6):633-45.

2. Lompré AM, Hajjar RJ, Harding SE, Kranias EG, Lohse MJ, Marks AR. Ca^{2+} cycling and new therapeutic approaches for heart failure. Circulation. 2010;121(6):822-30.

3. Venetucci L, Denegri M, Napolitano C, Priori SG. Inherited calcium channelopathies in the pathophysiology of arrhythmias. Nat Rev Cardiol. 2012;9(10):561-75.

4. Langenbacher AD, Dong Y, Shu X, Choi J, Nicoll DA, Goldhaber JI, Philipson KD, Chen JN. Mutation in sodium-calcium exchanger 1 (NCX1) causes cardiac fibrillation in zebrafish. Proc Natl Acad Sci U S A. 2005;102(49):17699-704.

5. Ebert AM, Hume GL, Warren KS, Cook NP, Burns CG, Mohideen MA, Siegal G, Yelon D, Fishman MC, Garrity DM. Calcium extrusion is critical for cardiac morphogenesis and rhythm in embryonic zebrafish hearts. Proc Natl Acad Sci U S A. 2005;102(49):17705-10.

6. Maack C, Cortassa S, Aon MA, Ganesan AN, Liu T, O'Rourke B. Elevated cytosolic Na^{+} decreases mitochondrial Ca^{2+} uptake during excitation-contraction coupling and impairs energetic adaptation in cardiac myocytes. Circ Res. 2006;99(2):172-82.

7. Kohlhaas M, Liu T, Knopp A, Zeller T, Ong MF, Böhm M, O'Rourke B, Maack C. Elevated cytosolic Na^{+} increases mitochondrial formation of reactive oxygen species in failing cardiac myocytes. Circulation. 2010;121(14):1606-13.

8. Drago I, De Stefani D, Rizzuto R, Pozzan T. Mitochondrial Ca^{2+} uptake contributes to buffering cytoplasmic Ca^{2+} peaks in cardiomyocytes. Proc Natl Acad Sci U S A. 2012;109(32):12986-91.

9. Rizzuto R, Pozzan T. Microdomains of intracellular Ca^{2+}: molecular determinants and functional consequences. Physiol Rev. 2006;86(1):369-408.

10. Perocchi F, Gohil VM, Girgis HS, Bao XR, McCombs JE, Palmer AE, Mootha VK. MICU1 encodes a mitochondrial EF hand protein required for Ca^{2+} uptake. Nature. 2010;467(7313):291-6.

11. Alam MR, Groschner LN, Parichatikanond W, Kuo L, Bondarenko AI, Rost R, Waldeck-Weiermair M, Malli R, Graier WF. Mitochondrial Ca^{2+} uptake 1 (MICU1) and mitochondrial Ca^{2+} uniporter (MCU) contribute to metabolism-secretion coupling in clonal pancreatic β-cells. J Biol Chem. 2012;287(41):34445-54.

12. De Stefani D, Raffaello A, Teardo E, Szabò I, Rizzuto R. A forty-kilodalton protein of the inner membrane is the mitochondrial calcium uniporter. Nature.2011;476(7360):336-40.

13. Baughman JM, Perocchi F, Girgis HS, Plovanich M, Belcher-Timme CA, Sancak Y,Bao XR, Strittmatter L, Goldberger O, Bogorad RL, Koteliansky V, Mootha VK. Integrative genomics identifies MCU as an essential component of the mitochondrial calcium uniporter. Nature. 2011;476(7360):341-5.

14. Szalai G, Csordás G, Hantash BM, Thomas AP, Hajnóczky G. Calcium signal transmission between ryanodine receptors and mitochondria. J Biol Chem. 2000;275(20):15305-13.

15. Pacher P, Csordás P, Schneider T, Hajnóczky G. Quantification of calciumsignal transmission from sarco-endoplasmic reticulum to the mitochondria. JPhysiol. 2000;529 Pt 3:553-64.

16. García-Pérez C, Hajnóczky G, Csordás G. Physical coupling supports the local Ca^{2+} transfer between sarcoplasmic reticulum subdomains and the mitochondria inheart muscle. J Biol Chem. 2008;283(47):32771-80.

17. de Brito OM, Scorrano L. Mitofusin 2 tethers endoplasmic reticulum to mitochondria. Nature. 2008;456(7222):605-10.

18. Szabadkai G, Bianchi K, Várnai P, De Stefani D, Wieckowski MR, Cavagna D,Nagy AI, Balla T, Rizzuto R. Chaperone-mediated coupling of endoplasmic reticulum and mitochondrial Ca^{2+} channels. J Cell Biol. 2006;175(6):901-11.

19. Min CK, Yeom DR, Lee KE, Kwon HK, Kang M, Kim YS, Park ZY, Jeon H, Kim do H. Coupling of ryanodine receptor 2 and voltage-dependent anion channel 2 is essential for Ca^{2+} transfer from the sarcoplasmic reticulum to the mitochondriain the heart. Biochem J. 2012;447(3):371-9.

20. Luo M, Anderson ME. Mechanisms of altered Ca^{2+} handling in heart failure. Circ Res. 2013 Aug 30;113(6):690-708.

21. Marks AR. Calcium cycling proteins and heart failure: mechanisms and therapeutics. J Clin Invest. 2013;123(1):46-52.

22. Venetucci L, Denegri M, Napolitano C, Priori SG. Inherited calcium channelopathies in the pathophysiology of arrhythmias. Nat Rev Cardiol. 2012;9(10):561-75.